POLITECNICO DI TORINO

Master of Science program in ARCHITECTURE FOR THE SUSTAINABILITY DESIGN

Thesis of Master degree

Active Transparent Facades: Experimental and Numerical Evaluation on Daylighting

Supervisors
Dr. Valerio Roberto Maria Lo Verso
Dr. Fabio Favoino
Dr. Luigi Giovannini

Candidate
Alireza Norouziasas

Academic year 2020/2021

Abstract

The proper use of daylight is a challenge in buildings due to the energy consumption, performance, and visual comfort of users. Given the widespread usage of glass facades in buildings, the need to consider and evaluate visual comfort and reduce glare is raised. Glare is a prevalent issue in modern buildings with large transparent facades, which not only reduces occupant comfort but can also degrade building energy performance. The use of image-based visual comfort analysis to identify glare and estimate occupant visual comfort with a place has a high potential. In terms of designing buildings with occupant visual comfort in mind, architects have to estimate glare using simulations rather than images. However, the image-based glare analysis is highly accurate, but on the other hand it is a significantly time-consuming procedure.

In this study, visual comfort and daylighting conditions in the presence of Double Skin Facades (DSF) were numerically and experimentally analyzed. Six points have been considered to assess visual comfort in three different scenarios. Scenario one was considered when the Venetian blind was pulled up. Scenarios two and three were with the Venetian blinds down, with the tilt angle of 0° and 30°, respectively. The image-based measurements have been carried out for analyzing glare conditions and compared with simulation results. The influence of the Venetian blind with various tilt angles on daylighting as expressed through a set of dedicated indicators was assessed.

The correlation of annual glare and point-in-time glare analysis was carried out to decrease the time of calculation and increase the accuracy of glare estimation. According to the results, the point-in-time Daylight Glare Probability ($DGP_{point\text{-}in\text{-}time}$) value in Diva was higher than the corresponding value in Honeybee almost for all the simulated time. The differences with the CIE Overcast Sky model were lower than what observed under a CIE Clear Sky. However, the disparity was significant so that in some simulated points, the $DGP_{point\text{-}in\text{-}time}$ values tripled than the $DGP_{point\text{-}in\text{-}time}$ in Honeybee. By assessing the $DGP_{point\text{-}in\text{-}time}$ and annual Daylight Glare Probability (DGP_{annual}) for each simulated hour, the closer the evaluated points are to the window, the more the value of glare classifications is inconsistent. The DGP_{annual} estimated the glare classes with high

accuracy. The estimation rate of DGP_{annual} for discomfort glare classes were 100%, 90.74%, and 85.42% in scenarios three, two, and one, respectively.

Acknowledgements

First of all, I would like to thank all my professors for the quality of learning they offered during the last three years at Polito University. Acknowledgments also go out to Dr. Luigi Giovannini have been of great help during the thesis process. The technical part of this research was a big challenge for me, especially in the lack of experts who work on the used program to get data from. Then, I would like to thank Dr. Gabriele Piccablotto for taking the time to answer my questions regarding the measurement instruments and applications. I am very grateful for the help of Dr. Peiman Pilechiha, as without his advice, my learning process on Grasshopper and Honeybee would not have gone as smoothly. I would like to express my deepest gratitude to my family and friends for their love and support during my thesis work from beginning to end.

Last, but not least, I am especially thankful to my supervisors Dr. Valerio R.M Lo Verso and Dr. Fabio Favoino, for all the attention given to this thesis, their availability, even in the context of the coronavirus, and all their advice.

List of figures

List of tables

List of acronyms

DSF	Double Skin Facade
DF	Daylight Factor [%]
sDA	Spatial Daylight Autonomy [%]
cDA	Continuous Daylight Autonomy [%]
IES	The Illuminating Engineering Society
DGP	Daylight Glare Probability
DGPs	Simplified Daylight Glare Probability
$DGP_{point\text{-}in\text{-}time}$	Point-in-time Daylight Glare Probability
DGP_{annual}	Annual Daylight Glare Probability
ASE	Annual Sunlight Exposure [%]
DA	Daylight Autonomy [%]
EPW	EnergyPlus Weather files
CGI	CIE Glare Index
UDI	Useful Daylight Illuminance
GH	Grasshopper
HB	Honeybee
CFS	Complex Fenestration Systems
LB	Ladybug
U-value	Heat transmission coefficient [W/m²K]
Tvis	Visible Transmittance
low-E	low-emissivity

Table of Contents

1. Introduction

Daylight is a crucial resource for life, one of nature's core unchanging forces, a major factor that may generate important and evocative architectural experiences, determining moods and space quality. Daylight is the clearest, softest, easiest and cheapest structural material available in producing qualities and objects needed by the human environment. Attention to human needs has become fundamental to improving building occupants' well-being, health, and safety.

Creating a sustainable architecture should be the central point of every professional's work. Therefore, it is necessary to study the building materials and the technologies and strategies that can be implemented to limit the environmental impact.

In fact, daylight plays a significant role in terms of occupant comfort and health, as well as energy savings. Over the last few years, the energy-saving elements of electric lighting in buildings have gained considerable attention as part of an integrated approach to predicting and calculating a building's overall energy consumption [1]. In terms of health and well-being, studies have demonstrated that daylight, with its diversity in intensity and spectrum, is critical in activating the human circadian rhythm, impacting 'human variables' such as sleep quality, drowsiness, and vitality, alertness, and productivity [2,3].

The utilization of daylight in buildings, with its fluctuations, spectral composition, and provision for external views, is critical for occupant comfort and well-being. In the offices, for example, daylight may have a good impact on office personnel's health, enhancing efficiency, and resulting in more advantages for increased productivity. A daylight strategy, if well developed, may also result in substantial energy savings, as long as it minimizes energy usage for artificial lighting and eliminates glare and other visual discomforts (such as contrast, adaption issues, and internal reflections). However, the total energy efficiency of windows is also determined by thermal factors (for example, solar gains and heat losses via glass) and their balance against heat output from artificial lighting systems [4].

Within this thesis, a particular discipline deals with both human health and respect for the environment. Daylighting is a phenomenon that, if studied carefully, can be a winning weapon for the objectives of well-being, comfort, energy-saving, and environmental sustainability.

1.1. Background information and problem statement

Providing user comfort in the interior of the building has various aspects, the most important of which is visual comfort. Providing lighting conditions in such a way that users' visual comfort is provided and visual stimuli are received from the environment can be influenced by various factors, including the amount of light and how it is distributed, annoying reflections, glare, and light color temperature [5].

In order to evaluate two critical factors affecting the visual comfort associated with daylight, namely the amount of light received and the absence of annoying glare. In terms of 'conventional' photopic needs, the complex issue of visual comfort is often handled in design practice through a variety of factors such as workplane illuminance (Ewp), vertical illuminance (Ev), glare indices, and luminance distribution in the occupants' visual field. Photometric indices are divided into static and dynamic groups regarding the period under evaluation and the sky conditions. The evaluation by static indicators is only for a short time, and calculations are performed for a steady-state, while dynamic indicators are based on design parameters, climate, and changes in sky conditions. Consequently, lighting changes based on meteorological data assess the space's lighting conditions and the users' visual comfort during a year and provide more comprehensive results [6].

Dynamic indices can be calculated through dynamic simulations that use the so-called climate-based daylight modeling CBDM [7]. Properties such as the geometry and shape of space, the properties of materials, and light sources (sun and sky) are input data for the software. Also, a network of sensors (grid points) at a certain height (usually at the work surface height, but also aligned at the eyes of occupants) is set to calculate daylighting across a space. The relevant indicators are calculated with the help of lighting data obtained at each of these sensors' locations to determine whether it is possible to assess the insufficiency, appropriateness, or excess of light in different parts of the study space [8].

Discomfort glare is a major factor in visual comfort. However, due of the inherent uncertainty concerning the nature of this multi-faceted psycho-physiological phenomena, which has both a temporal and a spatial reliance, as well as a dependent on visual activity, it is seldom addressed during the design phases [9]. In the presence of daylight, glare is impacted by the time-varying brightness distribution of the sky dome and interior surfaces, which may shift dramatically, as can glare felt from different positions and view directions inside the same room.

A variety of daylight glare indices have been suggested, with the Daylight Glare Probability DGP gaining widespread acceptance [10]. Nonetheless, because to the complexity and/or the length of time required for their computation, their incorporation into the design process has long been limited. The DGP and luminance ratios have a larger link with user happiness than horizontal illuminance [11], but the horizontal illuminance distribution across the workplane (E_{wp}) is the easiest to forecast, model, and test in-situ. This explains why, despite the fact that E_{wp} measures visual performance rather than visual comfort, the prevalent practice in the design process is still centered mostly on this parameter.

One of the dynamic indicators for measuring the amount of light is the useful daylight illuminance (UDI), the ratio of the period of occupation during a year in which the horizontal brightness at a certain point is within a specific range. The presence of low- and high-brightness values divides the estimated time range into three parts: the amount of time that daylight is too low ($UDI_{underlit}$), sufficient (UDI_{useful}), or so high ($UDI_{overlit}$) that it leads to visual discomfort [12].

The values set as the upper and lower limits for this index vary in different sources, but generally, 300 to 3000 lux is recommended as the light adequacy range [13]. Daylight autonomy (DA) is another dynamic indicator that shows the adequacy of daylight indoors is equal to the percentage of the period of space occupied during a year. The amount of light required at a given point in space can be provided by natural light alone.

Illuminating Engineering Society (IES), recommends spatial daylight autonomy ($sDA_{300/50\%}$) for light adequacy analysis; That is, the percentage of surface points that receive brightness above 300 lux in at least 50% of the occupancy time from 8 a.m. to 6 p.m., and the minimum acceptable value for it is 55% [14].

1.2. Daylight challenges

For daylight design to be effective and appropriate, it is necessary to start on a larger scale before considering how light enters the building and the systems that enhance the quality of indoor lighting. At this stage, the relationship between the site and the building, and the relationship between the building physics and daylight, is examined.

1.2.1. Effect of site location and obstructions on daylighting

The orientation of the building towards the site and measuring the effect of site obstruction are considered. The effect of site blockage is shading, which is caused by natural and abnormal barriers on the site. In order to have an adequate access to the sunlight, in the northern hemisphere, window walls should be 90 ° to the south. A slight orientation to the east causes solar heating in the morning and avoids overheating in the summer afternoon [15]. To get the desired daylight, the building should not be located close to large obstacles. The best way to estimate the optimal distance is to provide a cross-section of the design and the surrounding obstacles. If the beam passing through the highest obstacle point does not form an angle of more than 25 ° with the horizon line after hitting a point at the height of 2 meters, the building in question may have an adequate daylight [16].

1.2.2. Daylight and building physics

The first point to consider in using natural light in space is its entry into indoor spaces, separated from the facade's outside environment. The primary way natural light enters space is to use openings in the shell. There are two distinct areas for using daylight indoors. The peripheral parts of the building connected to the building shell have direct access to natural light. The inner parts of the building that are not directly connected to the building shell and provide natural light are only possible using transmission systems.

Before examining the specific systems used to allow daylight to enter the core parts of the building, the physical factors affecting the efficient use of daylight in indoor spaces are discussed. These factors include volume density, volume porosity, and geometric properties of the space. Volume density expresses the relationship between the volume and the building envelope. In buildings with lower spatial density, it is possible to use more natural light. Creating porosity in the volume through spaces such as the central courtyard allows light and ventilation for the central parts. The geometric properties of the space are essential in lighting design. Two spaces with different dimensions and the same spatial proportions have the same quality of natural light in the same environmental conditions. Therefore, proportions are more critical in daylighting than dimensions [17].

1.2.3. Lighting admitted indoors

Daylighting systems are divided into three groups according to the direction of light entering space. Lateral transmittance components let the light into the space laterally, and by moving away from them, the brightness of the space is significantly reduced. Zenithal components allow the light to enter the space vertically. These elements create a more uniform distribution of light in spaces compared to lateral daylighting systems. The components of the general translucency allow light to enter from above and to the sides. Therefore, it creates a high brightness and uniformity of light. These elements need a radiation controller because they provide too much radiation and solar gain, thus overheating the indoor space [18].

1.2.4. Window as a key factor for lighting entrance into buildings

Natural light enters indoor spaces often through windows. There are different types of windows, but in choosing their dimensions and appearance, less attention is paid to the issue of exposure. The aesthetic aspect and the appearance of the window in the building facade are considered mainly by designers. In terms of energy consumption, its thermal role is more critical. Since windows are good elements for providing light in the building, they need to pay attention to their solar control [19].

Calculating the level of window glass and the amount of exposure depends on several factors. These factors include materials, design, size, and exterior and window-related elements. Outside the window, sunlight can be dimmed by trees or elements such as lattice panels. Although these elements emit direct sunlight, they often reduce the amount of light entering the space through the window [20]. This reduction is compensated by increasing the size of the window. Windows need shading in the summer sun. The presence of trees reduces the amount of sunlight received in summer, while the amount of incoming light increases in winter.

1.2.5. Daylight and heat gain

The lighting, heating, and ventilation of a building, natural or artificial, are interdependent. The improper use of glass in incorrect places, such as the western wall of the building in the hot climates, and excessive use of glass surfaces in the hot or cold regions paved the way for undesirable heat gains or losses. Consequently, in this case, reducing the demand for heating or cooling is necessary.

In general, a lack of proper design in the use of daylight causes excessive heat intake. For example, the everyday use of glass surfaces leads to high demand for electric lighting. In this way, the elements that produce electric light generate heat and increase the cooling load of the building. Also, when solar radiation enters the building, it also brings thermal energy in, which causes a load on the building's cooling system. Therefore, to prevent the creation of undesirable heat caused by sunlight, it is necessary to pay attention to the dimensions and position of the window and provide solar shading devices in the needed places. In the case of proper lighting design, daylight is the most efficient type of source. Therefore, daylighting techniques and reducing electricity consumption minimize the load on the building's cooling system.

1.2.6. Daylight and human behavior

Architectural and environmental conditions are very influential on the behavior and performance of space users. Therefore, utilizing environmental capabilities provides the possibility of managing user behavior to achieve designers' goals. Light, as an environmental factor in occupied spaces, has a significant effect on human behavior. Changing the intensity of light, its type, and its resulting phenomena such as glare, led to different reactions in humans. For example, the type of fluorescent light bulb causes fatigue, confusion, and stress. It happened since these lamps emit x-rays and radio waves and do not have the full range of colors, thus reducing the productivity of occupants [21].

1.3. Motivation

Care and respect for our planet are topics that have taken hold in the architectural field for some decades. The answer to these demands in architecture has emerged in the form of buildings such as the "green buildings", "zero impact buildings", or the "passive houses", which minimize or even eliminate the energy requirement necessary to keep the environment cool or warm. These new attentions have led to concepts such as energy saving. Using local resources and recycling has become a "must-have" for everyday architecture.

Glazed facades are most common in building sectors, particularly office buildings. Glassed surfaces allow natural light to enter spaces and interact with the outside world and surroundings, particularly with a view of the surrounding metropolitan area. Furthermore, significant glass sections can lessen the impression of enclosure for occupants and enhance the comfort of employees who spend most of their time in that office room, where the external visual contact significantly influences the occupant's wellbeing. As a result, work productivity will improve.

It is widely understood that daylight and visibility promote employee health, comfort, and a good work environment and that they should thus be addressed for indoor spaces. Understandably, the need to reduce visual discomfort and glare is inevitable for daylit space users [22]. Considering the widely used glazed facades in buildings, the importance of consideration and evaluation of the visual comfort and decreasing the glare is increased. However, the glare issue has been investigated by researchers for many years, it is quite a complex problem. Therefore, finding an acceptable solution for the glare phenomena is hard. As a result, it is extremely tough for the designer to determine how to reduce glare performance as feasible. Valid criteria help designers make better choices between different solutions, leading to a range of designs that balance daylight penetration and visual comfort [23].

Changes in the intensity and quantity of light during the day can affect the visual performance of the occupants. Increasing the intensity of daylight can cause visual dysfunction and consequently glare occurrence. Despite architects' desire to use more daylight, glare is given insufficient consideration. As a result, the visual comfort and glare induced by daylight should be carefully evaluated because the lack of visual comfort can interfere with effective daylight use. It emphasizes the significance of this research.

1.4. Objectives

This study investigates the applicability of active facades (DSF) to improve the occupant's visual comfort in the building ultimately. The analysis includes experimental and numerical evaluation of daylighting performance and computer modeling results. Ultimately, this study aims to identify the practicality of dynamic facades concerning glare predictions and their correlation with illuminance. Also, finding the correlation of annual glare and point-in-time glare analysis paves the way for scheduling the shading devices with annual glare analysis instead of a point-in-time . The project is a pilot study, and four main objectives are as follow:

1. Comparison and analysis of the annual and point-in-time glare in double skin facades.
2. Finding a framework for conducting an annual glare analysis instead of a point-in-time glare analysis.

3. Understanding the correlation of the annual glare analysis and point-in-time glare analysis.
4. Demonstrating the accuracy of glare prediction when the annual glare analysis was used instead of point-in-time analysis.

This study aims to investigate the applicability of active facades for increasing the adoption of annual-climate-based glare metrics and the enhancement of daylighting in the interior spaces of buildings, to scale opportunities for more healthy, productive, and energy-efficient spaces for occupants.

The main research questions of this thesis are as follow:

- Research Question RQ1. Which simulation tools are more accurate and capable in terms of glare analysis?
- Research Question RQ2. How can glare analyses be simplified through doing annual glare analysis instead of point-in-time glare analysis?
- Research Question RQ3. What is the correspondence degree between the annual glare analysis and point-in-time analysis?

Therefore, the whole work evaluates visual comfort, glare exploiting, and dynamic facade through an experimental characterization and numerical simulation analysis.

1.5. Structure of the thesis

The thesis is structured as follows. Chapter two: focuses on introducing, reviews and presents daylighting measurements, visual comfort, modeling tools, glare metrics, and adaptive façades technology. This section provides a quick overview of the daylighting metrics used to analyze visual comfort and the impact of discomfort glare. It then briefly discusses the most recent modeling tools for daylighting performance before introducing a new categorization for measuring visual comfort and glare risk. After that, the customized approach for answering the research objectives, as well as the entire approach of simulation procedure, case study, and experimental analysis, are then discussed in chapter three. Also included are the existing design tools and blueprints that were utilized for simulation are discussed in this chapter.

Then, chapter four will present the results obtained by following the methodology. According to the methodology, different indicators of daylight and glare are simulated. Simulations were used to perform generalizable results. The introduced DSF was modeled and simulated using Honeybee in Grasshopper and Diva for Rhino. The results of appropriate indicators for evaluating daylight and glare are prioritized and selected. Thus, the effect of the Venetian blind with different degree angles on the selected indicators was investigated in different scenarios. Finally, in chapter five, the strengths, challenges, and limitations are introduced and suggestions are made for future studies are discussed.

2. literature review

This literature review focuses on gathering state of the art related to the thesis: daylighting metrics, visual comfort, simulation tools, glare metrics, and adaptive façades technology.

This section briefly describes the list of daylighting metrics to assess visual comfort and the influence of discomfort glare. Then, it briefly reviews the most adaptive façade with the focus on double-skin facade for daylighting performance and finally introduces a new classification for assessing visual comfort and risk of glare.

2.1. Visual comfort

The term "visual comfort" refers to "a subjective state of visual well-being caused by the visual surroundings" [24]. Even though the description indicates a subjective dimension of comfort, many physical parameters of the visual environment are described and utilized to evaluate its quality objectively. Luminance distribution, illuminance and its uniformity, glare, color of light, color rendering, flicker rate, and quantity of daylight are all characteristics that define visual situations [25].

One of the instruments for providing visual comfort is the algorithm for regulating shade devices (e.g., manual, cut-off, closure during high irradiation). It has a considerable influence on solar radiation flux and, as a result, illuminance distribution, visual and thermal comfort, and, last but not least, a building's energy requirement. Because many current automated shade control methods do not result in increased visual comfort or an instant increase in thermal comfort, they are frequently rejected by consumers [26].

In this way, not only all its benefits can be obtained from light, but also the relative energy and economic savings, which lead to higher scores, at an architectural level, in certifications and energy protocols.

2.2. Quantifying the visual well-being

The assurance of internal visual comfort is a vital component for the quality of life in indoor spaces. It must be such that users can carry out the activities planned for that room safely and satisfyingly.

Various criteria can be used to assess brightness levels and serve as visual well-being indices; some of these are recognized by national and international legislation that mandates the achievement and exceeding specified minimum standards. In terms of light, these minimum levels must be met without surpassing the verification, as the purpose is to maintain energy efficiency and visual well-being without jeopardizing them. Additional visual discomfort indicators, or metrics, show when the comfort limitations have been exceeded in this regard. Illuminance, uniformity, glare, and luminance contrast, which apply to both natural and artificial light, will be discussed in this part, followed by chromaticity and flickering, which are more relevant to the second component. In addition to being calculated for regulatory control, these metrics can be utilized in the energy sector to get recognition, such as protocols and certificates, which allow raising the added value of properties by partnering in consumption reduction and safeguarding - biennial. Frequently, designers focus on the effortless fulfillment of legal requirements, which do not always meet quality and proper quantity requirements. For this reason, in addition to the amounts covered by the regulation, extra quantities contribute to the user's visual well-being and safety.

2.3. Methods for describing discomfort glare

An excellent daylighting design aims to offer enough light for efficient visual performance and provide a comfortable and pleasing atmosphere appropriate for the purpose. The problem of glare is intimately tied to the comfort component of a daylighting design. Only the subject's characterizations and physical elements may be used to estimate the amount of glare (e.g., source luminance, the solid angle of the glare source, background luminance, etc.).

The author will offer a collection of past experimental investigations on subjective glare perception in the following sections.

2.4. Assessment of visual comfort

Although the sun is needed to create natural light in a building, this light eventually turns into heat. The amount of radiation required for each building must be provided according to its type and climatic conditions. Due to the importance of sunlight depending on the type of climate in the region and different seasons.

Currently, daylight has been developed as a design strategy to reduce lighting energy consumption and improve users' visual comfort and productivity in space. Natural light and visual communication with the outside environment in human living spaces, including work environment, education, recreation, etc., in addition to increasing efficiency and productivity, reduces anxiety, improves behavior, and maintains and increases health.

Achieving visual comfort in a daylighting design is accompanied by the risk of glare for occupants in a building [27]. Changes in the intensity and quantity of light during the day affect the visual performance of the audience. Increased daylight intensity caused visual dysfunction and glare. Despite the architects' attention to using as much daylight as possible, they pay less attention to the issue of glare. Therefore, the visual comfort and glare of daylight should be carefully considered; because the lack of visual comfort can disrupt the use of daylight.

The glare estimation is only possible by classifying and analyzing the glare source employing subject and physical factors such as the source of luminance, the background luminance, the solid angle of the glare source, etc [26].

Light distribution is measured in illuminance, while contrast ratios related to glare conditions can be perceived in luminance values. The indexes used to describe visual comfort can be point-in-time and annual-based metrics. Table 1 shows an overview of some of the primary metrics currently in use.

Table 1. The annual and point-in-time glare and daylight metrics

Point-in-time Metrics	
Illuminance (Ep)	Amount and distribution of light
Luminance (L)	Surface 'brightness'
Daylight Factor (DF)	Amount and distribution of light
CIE Glare Index (CGI)	Glare
Unified Glare Rating (UGR)	Glare
Discomfort Glare Probability (DGP)	Glare

Annual-based Metrics	
Daylight Autonomy (DA)	Amount and distribution of light
Daylight Glare Probability (DGP)	Glare
Continuous Daylight Autonomy (cDA)	Amount and distribution of light
Useful Daylight Illuminance (UDI)	Amount and distribution of light
Spatial Daylight Autonomy (sDA)	Amount and distribution of light
Annual Sunlight Exposure (ASE)	Glare proxy: direct sun in space

2.4.1. Amount and distribution of light

The metrics essentially utilized in order to get the amount, as well as propagation of light, are given below.

2.4.1.1. Luminous flux (Φ)

The luminous flux (Φ) describes the quantity of light emitted by a light source. The unit of luminous flux is Lumen (lm). The luminous efficiency is the ratio of the luminous flux to the electrical power consumed (lm/W). It is a measure of a light source's economic efficiency.

2.4.1.2. Luminous intensity (I)

The luminous intensity (I) describes the quantity of light that is radiated in a particular direction. It is a helpful measurement for directive lighting elements such as reflectors. It is represented by the luminous intensity distribution curve (LDC).

2.4.1.3. Illuminance (E)

Illuminance (E) is the total luminous flux incident on a surface per unit area expressed in lux. Illuminance describes the quantity of luminous flux falling on a surface. Relevant standards specify the required illuminance like EN12464-1 [25]. The illuminance Equation 1 includes illuminance of a surface (*p*) in lux (*Ep*);

luminous flux incident calculated based on the light source and reflecting properties of neighborhood surfaces (*dØ*) and area of the surface (*dArec*) [28].

$$Ep = \frac{d\emptyset}{dAreceiving}\,[lx]$$

Equation 1. Illuminance equation

The summary of the definitions mentioned above has been presented in Figure 1.

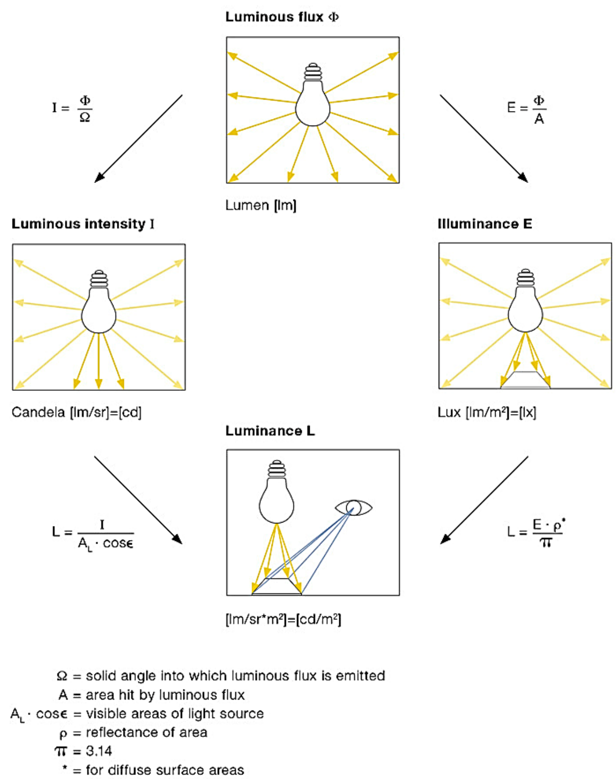

Figure 1. Summary of the basic parameters of lighting

2.5. Glare indexes

Glare is defined as "the annoyance, discomfort, or loss of visual performance and visibility caused by luminance within the visual field that is sufficiently greater than the luminance to which the eyes are acclimated" [29].

Over the last 60 years, researchers have studied discomfort glare. There has always been considerable agreement on the major physical parameters that determine the subjective glare sensation: (i) luminance of glare sources in one's visual field; (ii) adaptation level, typically identified as the luminance of background in one's visual field or as the vertical illuminance at eye-level; (iii) solid angle subtended at eyes by the glare source; and (iv) position of the glare source in one's visual field [30].

According to Pierson et al. [27], the discomfort glare is caused by two factors: (i) a too high brightness contrast between the glare source and the adaption level. This contribution to glare is commonly known as 'contrast glare'. (ii)the amount of light reaching an occupant's eyes is excessive. Discomfort is felt even if the contrast is adequate since the occupant's eye cannot adjust to such bright light. This contribution to the glare is known as 'saturation glare'.

In principle, glare caused by daylight can be placed into three main categories: disability glare, discomfort glare, and glare reflections. Disability glare occurs when the amount of light is excessive, and the occupant is unable to see; or discomfort glare occurs when a range of brightness exists in a field of view, causing visual impairment and eye fatigue [28]. Glare reflections degrade contrast on visual display units (VDUs) and can significantly affect office environments. The principal used glare indexes, and metrics are described below.

In a study where visual comfort assessment from a group of 45 people was compared to several illuminances and luminance-based metrics derived from HDR luminance images, Van Den Wymelenberg and Inanici [31] discovered that Ev and other simple metrics (mean and standard deviation luminance of the scene) outperformed complex glare indices and also set preliminary thresholds values between comfort and discomfort (BCD) for Ev, in the range 875–1250 lux, while The collection of HDR photos utilized in this investigation was reanalyzed in a later study by Jakubiec et al. [32], and the threshold value Ev > 1500 lx was shown to be capable of identifying 54.7% of participant discomfort.

To reliably quantify and assess observed levels of glare, many discomfort glare indices have been established. However, existing glare indices provide vastly disparate ratings of the identical glare situation [33]. Many experts have conducted validation tests on the glare indices. However, there is still no clear guidance on how to use the glare indices correctly. Extensive human subject research was conducted to corroborate prior research findings and further understand how existing glare indices assess glare under different daylit circumstances.

2.5.1. Luminance (L)

Luminance is a photometric measure of the luminous intensity per unit area of light traveling in a given direction. Luminance is the only essential lighting parameter that is perceived by the eye. On the one hand, it describes a light source's impression of brightness, and on the other, a surface depends mainly on the degree of reflection (color and surface). Equation 2 includes the luminous intensity (dl) at an angle (y) resulting between the surface normal and the emission point over the visible area of the surface ($dAvisible$).

$$Ly = \frac{dly}{davisible}\,[cd/m^2]$$

Equation 2. Luminance formula (L)

However, there is no consensus on the maximum brightness threshold for glare prediction Wienold and Christoffersen [10] proposed the following thresholds:

“acceptable” glare: 2000 cd/m2

“just uncomfortable” glare: 4000 cd/m2

“intolerable” glare: 6000 cd/m2

Glare may be defined in three ways: according to the process that caused the glare, according to an individual's perceived degree of glare intensity, and according to the glare's outcomes. Many current glare indices, such as the DGP (Daylight Glare Probability), DGI (Daylight Glare Index), UGR (Unified Glare Rating), VCP (Visual Comfort Probability), and CGI (CIE Glare Index), are concerned with determining the perceived degree of glare intensity. DGP and DGI were created expressly for daylight glare, which must be managed differently from the visual discomfort caused by electrical light sources [34]. The glare indices' formulae appear complicated but utilize the same variables with different weighting factors. Background mean luminance, glare source luminance, glare source position, the solid angle of glare sources, vertical illuminance, and direct vertical illuminance are critical data to collect in order to determine the following glare indexes.

2.5.2. CIE Glare Index (CGI)

This index was presented by Einhorn [35] and adopted by the International Commission on Illumination (CIE). The CGI calculation includes illuminances by direct (*Ed*) and diffuse light (*Ei*) (Equation 3). This metric developed only for artificial light, such as British Glare Index (BGI) and Visual Comfort Probability (VCP) not included in this literature review.

$$CGI = 8\,log\left[2\,\frac{1+(Ed/500)}{Ed+Ei}\sum_{i=1}^{n}\left(\frac{L_{s,i}^{2}\times\omega s,i}{P_{1}^{2}}\right)\right]$$

Equation 3. CIE Glare Index (CGI)

In a study conducted by Jakubiec and Reinhart [36], authors claimed that CGI thresholds of less than 13 indicate imperceptible glare and more than 28 intolerable glare.

2.5.3. Unified Glare Rating (UGR)

For the assessment of discomfort glare in interior lighting, the CIE proposed the Unified Glare Rating (UGR) [37].

The UGR is calculated through the following equation:

$$UGR = 8\,log\left[\frac{0.25}{L_b}\sum_{i=1}^{n}\left(\frac{L_{i}^{2}\times\omega_{i}}{P_{i}^{2}}\right)\right]$$

Equation 4. Unified Glare Rating (UGR)

Where:

L_b the background luminance

L_i the luminance of luminaire i

ω_i the solid angle of luminaire i

p_i the Guth position index of luminaire i.

The luminance is calculated by dividing the light intensity in the direction of the observer by the apparent size of the luminaire's luminous portion. Initially, the Guth position index is only supplied for the upper visual field and is calculated by interpolating between tabular values.

The majority of lighting systems result in UGR values in the practical range of 10–30. The suggested limiting UGR values, according to EN 12464-1 [25], comprise a sequence with steps of noticeable increases in glare sensation: 10, 13, 16, 19, 22, 25, and 28. Observers frequently need to use a scale based on Hopkinson's [38] criteria to quantify uncomfortable glare feeling. A correlation between UGR and Hopkinson's criterion is required. According to EN 12464-1 [25] and Geerdinck [39], three UGR units equate to one Hopkinson criteria step, and the following relationship may be discovered: UGR 10 = unnoticeable, 13 = barely perceptible, 16 = perceptible, 19 = barely tolerable, 22 = unacceptable, 25 = barely unpleasant, and 28 = extremely uncomfortable. Lighting systems with a UGR of less than 10 are deemed to be non-inconvenient [25].

2.5.4. Daylight Glare Probability (DGP)

Unlike prior glare metrics, DGP considers the illuminance value experienced by the observer in addition to the luminance contrast ratios between the background and the glare source. As a result, this metric frequently has good correlates with occupant surveys on glare perception. The fact that this metric is only applicable for vertical illuminance values above 380 lux and DGP values between 0.2 and 0.8 is one of its limitations. Equation 5 shows the formula for the calculation of DGP:

$$DGP = 5.87 \times 10^{-5}\, Ev + 0.0918 \times log_{10} \left[1+\sum \left(\frac{L_{s,i}^{2}}{E_{v}^{1.87}} \times \frac{\omega s,i}{P_{i}^{2}}\right)\right] + 0.16$$

Equation 5. Daylight Glare Probability (DGP)

Where in DGP equation uses vertical eye illuminance (*Ev*), the luminance of the light source (*Ls*), the solid angle of the source seen by an observer (ωs), and a position index relative to azimuth and elevation (*P*).

The proposed cutoff point by Wienold [40] is:

- Imperceptible glare: DGP ≤ 0.35
- Perceptible glare Disturbing glare Intolerable glare: 0.35 > DGP ≤ 0.40
- Disturbing glare: 0.40 > DGP ≤ 0.45
- Intolerable glare: DGP > 0.45

Another study [31] published recommendation thresholds for DGP as follow:

- Likely to be comfortable: DGP < 23% or 0.23
- Bounded between comfort and discomfort (BCD): 23% or 0.23 > DGP < 25% or 0.25
- Likely to be uncomfortable: DGP >25% or 0.25

Wienold et al. presented a simplified DGP (DGPs), also known as annual DGP, for dynamic simulation in 2007. The DGPs, which serve as the foundation for the proposed glare reduction technique, further decrease computing time by skipping picture formation accounting for the vertical illuminance contribution. The simplified metric can be applied to any virtual sensor positioned at a viewpoint of interest, as long as no direct sunlight or specular reflections reach the sensor (Equation 6). The equation considers vertical eye illuminance but applies a simplified computation to the principal glare sources that ignore indirect ambient reflections and do not incorporate the exact lighting distribution. This approach cut simulation time in half and produced results that were comparable to DGP.

$$DGP_s = 6.22\times10^{-5}\, Ev + 0.184$$

Equation 6. Simplified Daylight Glare Probability (DGPs)

2.6. Daylighting performance within a space

LEED is an American certification standard for sustainable building certifications. This standard takes into account energy consumption, occupant comfort, and others. It focuses on the environmental (52%), economic (5%), and social (43%) aspects.

The limits of LEED v4's annual climate-based criteria have been a regular topic of controversy in the academic and practice sectors. Reinhart released a technical opinion in 2015 on the rigorous direct sunlight requirement in LEED v4, advocating the use of direct sunlight criteria only in job areas that require greater management of direct sun incidence [41].

LEED 4.1 provides points for good vistas, good interior illumination, and enough daylighting (2.7%). Table 2, LEED 4.1, is advanced in terms of daylight metrics: Spatial Daylight Autonomy (sDA) and Annual Sunlight Exposure (ASE).

Table 2. Daylight and visual comfort specified by LEED 4.1

LEED 4.1	
Glare measure and control	✔
Lightning contractibility	✔
View out	✔
Internal and external lighting	✔
Daylight factor (DF)	✔
Illuminance level	✔
Daylight Autonomy	✔
Spatial Daylight Autonomy (sDA)	The minimum value for visual comfort
Annual Sunlight Exposure (ASE)	The maximum value for visual comfort

2.6.1. Daylight Factor (DF)

The daylight factor (DF) is one of the most well-known static indicators for measuring the amount of light in space. DF was introduced in 1892 by Trotter. Its value equals the ratio between the brightness inside the space and the brightness outside the space in an unobstructed environment under cloudy sky conditions [42]. The DF can be expressed as:

$$DF = \frac{E_{indoor}}{E_{outdoor}} [\%]$$

Equation 7. Daylight Factor (DF)

The thresholds suggested for DF are between 2% and 5%, where 5% or more represent daylight interiors substantially, and 2% or less characterize that electric lighting is likely to be used [43]. It is worth mentioning that one of the most significant limitations of this metric is excluding direct sunlight. The direct sunlight's impact on both illuminances must be considered separately and is omitted. The higher the DF, the more natural light is available in the room.

2.6.2. Spatial Daylight Autonomy (sDA)

A daylight metric called Spatial Daylight Autonomy is a daylight metric created for a more precise measurement to guide designers to attain the sufficiency of daylight illuminance across a space, by including the internal daylighting distribution rather than an average daylight level.

It specifies the proportion of each analysis grid that has investigated region that satisfies a minimum daylight illuminance level during a certain fraction of the operational hours each year (50 percent regarding IES- LM-83-12). The minimum illuminance is often specified based on the room type: office, education, healthcare, or another. For example, If the investigated room is an office, the minimum illuminance according to the standard EN 12464-1: lighting and illumination of workplaces are set to 500 lux on the work zone (Figure 2). The IES-LM-83-12, on the other hand, has a threshold of 300 lux.

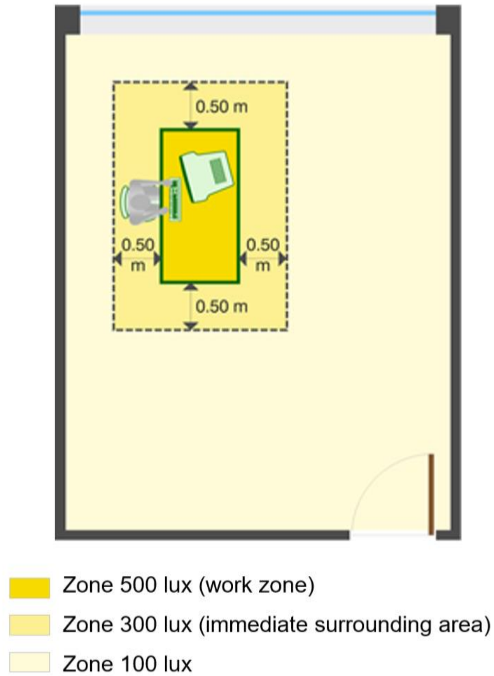

Figure 2. The minimum required illuminance in an office room [25]

This dynamic daylight meter (sDA) is based on hourly measurements using either manual or electrically controlled window blinds, which are adjusted depending on the quantity of direct sunlight that flows through windows into space to preserve visual comfort. The blinds open and closed following the IES LM-83-12 suggestion; when more than 2% of the analysis grid points get 1000 lux or more (direct sunlight), blinds will close simultaneously for each window group until fewer than 2% receive direct sunlight.

As specified in the option 1: LEED v4.1 Daylight and Quality Views Calculator, LEED specifies a 300 lux requirement for 50 percent of yearly sunshine hours over a percentage of the occupied space. The $sDA_{300/50}$ percent value is 75 percent, 3 points are awarded, 55% for two points, and 40 percent for one point [44].

Table 3. Three points for daylight floor area: The average Spatial daylight autonomy $sDA_{300/50\%}$ [44].

	New construction, Data center, Schools, Warehouses, and Hospitals	Healthcare
sDA (for regularly occupied floor area) at least:	Points	Points
40%	1	1
55%	2	2
75%	3	Exemplary performance
Each regularly occupied space achieves $sDA_{300/50\%}$ value of at least 55%	Exemplary performance or one additional point if only 1 or 2 points are achieved above.	Exemplary performance or one additional point if only 1 point is achieved above.

Figure 3 shows that 65 percent of the surface of a working plan on a level of 0.76m obtains a minimum illuminance value, which in this case is 300 lux, throughout at least 50 percent of the total yearly operational hours from 8:00 to 18:00 [45].

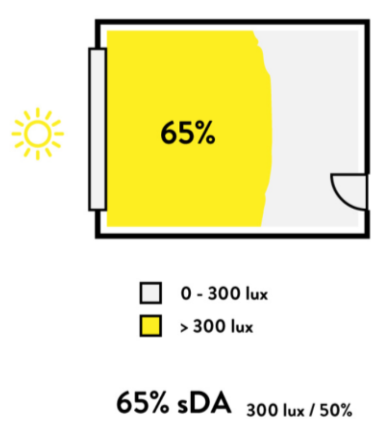

Figure 3. An example of sDA

It is represented by the following:

sDA 50% > 300 lux (8:00-18:00)

The sDA300lux/50%= 65% ; hence, in LEED v4.1, this number exceeds the permitted threshold for enough daylight.

2.6.3. Annual Sunlight Exposure (ASE)

It was introduced in 2012 by Illuminating Engineering Society [45]. The ASE metric looks at direct sunlight as a potential source of visual discomfort, measuring the percentage of floor area that exceeds a specified direct sunlight illuminance level for a specified number of hours. By means of ASE, the visual discomfort and potential overheating problem can be investigated at the same time.

The IES recommends a relative value with smaller sunlit regions exposed to no more than 1000 lux of direct sun for more than 250 hours per year. Even though there is no obvious cutoff point for this statistic, the standard states that it is based on supporting research by Mardaljevic et al. [46], 10% or more areas result in unsatisfactory visual comfort, 7% neutral, and 3% acceptable spaces.

Figure 2-4 illustrates that 8 percent of the surface of a working plan on a level of 0.76m gets daylight over the maximum recommended illuminance value, which is 1000 lux, during more than 250 hours of the total yearly operational hours from 8:00 to 18:00.

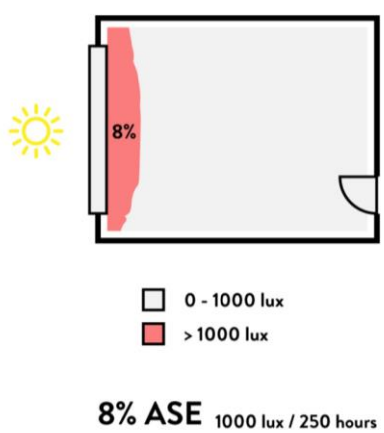

Figure 4. An example of ASE

It is represented by the following:

ASE 8% > 1000 lux (8:00-18:00)

The ASE1000ux/250h ratio is 8%. This number falls below the permitted level for visual comfort in LEED v4.1, less than 10%.

In addition to the thresholds recommended, the IES simulation method is used to calculate ASE before operable shades are deployed to block direct sunlight. The LM-83-12 document recognizes that the ASE metric does not address other sources of glare besides direct sunlight [45].

2.7. Adaptive façade classification

Over the last decades, there has been an increase in novel building exterior materials and façade components. Façades serve numerous duties as mediators between the external and inside of a structure, all of which impact its performance [47]. These revolutionary building envelopes strive to increase energy efficiency, tenant comfort, health, and environmental effect [48]. These are dynamic building envelopes that can adjust to changing boundary circumstances. They are also known as adaptive façades. These unique building façades can adjust to outside climatic circumstances and dynamic occupant requirements, ensuring step-change advancement in energy performance. The terms "dynamic" or "adaptive" relate to a façade's ability to benefit from or respond to boundary circumstances in order to increase performance and occupant demands [49]. These systems can be built on-site or prefabricated and preassembled. This term is consistent with EU COST Action TU1403 " Adaptive Façades Network " [50]. This Action's goals are to define adaptable façades and to share technological expertise at the European level.

Several technologies are now available on the market, while others are still in the testing stage. In this context, it is critical to provide an overview of these technologies, according to various frameworks and review research [48,51–53]. The products or kinds of dynamic envelopes existing are provided in the sections that follow. The goal of COST Action TU 1403 was to establish a generic framework, standardized methodology, and tools for quantitatively evaluating the performance of adaptable façades. The book brings together the research and experience of numerous European experts to propose a standardized strategy that can facilitate the integration of adaptable façades in buildings. According to them, switchable glazing, dynamic solar shading, dynamic insulation, and 12 multipurpose façades are the most promising adaptive façades for buildings [50]. According to these sources, there appear to be four primary families of dynamic building envelopes:

- Switchable windows
- Movable shading devices
- Solar active façades
- Active ventilative façades

2.7.1. Solar active façades

Solar active façade is one of the adaptive façade families that this study mainly deals with this class of façade. As the name implies, active solar technologies are implemented with the assistance of the sun. They influence thermal comfort and energy savings in addition to managing solar gain and the amount of daylight. Their performance depends entirely on chemical, physical, and biological reactions between materials and the light and temperature changes [51]. With the help of in-depth experts' specialists, categorize four technologies in this family type:

- Double-skin façades
- Green roofs and façades
- Building-integrated photovoltaics
- Phase change materials

This thesis mainly focused on the evaluation of double skin façade on daylighting and glare. Therefore, in the following section, double skin facades are presented.

2.7.1.1. Double-skin façade

The Double Skin Façade (DSF) is a glazed system with two glazed surfaces, known as skins, and a large air cavity between the two skins. In contrast to a triple-glazed window, the DSF may install shielding devices inside the cavity and even manage airflow via moveable vents generally located at the top and bottom of the window. Double-skin façades have been employed to maximize the quantity of light and heat intake into the structure. Typically, roller blinds or other shading devices are fitted between the two levels to manage daylight.

Various double-skin facades (DSFs) have been created and installed in both new and renovated structures. A DSF typically has a hardened single-glazed pane on the exterior and an insulated double-glazed unit on the inside [54–56]. Solar-control glazing and clear low-emissivity (low-E) coatings can also be employed [57,58]. The air in the cavity between the two skins can be vented naturally or mechanically, and the width of the cavity can range from 0.20 m to more than 2 m [59]. The DSF system might vary based on the configuration of the air cavity sections. The shaft-box window, the corridor façade, the multi-story DSF, and the box-window façade are all variations. Figure 5 presents an example of DSF in non-residential buildings.

Figure 5. The example of DSF; Eurotheum DSF, Germany. From the left: The face; DSF interior; Shading devices [60]

The glass of DSF buildings' windows has varying Thermal transmittance (U-value) and light transmittance. These values are often chosen from commercially available materials that are regularly utilized in office buildings to provide adequate quantities of daylight. The light transmittance for both interior and exterior windows is estimated to be 0.76 for modeling purposes, with the profile's U-value considered to be 1.8 W/m^2 K [58].

Analyzing the DSF has allowed us to list positive and negative feedback regarding this technological solution, concerning where it was built and how it was created. A DSF system has advantages and disadvantages compared with a standard facade window. The advantages include good acoustics, ideal thermal insulation, and wind pressure effect reduction. Meanwhile, the disadvantages involve high cost, lack of fire safety information, and reduced available space.

From the literature can be found that daylighting received less attention compared with other strategies applied in existing DSF buildings, although DSF systems admit daylight into buildings without causing glare.

Daylighting solutions include increasing daylight and reducing heat input. One of the essential ways to increase facade performance is using a shade system. Researchers, architects, and engineers have extensively studied the uses of various shade systems, such as Venetian blinds, roller blinds, overhangs [61,62]. Typically, roller blinds or other shading devices are fitted between the skins to manage daylight [63].

2.8. Movable shading devices

Building facades are expected to be multifunctional in today's world, such as dynamic shading devices are technologies capable of meeting these high-performance demands. Examples are Venetian blinds, prismatic film, glass frits, louvers, and many other items. These kinds of technologies can be static or dynamically controlled depending on the strategies chosen. Several studies have shown that such shadings can reduce glare and improve visual comfort [64].

- Passive that is static shading devices and included fixed or manually adjustable. Their improvement is based on a parametric study.

- Active that gathers the motorized and automated or dynamic shading devices. It primarily means simple motion mode.
- Hybrid that maintains biomimetic-based systems (shape morphing skin). A control method must be established for them, which could be intrinsic or extrinsic, using actuators in the case of switchable glazing [52].
- Photovoltaic panels that are integrated into the structure [64].

Because they incorporate a control approach, active, hybrid shading devices and integrated photovoltaic panels are considered intelligent technologies. Internal, mid-pane, or external shade devices are some options.

Shading is an essential aspect of fenestration system design for commercial and office buildings until a balance is reached between the necessity for daylighting and the need to limit solar gains. Motorized shading systems are more sophisticated in terms of adjutancy than adjustable shading devices since they operate using electrical motors. In comparison to models with simple geometries, their design is constrained, despite their more sophisticated construction. However, because of the motorized aspect, it has been demonstrated that occupants adjust the shade devices more frequently to their needs, improving the thermal and visual comforts. In any case, it is entirely dependent on the user's actions. Commonly, motorized shadings are used in DSF [65].

2.9. Daylight simulation software

2.9.1. Simulation tools

The usage of simulation tools has risen dramatically over the last two decades. The changing compliance requirements of codes and standards have led to the broad acceptance of computer modeling [66]. When a building is in the design stage, design teams and consultants frequently employ simulation tools to examine visual comfort and glare daylighting metrics. Therefore, this section aims to review to identify cutting-edge simulation tools utilized by construction project design teams in the early design stages of the project to help the decision-making process. This study's major goal is to review for identifying cutting-edge simulation tools utilized by construction project design teams in the project's early design stages to help the decision-making process.

2.9.1.1. RADIANCE

The RADIANCE was introduced in 1994 [67]. RADIANCE helps experts conduct advanced calculation techniques in most daylighting simulation software in existence. As the Radiance is a command-line-based program, it requires high expertise to be used while at the same time providing higher control over the parameters. This program is open-source software, and it has been validated many times, presenting high accuracy results for different sky conditions, overcast and clear sky [68,69]. The inputs in Radiance include geometry, materials, date, time, and sky conditions. Images, numerical values, or contour plots of Radiance such as luminance and color, irradiance, and glare indices are some of the results of RADIANCE. It also can provide complex fenestration systems (CFS) and automated shading systems. Direct, specular indirect, and diffuse indirect components are three main simulation methods in RADIANCE computing with a combined Monte Carlo and deterministic ray-tracing algorithm. The method consists of tracing light rays from a viewpoint backward to the lighting sources.

2.9.1.2. DAYSIM

DAYSIM is a verified command-line-based software explicitly developed to perform annual daylighting calculations [70]. It combines RADIANCE a backward ray-tracing algorithm with the Daylight Coefficient approach [71] and the Perez “all-weather sky model” for computing hourly illuminance values during a year [72]. The Standard Daylight Coefficient approach uses a discretized sky to simulate a continuous sky specified by the Perez all-weather sky model. Grasshopper, Rhinoceros, Sketchup, and Ecotect are some of the interfaces of DAYSIM. The outputs include a range of climate-based daylighting metrics (e.g. DA, UDI, and annual DGP), hourly occupancy and blind use schedules, and electric lighting loads that can communicate with EnergyPlus and other energy modeling software. DAYSIM can compute automated shading systems and complex fenestration systems (CFS) [73].

2.9.1.3. DIVA

Design Iterate Validate Adapt (DIVA) is a Rhinoceros and grasshopper plug-in and a user-friendly interface for the RADIANCE and DAYSIM engines [74]. It was developed ad in 2009 and 2011 by the Graduate School of Design at Harvard University an add-on for the 3D-Cad modeler Rhinosceros, and it is administered by Solemma LLC [75]. A weather file, materials defined by RADIANCE parameters, sensor grid points are inputs and three main groups of simulations: "daylight images," "daylight grid-based," and "thermal single-zone." DIVA utilizes RADIANCE backward ray-tracing for calculation Daylight Factor and scene visualizations under CIE overcast or clear skies, and DAYSIM to calculate annual-climate based metrics. Daylight performance metrics like point-in-time and annual-climate-based are the output of DIVA, which automatically loaded into the Rhinoceros scene with color mapping or exported to WXfalsecolor for rendering image results. Other outputs include hourly occupancy schedules, dynamic shading schedules, and electric lighting loads used in EnergyPlus for energy modeling analysis [74].

2.9.1.4. Grasshopper, Ladybug and Honeybee

Grasshopper is a graphical algorithm and a plug-in for Rhinoceros providing parametric design generation. It is an interface for DIVA providing advanced control over the parameters of RADIANCE and DAYSIM scripts. There are two open-source plug-ins for daylighting and energy analysis: Ladybug and Honeybee in Grasshopper [76]. Ladybug relies heavily on weather data files. LB may analyze and visualize several diagrams in 2D or 3D by importing an EnergyPlus Weather file (.epw), such as radiation-rose, sun-path, or execute radiation analysis. It offers the advantage of assisting designers in the design decision-making process, particularly during the early stages [77]. However, Honeybee is a Grasshopper plugin that uses Ladybug's climatic weather file. In terms of obtaining more sophisticated investigations, the Honeybee plugin is used. It can be used to simulate indoor or outdoor comfort, lighting, daylighting, or energy. Honeybee uses EnergyPlus, Radiance, Daysim, and OpenStudio energy and daylighting simulation features in Grasshopper [78]. The Honeybee plugin allows progress from early analysis to more extensive and advanced analysis [77].

2.9.1.5. Evalglare

Evalglare is a RADIANCE and command-line-based program to evaluate glare sources and calculate DGP using 180-degree fish-eye images. The program was developed based on the glare prediction model developed by Wienold and Christoffersen [10]. The horizontal and vertical angles (-vh –vv) are inputs, measured vertical illuminance (-i), and a 180-degree fish-eye image. The output "-c frame" detected color glare sources looking at each image pixel to calculate the average luminance coloring the pixels that exceed this threshold with glare source color. The Evalglare provides results related to DGP and other glare indexes.

2.9.1.6. WXFalseColor and HDRScope

HDRScope and WXFalseColor are two interfaces using RADIANCE for HDR image processing and lighting analysis. This software allows for displaying Radiance RGBE images and luminance values in lux in an interactive environment. HDRScope was developed by Kumaragurubaran and Inanici [79] at the University of Washington, and WXFalseColor was developed and is maintained by Bleicher [80].

2.10. Daylight simulation inputs

Generally, daylighting models need to have three fundamental parameters: geometry, material properties, and light sources like sun and sky distributions. However, the new modeling applications had provided extensive features to create three-dimensional geometries; there are still many complexities regarding material properties [66].

Material specifications and characteristics can have a simplistic application, such as diffusing reflectance and transmittance, or more accurate approaches such as material specularity. In terms of having more accurate computation of complex material properties like translucent panels, curved reflective blinds, and prismatic films, simulation models use bi-directional scattering distribution functions (BSDF). BSDF includes both bi-directional transmittance distribution function (BTDF) and bi-directional reflectance distribution function (BRDF) [81]. BRDF function can predict diffuse, directional, and specular materials by computation of the wavelength, surface roughness, incoming and outgoing light direction [82]. These calculations were first developed in laboratory testing of actual material properties and became available in simulation programs.

Another critical parameter for daylighting simulation is Light sources. Simulation software defines daylight as a light source and calculates the sun's position concerning a skydome model where sun rays are diffusely or directly distributed. Although the sun's position is calculated based on the latitude and longitude of the case study, the sky condition (e.g., clear, intermediate, and overcast skies) is hard to predict [71]. Therefore, daylight coefficients are used to estimate daylight distribution for various sky conditions. The common sky models for simulation tools are as follow:

CIE sky model, developed by the International Commission of Illumination. CIE sky models are generic models predicting three sky conditions: clear, intermediate, and overcast [83]. These sky models can be created utilizing the "*gensky*" command in the RADIANCE software with a zenith irradiance (-*B*) and solar radiance (-*R*) inputs that can be calculated from horizontal direct and diffuse irradiance.

Perez All-Weather sky model is another most commonly used sky in simulations. Perez All-Weather sky model is an algorithm able to represent any type of sky condition based on direct and diffuse irradiance and is commonly used for annual daylighting simulations [72]. Perez All-Weather skies are also available in RADIANCE and can be constructed through the command "*gendaylit*" and using horizontal direct irradiance and horizontal diffuse irradiance (-*W*) input values.

Image-based sky model is a site-specific model based on high dynamic range (HDR) photographs of the skydome of a specific location [84]. This sky model can accurately anticipate the luminance distribution at the site, including the influence of the surrounding environment, such as buildings and threes. The photograph pixels inform the luminance through an Image-Based Rendering technique used in the simulated environment.

Ubbelohde and Humann [85], investigated four lighting simulation tools and found that the sky inputs were one of the most impactful parameters over the daylighting simulation results. The study results showed that RADIANCE and Lightscape provided more detailed inputs for sky models and could yield results close to actual measurements.

2.11. Daylight Simulation methodologies

The four currently calculation approaches in simulation tools are as follow:

1. direct calculations, including physical equations like the lumen method.

2. Ray tracing approach, which is a scene-dependent algorithm that computes direct illumination, specular surfaces, and reflections by tracing rays from the light source to the observer's eye (forward ray tracing) and from the observer's eye to the light source (backward ray tracing) or both ways [86].

3. Radiosity algorithm determines radiometric values to surfaces in the scene, independent of view, to calculate heat transfer [87].

Deterministic and the Monte Carlo methods are two common approaches for assessment ray tracing and radiosity simulation algorithms.

Figure 6 depicts the schematic of three major lighting simulation tools algorithms.

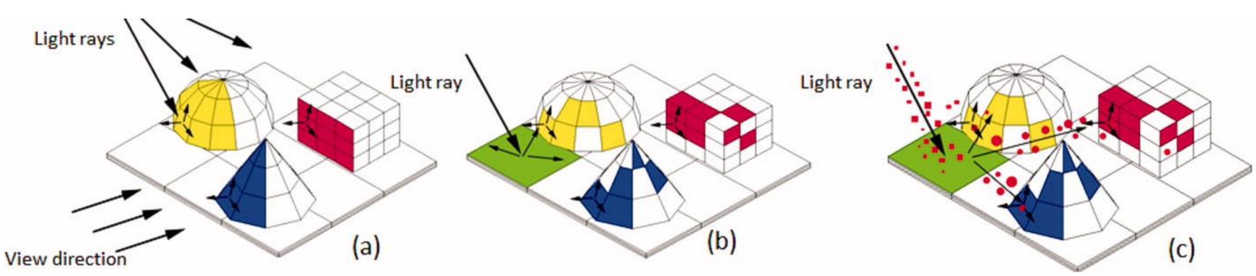

Figure 6. (a) Ray tracing, (b) radiosity and (c) photon map [66]

Ward et al. [88] introduced the Bidirectional Scattering Distribution Functions (BSDF) for RADIANCE. McNeil and Lee [89] validated the RADIANCE three-phase method of BSDF, and this method was groundbreaking to speeding annual simulations of complex fenestration systems (CFS) in daylighting models. In 2008, a five-phase method for dynamic daylighting simulations was introduced by Bourgeois et al. [90] to render BSDF more precise. BSDF can be measured in a laboratory or computed with Window7 software [91] and RADIANCE.

3. Methodology

In this chapter, different steps of the methodology were explained. Based on research questions, as previously mentioned in chapter one, were as follow:

RQ1. Which simulation tools are more accurate and capable in terms of glare analysis?

RQ2. How can glare analyses be simplified through doing annual glare analysis instead of point-in-time glare analysis?

RQ3. What is the correspondence degree between the annual glare analysis and point-in-time analysis?

In order to answer the research questions, first, using the literature review, the glare and daylight were evaluated, and indicators were selected. Then, a test located on the roof of the Politecnico di Torino University, DSF, was selected as a case study to examine the conditions of visual comfort experimentally. After that, since field measurements of daylight levels throughout the year are costly and time-consuming, the simulation results after validation with actual data were used to analyze annual glare. The 3D models conducted in Rhino were then created in Grasshopper, which is a plug-in for Rhinoceros 3D. The model was created to be the same size as the actual conditions of the DSF, and the simulation was performed using the Diva in Rhino and Honeybee tool in the Grasshopper. The Honeybee environment supports a set of performance evaluations using validated tools such as Radiance. The software uses the Radiance engine to visualize lighting conditions, the Daysim engine to evaluate climate-based metrics and annual maps, and the Evalglare engine for glare analysis, and is capable of simultaneously evaluating dynamic criteria. The support of various reputable daylight evaluation engines from Honeybee confirms the validity of this software in simulation. Critical glare hours were also obtained through the Ladybug plug-in in the Grasshopper environment.

3.1. Description of the research methods

This research was based on empirical research and a quantitative method, depending on the measurement, modeling a case study, and investigating simulations of different scenarios. To this end, a case study, TWIN cell with double skin façade located at the roof of Politecnico Di Torino, has been selected. The meteorological data were gathered from EnergyPlus weather data for Torino city. Observation, simulation, measurement, and documentation study were used for collecting the data. The final results of the simulation have been validated through a comparison of the actual data measured on-site. Finally, the results have been evaluated with a comparative study to understand the correlations between results.

The structure was divided into five main steps, starting with modeling and ending with evaluating the results. The simplified workflow of this research is illustrated in Figure 7 and is described in the following sections.

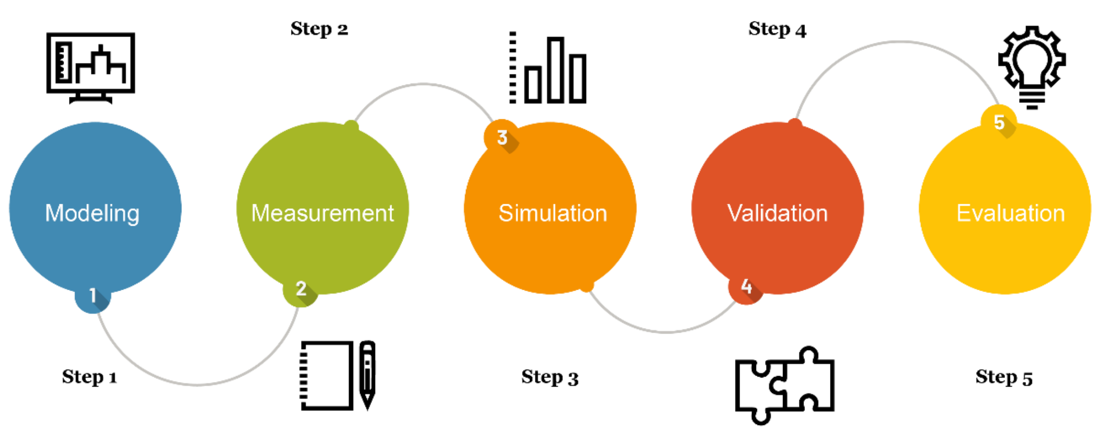

Figure 7. The thesis workflow

3.2. Conceptual study framework

The methodology of this thesis consists of 5 steps, as can be seen in *Figure 8*.

Step 1 of the thesis methodology was data collection. After selecting the DSF as a case study for this research, EnergyPlus Weather File (EPW) related to Torino has been used as meteorological data. The modeling based on the data related to geometrical and optical information of DSF has been done in Rhino. At the measurements stage, different types of measurements have been taken. The light reflectance properties of the materials used as finishing in DSF has been measured through a contact spectrophotometer: the Konica Minolta CM-2600d was used for the purpose. Then, horizontal and vertical illuminance has been captured via illuminance meter sensors located at the middle of the test cell. For glare analysis and creating the actual sky condition, Global Horizontal Irradiance (GHI) and Diffuse Horizontal Irradiance (DHI) were measured by different Pyranometers positioned outside the facility. After that, the luminance condition of interior surfaces was captured in different points employing an HDR camera (Canon EOS D650), that provided luminance maps. The TehcnoTeam LMK advanced mobile camera was used for the purpose. The detailed information regarding the instruments utilized for the measurements and the measurements are described in the following subsections. Six points in the test cells have been selected for illuminance and glare evaluation in Diva for Rhino and Honey bee for Grasshopper. Three of these points were perpendicular to the window. The other three points have a 45-degree view direction toward the window. Three scenarios have been developed to test the effect of Venetian blind on daylighting and glare. Scenarios one were performed with the Venetian blind up, and scenarios two and three were performed with the Venetian blind drawn with slat tilt angles of 0° and 30°, respectively.

At the simulation data set stage, all the gathered information has been simulated through different simulation software programs. The illuminance, glare occurrence, daylight quality was simulated in this study. In Grasshopper and Diva for Rhino, Honeybee simulates the horizontal and vertical illuminances at each reference point. For glare analysis, point-in-time discomfort glare probability and annual discomfort glare probability has been assessed through Honeybee and Diva. Then the results of both software were compared. After that, the results were compared to the actual glare measurements in the test cell through an HDR camera at reference points. The images' luminance map and $DGP_{point-in-time}$ amount have been compared with simulation results to validate the model.

After model validation, the simulation has been done for 8 days in a year and four times on each selected day. Then the results of the DGP_{annual} and $DGP_{point-in-time}$ were compared and evaluated to define their correlations. In the end, some recommendations were provided for doing the DGP_{annual} instead of $DGP_{point-in-time}$, as it was the main purpose of this study.

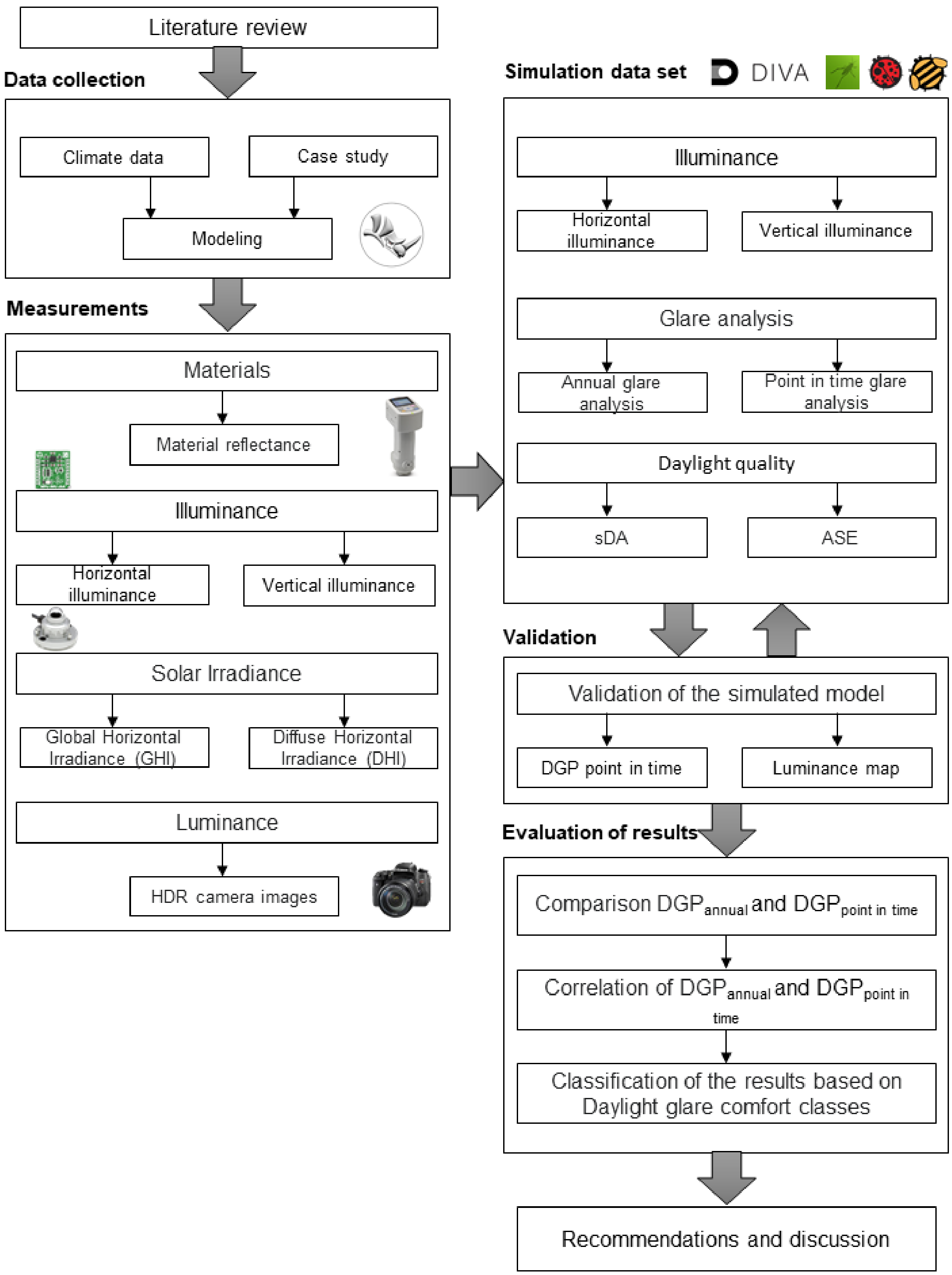

Figure 8. Conceptual study framework

3.3. Methods and model description

Since field measurement of daylight levels is costly and time-consuming throughout the year, simulation results were used to analyze the visual comfort of spaces in this study. 3D models are created in Rhino software with the same size as the real condition of the DSF test cell (Figure 9).

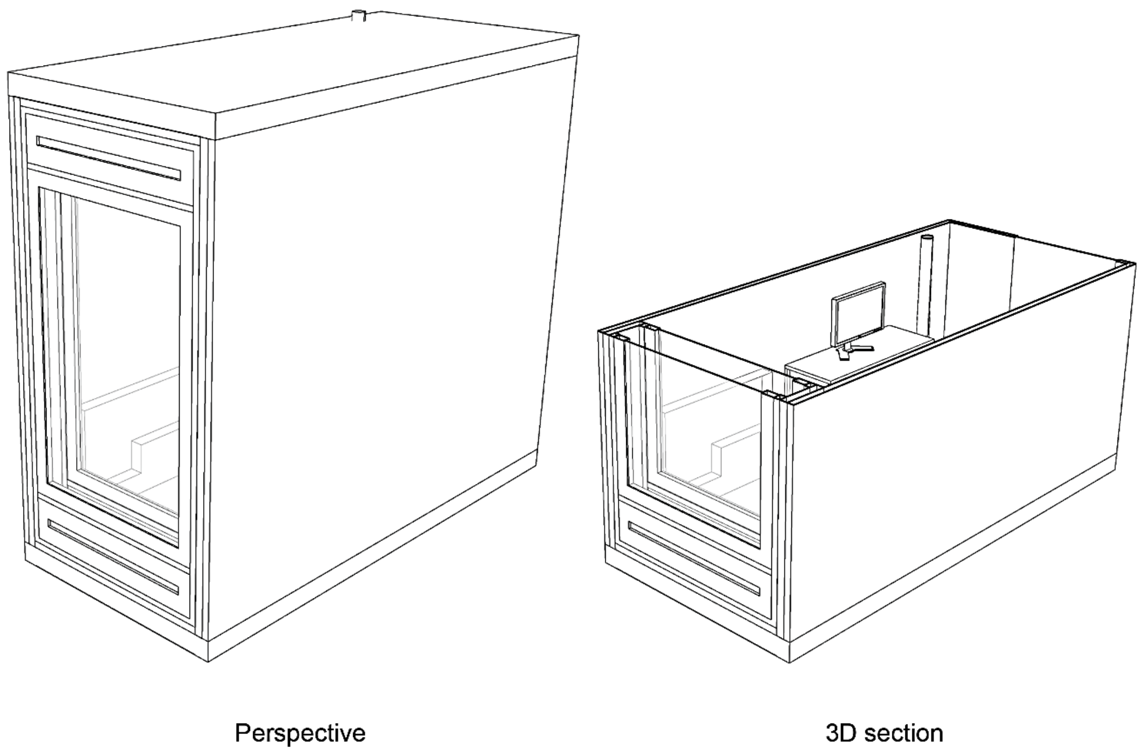

Figure 9. simulation model geometry

The simulation was performed using RADIANCE via the Diva plug-in version 6. The DIVA supports a set of performance evaluations using validated tools such as Radiance. In order to calculate the indicators of daylight autonomy and annual penetration of sunlight.

Researchers in several studies have confirmed the validity of Diva software. In a study by Suk and Schiler [33], the validity of Diva software was evaluated by measuring the ambient brightness by luminance meter and comparing it with the simulation results by the software. The simulation software approved the results. In a similar study, Mirinen et al. [92], comparing field results and simulation results, considered this software valid for daylight simulations. Bian and Ma [93] for investigating the effect of time on visual comfort, conducted a study based on people's mental evaluation and simulation. In their research, they examined the reliability and validity of Diva software.

Also, the same 3D models in the Grasshopper, a plug-in for Rhinoceros, have been created for comparison with DIVA results. Simulations were implemented using the Honeybee tool in the Grasshopper. Honeybee supports a set of performance evaluations using validated tools such as RADIANCE. The software uses the RADIANCE engine to visualize lighting conditions. The Daysim engine evaluates climate-based metrics and annual analysis and simultaneously evaluates dynamic and static criteria. The primary use of Daysim is to simulate the annual brightness using weather data. The main difference is speeding up the calculations relative to the RADIANCE by simplifying the skydome and limiting the number of Ray-tracing. Another difference between this two software is the existence of an algorithm to predict the behavior of residents and their performance in the face of receiving daylight. The Evalglare engine is used for glare analysis. The support of various reputable Honeybee daylight evaluation engines confirms the software's credibility in the simulation. Critical glare hours were also obtained through the Ladybug plug-in in the Grasshopper environment.

3.3.1. Simulation model inputs

The main inputs of the software are the space geometry, the reflection coefficient of the surfaces, and the light transmission coefficient of the windows. In addition, the results obtained from the RADIANCE depend on the determination of Ambient edgy values, where Ambient bounce indicates the number of reflections between surfaces, and Ambient division and Ambient sampling indicates the number of ambient super-samples. Ambient resolution determines the control of maximum error, evaluation of the direction, and endpoints of sampling. The RADIANCE parameters used in this study are based on the values recommended in the standard of IES LM-83-12 [94].

To evaluate the daylight situation using sDA, UDI, and DF indices, a 10 by 10 cm grid of sensors was used, located over the desk level (80 cm above the floor), and simulations have been performed.

For glare and illuminance analyses, six reference points have been considered in the test cell. Three scenarios have been developed to test the effect of Venetian blinds on daylighting and glare. Scenarios one and two were performed with the Venetian blind lifted, and scenarios three and four were performed with the Venetian blind drawn with slat tilt angles of 0° and 30°, respectively. As illustrated in Figure 10, points were located with different distance and view directions to the window surface. Point A was the farthest point from the window, with 3.35 m distant from the window. Point B is located at 1.75m from the window, which is also the middle of the cell (the same position as the illuminance sensors). Point C was located close to the window surface, exactly 0.5 m to the window. Points A, B, and C have a 0-degree view direction while A', B', and C' look to the window with a 45-degree angle. These points were located at the occupants' eye level (1.2m) looking to the window.

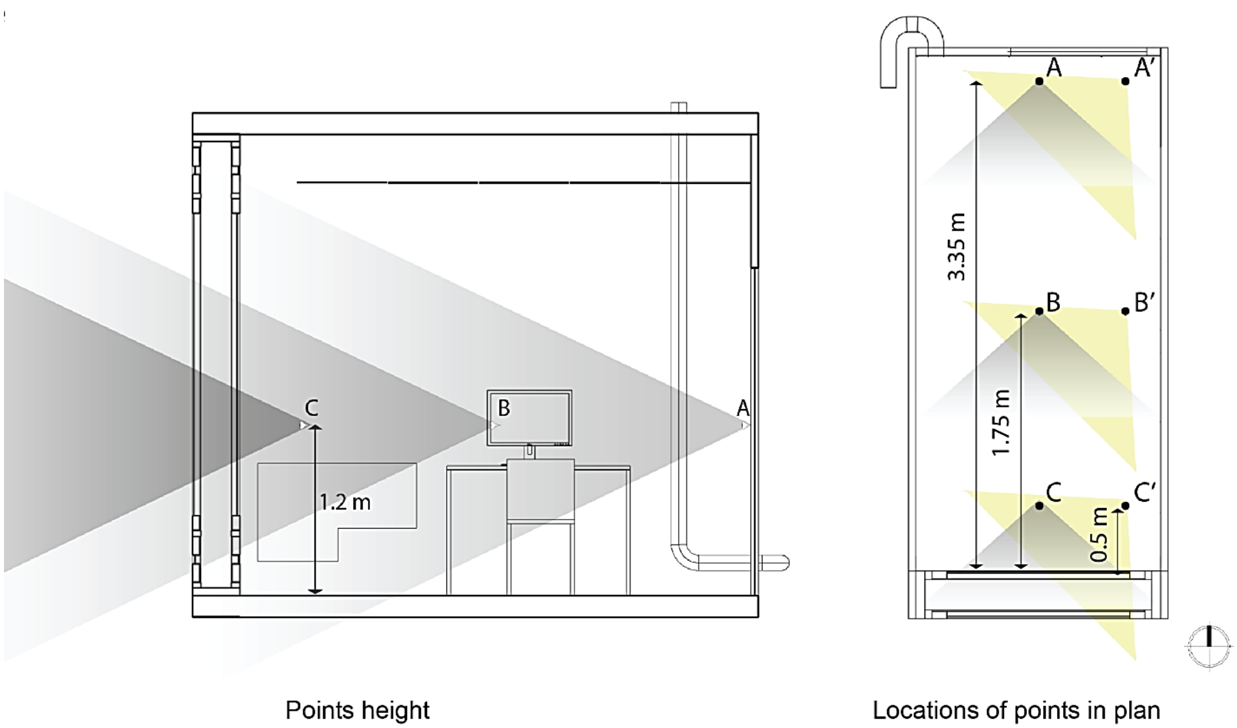

Figure 10. Location of reference points in DSF plan and section

Total hours of a year were considered for annual simulation, while March, June, September, and December were selected for point-in-time simulations. For the comprehensive evaluation, different days in these months were analyzed. March 21 and September 21 were selected as equinoxes and June 21 and December 21 as summer and winter solstice, respectively. One more day close to these days with different sky conditions was selected based on the sky condition (from the EPW file) to better understand the daylight and glare conditions. For example, if December 21 was overcast, another sunny day close to this date has also been selected and simulated. 9.00 a.m,12.00 p.m, 3.00 p.m, and 6.00 p.m. for each day has been simulated.

In general, all simulations have been conducted in three different conditions (scenario) regarding shading devices. The first scenario is the condition of the test cell without Venetian blind. The second scenario was when the Venetian blind was pulled down, and the blind slats had a 0-degree angle. The last scenario was for the Venetian blind with a 30-degree angle.

Summary

This research employed simulation tools such as DIVA-for-Rhino, Honeybee, and Ladybug in Grasshopper and RADIANCE command lines. Other computer programs, including Lmk LabSoft, HDRScope, WXFalseColor, and Evalglare, were utilized to examine the glare in the HDR photos. The use of these tools is briefly discussed in the following subsections.

3.4. Experimental characterization

3.4.1. Double skin façade test cell

The case under study is the DSF installed in the TWINS (Testing Window Innovative System) cell, located on the roof of the Energy Department of the Politecnico di Torino (Figure 11). The cell has internal dimensions 1.6m x 3.5 m x 3.00 m; these dimensions are not random as they are inspired by the dimensions of the facades used for buildings such as offices (Figure 12).

Figure 11. The DSF test cell

The DSF under analysis was developed with the aim of maximizing the flexibility of the facade, in particular the facade under analysis consists of two parallel double glazing, which are identified as the skins of the facade; these skins are identical and possess an aluminum frame system. Each skin of the facade extends in width by 1.22 m in height by 2 m and is composed of a Double Glass Unit (DGU), composed by two glasses with a unitary thickness of 6 mm and a low-emissivity coating on the internal surface of the interspace between the two glasses of the DGU, this cavity is 16 mm thick and is filled with a mixture of 90% Argon and air. The two parallel skins form a 25 cm air cavity, which contains 4 fans in the upper part, which will be called "fans", directed vertically at a height of 2.6 m and which achieve a nominal flow rate of 220 m^3/h. The façade has four openings, called "vents", which allow the control of the air flow between the internal and external environment and have a width of 1.5 m and a height of 0.5 m.

In the cavity at a height of 2.6 m there is a "Venetian blind" type curtain, which through the use of an incorporated actuator allows you to control both the inclination angle of the slats and the descent of the curtain. When the awning is fully extended, the lower part is at a height of 40 cm and the awning has a length of 2.2 m, it is 3.5 cm laterally from the cavity wall while on the right side it is in contact. The motorized Venetian blind of the DSF was located between the cavity of the façade skins. The dimension of the is 3cm and can be controlled automatically with the system in the DSF

It consists entirely of opaque components, except for the south-facing facade on which the Double Skin Facade, object of study, is installed and is in conditions of non-shading from external elements. There is a door to access the cell in the north facade. Furthermore, the cell is mounted on a metal structure that raises it from the ground by 14 cm.

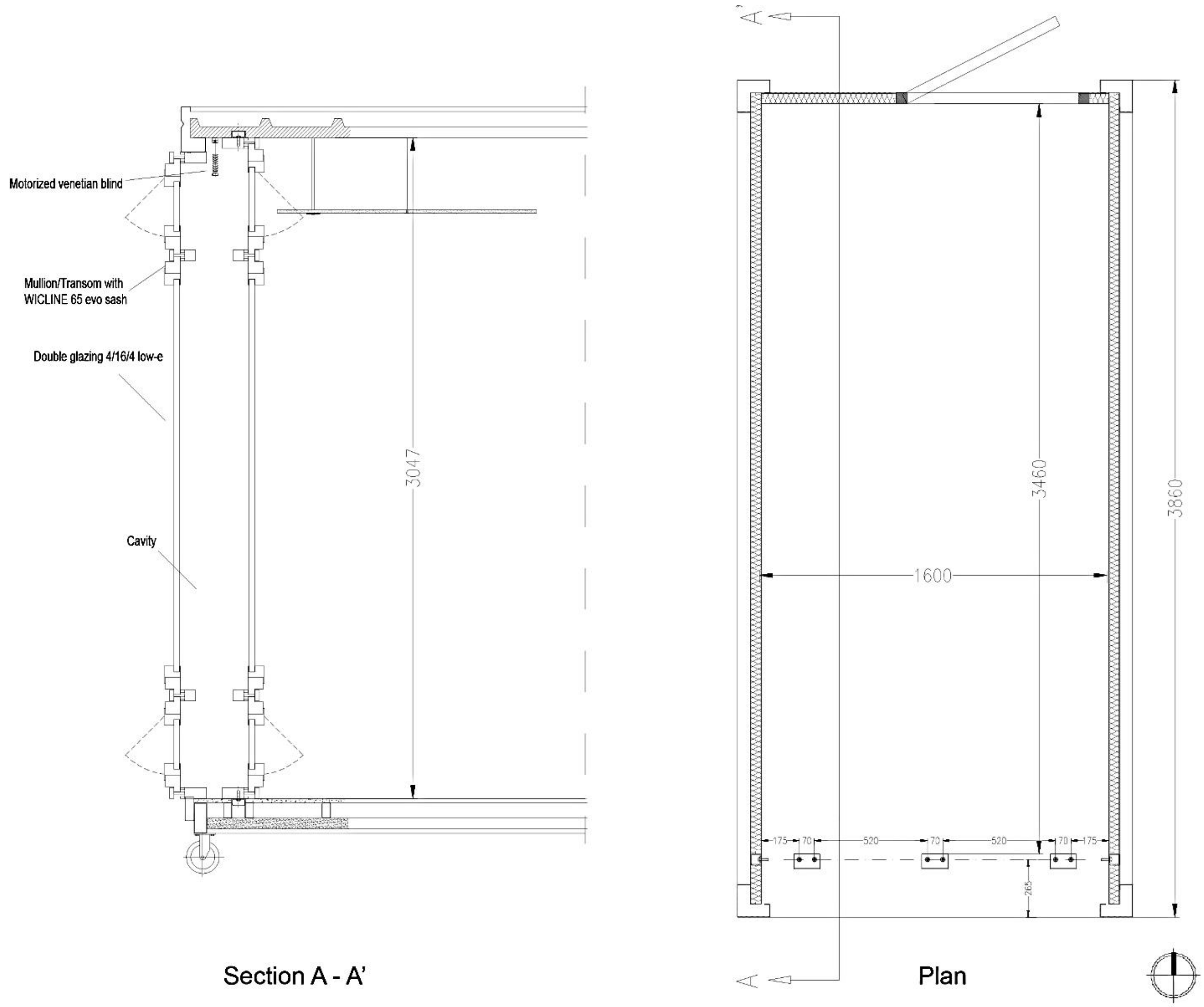

Figure 12. Technical drawings of the DSF

The ceiling and the cell walls are formed by sandwich panels of 48 mm, with double steel sheet and polyurethane foam, while the floor has been added a layer of linoleum to the sandwich panel.

3.4.1.1. Opaque components

The previous thesis carried out the experimental characterization of the cell [95,96]. From their works, the transmittances of the opaque walls were obtained. The frame of the DSF and the vent dampers are made of aluminum in both skins. The experimental characterization of the opaque components in the same test cell was carried out. The results obtained are reported below (Table 4):

Table 4. U-value of opaque components in DSF

Opaque component	U [W/m²K]
West wall	0.42
East wall	0.48
North Face	0.48
Ceiling	0.49
Floor	0.7
Door	0.53

3.4.1.2. Transparent components

The south-facing facade only has a glass window with a double glazing unit (DGU) and a low-emission film. In more detail, the DGU consists of:

- Clearlite_33_2 thickness 6.5 mm
- Air 10% / Argon 90% thickness 16 mm
- iTop_33_2 thickness 6.5 mm

The detailed information on the glazing components is presented in Table 5.

Table 5. The detailed information regarding the window

Tvis	**0.774**
Rfvis	0.123
Rbvis	0.13
Tsol	0.449
Rfsol	0.268
Rbsol	0.226
Abs1	0.172
Abs2	0.109
Tdw-K	0.187
Tdw-ISO	0.469
Tuv	1.01E-18

3.5. Material reflectance measurements

Hand-held spectrophotometers measuring color at a wavelength scale have become more affordable to use in field studies.

This study measured the material reflectance related to each surface by utilizing a spectrophotometer (Konica Minolta CM-600d Spectrophotometer). Figure 13 shows the spectrophotometer which used for measuring the material reflectance in this study. The measurement has been done based on an average amount of three-point measurements of each surface material type. For some surfaces, to increase the accuracy of the results, more points have been measured, such as floor and outdoor albedo.

Figure 13. Spectrophotometer Konica Minolta CM-600d

According to the study conducted by Jones and Reinhart [97], a photo of each measured surface was also captured. These images were used as reference and estimation of roughness values according to the visual appearance of the images. For converting the measured reflectance values of each surface to Radiance material definitions, the way has been used, as explained by Jakubiec et al. [98]. The values of each glass's optical and thermal properties were obtained from the manufacturer's data (presented in the previous section). Then, using the Window software, the BSDF of the

DSF were obtained in the absence of the blind and with the blind at different angles. For obtaining the transmissivity of the glazing, the transmittance was multiplied to the value of 1.09 as suggested by Quek et al. [7]. The measured reflectance amount of each material is presented in Table 6.

Table 6. The measured values of the reflectance of each surface

Surface name	Reflectance (%)
East wall	43.3
West wall	45.6
North wall	42.5
Floor	27.3
Roof (white tiles)	72.3
Roof (gray tiles)	70.1
Door	67.5
Venetian blind	13.0
Pipe	8.8
Steel box of ventilation	34.8
Ventilation fabric	20.6
Window aluminum frame	52.5
Table (top)	45.7
Table (drawers)	6.0
Chair	6.5
Device's box (orange)	24.7
Outside albedo	25.8

3.6. Illuminance and luminance measurements

Lighting measurements were often taken with photopic illuminance meters. The measurement of luminous flux density on a unit area is known as illuminance (lux or footcandle) [99]. Illuminance meters are affordable, widely available, and easy to use, allowing researchers to generate additional illuminance-based measures and practitioners to use them. In account of the fact that office lighting needs to dominate the creation of many lighting standards and recommendations [100], illuminance measurements were frequently taken at desk height. The eye-level vertical illuminances were measured increasingly more often. The research has shown that vertical illuminance correlates better with human perception than horizontal illuminance [31,101].

3.6.1. Illuminance measurements

In order to capture the illuminance of the spaces, two illuminance meters have been used. The illuminance meters were positioned in the middle of the test cell at eye level (1.20 m) and on the workplace (0.8 m). Horizontal illuminance at the hight of 0.8 m were captured through an illuminance sensor (LTR-559 Light and Proximity Sensor Breakout), While vertical illuminance was measured using an illuminance sensor (Adafruit VEML7700) at the eye position facing the window.

The Raspberry Pi 4 is a single-board controller incorporated in the cell, allowing measuring the variable relating to the DSF states and the boundary conditions (Figure 14).

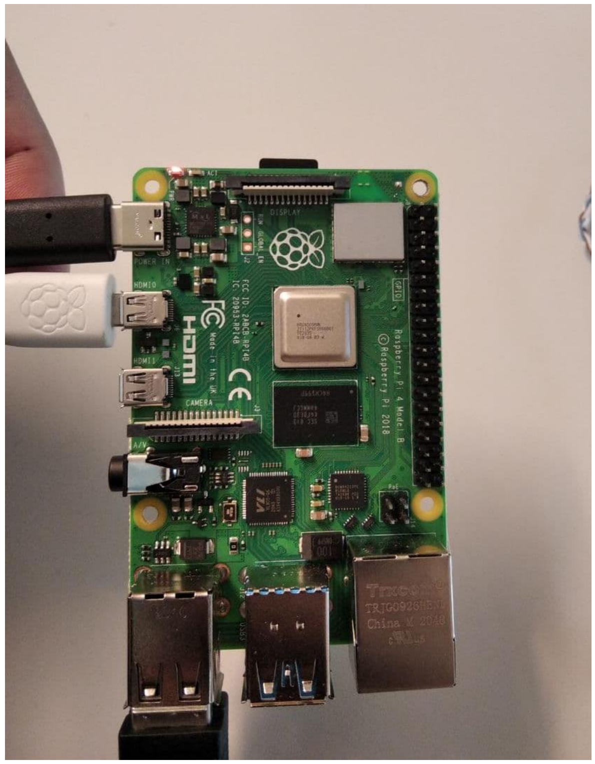

Figure 14. Raspberry Pi 4

The sensors that send information to the Raspberry Pi exploit the I2C type communication protocols used for low-level communication between integrated circuits. The Raspberry Pi controls the actuators present in the cell and receives data from the sensors. The controller, based on the inputs it receives from the user or from the decision-making processes for control, sends electrical signals to the actuators in the cell in order to set the DSF in the chosen configuration. The actuators have the task of controlling the Venetian blind. For example, pulling down or raising the blind and adjusting the angle of the slats. A Personal Computer receives data measured by the sensors and acquired by the devices. These sensors were connected to the Modbus and Data Taker, capturing illuminance values. The vertical and horizontal illuminances were captured on a time step of 10 seconds. However, the final values were averaged in minute time intervals. Figure 15 presents the illuminance sensors in the DSF test cell.

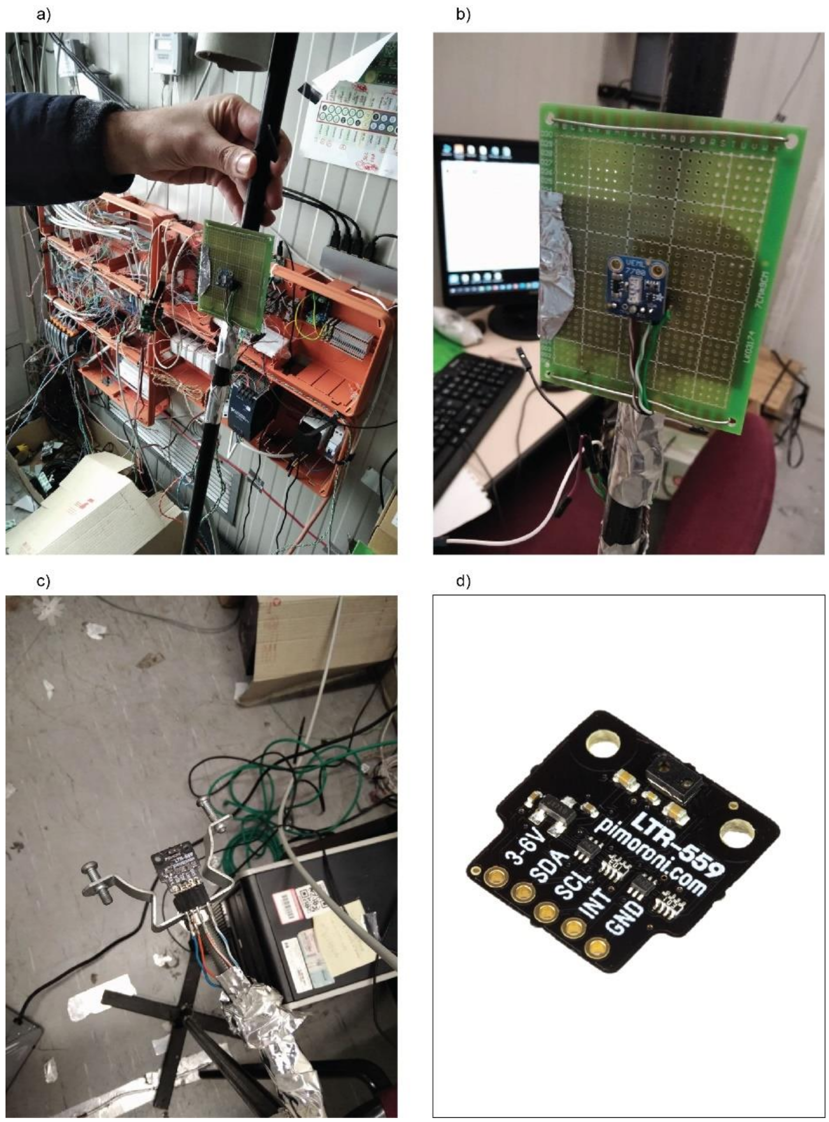

Figure 15. Illuminance sensors, a) and b) vertical illuminance sensor (Adafruit VEML7700) located at 1.2 m, c) and d) horizontal illuminance sensor (LTR-559 Light and Proximity Sensor Breakout) located at 0.8 m hight

3.6.2. HDR photography

In this study, with the aim of comparing software outputs with real conditions, measurements have been made for the amount of brightness at the desktop level and the amount of glare from the user's view of the windows. One of the field measurement methods for determining the amount of glare in a specific space and time is HDR photographs. The glare calculated by this method has been compared with the glare simulated in Diva and Honeybee software. HDR imaging is a photograph that allows a more dynamic range of light between dark and light points than conventional methods.

The purpose of this technique is to display the range of light intensities in natural scenes accurately. For capturing HDR images, the cameras with HDR shooting capability (SLR cameras) in completely fixed conditions (on the tripod) and with different exposure by changing the shutter speed taking some images from a scene. With the help of software such as photosphere, LMK Labsoft, and Aftab Alpha, the captured photos are merged, and the final image is created.

HDR images were captured with a digital camera (Canon EOS D650) (Figure 16). The methods used for measurements are in accordance with the recommendations proposed by [98,102]. The camera was installed on a tripod, capturing images with activated Auto White Balancing. The ISO settings were captured constantly at 100, the shutter speed at 1/15, and the activated EV setting between -2 and +2. The camera was positioned at six different positions and two different view directions. HDR photographs were captured at 6 points in the test cell to capture luminance values from their point of view. Three points A, B, C are located 3.3m, 1.75m, and 0.50m, respectively, with 0° view angle to the window. The other three points, namely A', B', and C', have 45 degrees to the window. The measurements for taking the images have been done in different blind conditions for each point. The condition without Venetian blind, and pulled down blind. Different blind angles have been selected 0, 15, 30, 45, 60, 75, and 90 degree blind angles were considered for this measurement. Figure 16 depicts the HDR photography under various blind conditions. Also, it is worth mentioning that the measurement has been done both in sunny and overcast sky conditions. The camera was already calibrated and had a calibration curve then, it was not needed to calibrate the lens of the camera again. The LMK-Labsoft 4 was used to produce the different exposure images, and then HDRScope [79] software was used for image post-processing and creating false-color images.

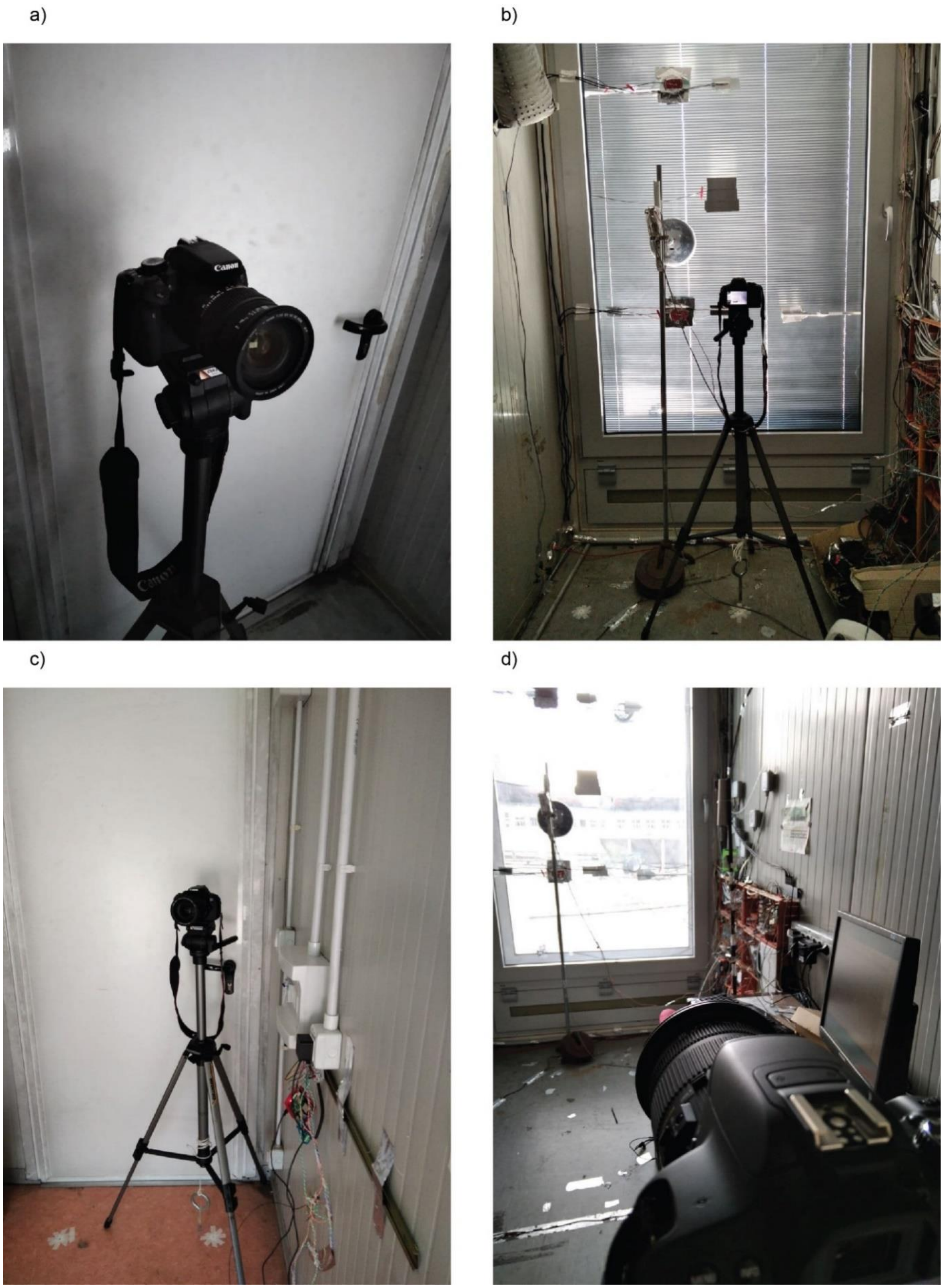

Figure 16. HDR camera; a) The camera; b) HDR photography with the presence of the Venetian blind; c) The camera and tripod; d) HDR photography without Venetian blind

3.7. Model validation

3.7.1. HDR photography versus simulated $DGP_{point\text{-}in\text{-}time}$

Experimental measures were taken in three days, May 14, 15, and 18 of 2021, in the presence of both clear and overcast days at different hours (Morning, noon, and afternoon), to evaluate the occupants' visual comfort and glare perception in different positions inside the test cell. The states without Venetian blind and with Venetian blind with different slat angles of 0°, 15°, 30°, 45°, 60°, 75°, and 90° has been investigated. The field measurement consisted of field measurement of vertical and horizontal illuminance and luminance levels. The HDR photography and calibration process followed the step-by-step procedure tutorial paper written by Pierson et al. [102]. The details of how measurements have been done regarding illuminances and luminance (HDR images) were explained in previous sections.

Intending to calculate Daylight Glare Probability (DGP) through an HDR camera, this task's camera settings were as the previous. A constant ISO 100 was set, with fixed aperture size (f/7.1) and variable shutter speed (1/4, 1/8, 1/15, 1/30, 1/60, 1/125, 1/250, 1/500, 1/1000). The camera was positioned at six points indicated as the exact location of the sensors in simulation.

Vertical illuminance at the eye level was simultaneously measured using a vertical illuminance sensor (Adafruit VEML7700) located 1.2 m above the floor (same height as the camera lens). Evalglare's measured illuminance values were compared to predicted vertical illuminance values, and the Evalglare '-i' option with externally measured illuminance was also employed [33]. Multiple exposure images were combined in LMK-Labsoft with the calibration file. Then, DPG calculation and glare analysis were assessed using Evalglare. The following example illustrates the command line used for evaluations on Evalglare for the 180° fisheye lens with [103]:

evalglare -vta -vv 180 -vh 180 -i (measured vertical illuminance) (output.hdr) where:

- *-**vt**t :* Set view type to t (for fisheye views should use ***-vt**a* or ***-vt**h* preferably)
- ***-vf** viewfile :* Get view parameters from the file
- ***-vv** val :* Set the vertical view size to value
- ***-vh** val :* Set the horizontal view size to *value*

It should be noted that the camera was not equipped with a fish-eye lens, and the images were taken with a perspective lens. Then the *-vv* and *-vh* were not equal to 180°, and the actual lens size should be inserted. Despite the fact that the 17mm lens captures a broad angle of view, it has a significantly narrower field of vision than an angular fish-eye view. In other words, it missed as much information as an angled fish-eye view [33]. It explains why fish-eye images would be more suitable for capturing a human's field of view than perspective images.

The DGP scales proposed by Wienold [40] were used in this investigation.

3.7.2. Simulated luminance map

In order to simulate the sky condition for the same time of measurement, the outside global horizontal irradiance and diffuse horizontal irradiance have been captured simultaneously. To this end, a pyranometer (Hukseflux lp02) with a shading band was installed on the roof of Politecnico University close to the test cell to capture the diffuse horizontal irradiance. Figure 17 shows the pyranometer (Hukseflux lp02) with its shading band. Another pyranometer measured the global horizontal irradiance, positioned near the test cell so that nothing shaded it (Figure 18).

Figure 17. The pyranometer with shading band for measuring diffuse horizontal irradiance

Figure 18. The pyranometer for measuring global horizontal irradiance

The irradiance values measured by these pyrometers were stored in the system and then inserted in simulation software (Diva and Honeybee), based on the capture time of each HDR image. Accordingly, with these amounts and selection creating the custom sky, the real sky condition has been simulated for the application, and the results were based on the measured sky.

3.7.3. Comparison of HDR photography and simulated DGP

The HDR photography has been conducted at six reference points and three different days for having various sky conditions from sunny to overcast. Images have been captured for 8 states depending on Venetian blind. The states of without blind and with blind and slat angles of 0°, 15°, 30°, 45°, 60°, 75°, and 90° has been investigated. These are only some images comparing the DGP amount and luminance in different points in real images and simulation results. These images have been selected from the condition without Venetian blind to have a higher DGP since the glare has not happened during measurements. The values of global horizontal irradiance (GHI) and diffuse horizontal irradiance (DHI) have been measured during the measurement time then extracted and used to create the real sky condition in Honeybee.

The calculated DGP amount of simulation and HDR images has been compared in Figures 19-22.

Falsecolor of captured by HDR camera 14.05.2021

Time: 14:31

Diffuse horizontal irradiance: 87 W/m2

Global horizontal irradiance: 115 W/m2

Glare : 29%

Falsecolor created by simulation in Honeybee

Simulation in Honeybee

Glare : 29%

Figure 19. Comparison of the results regarding DGP for HDR image and simulation at point A on May 14

Point B

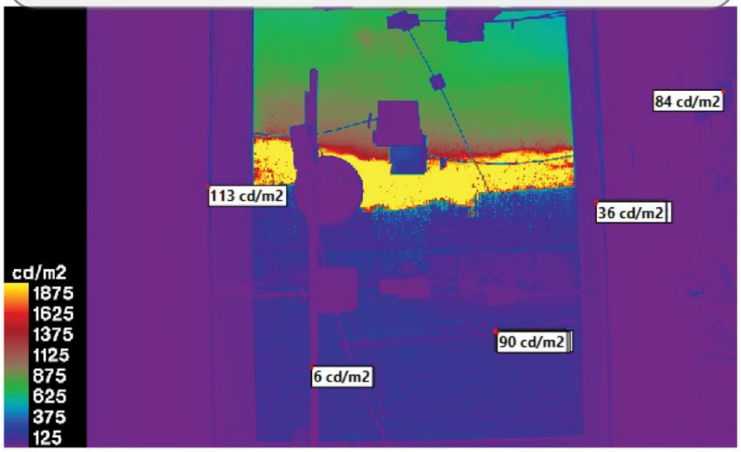

Falsecolor of captured by HDR camera 14.05.2021

Time: 13:52

Diffuse horizontal irradiance: 65 W/m2

Global horizontal irradiance: 85 W/m2

Glare : 20%

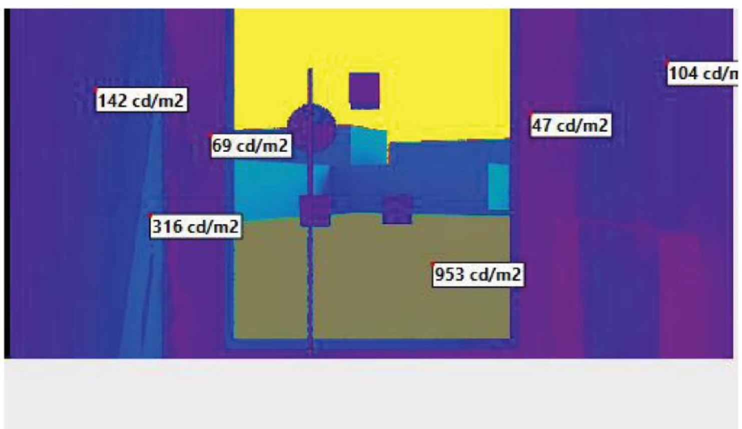

Falsecolor created by simulation in Honeybee

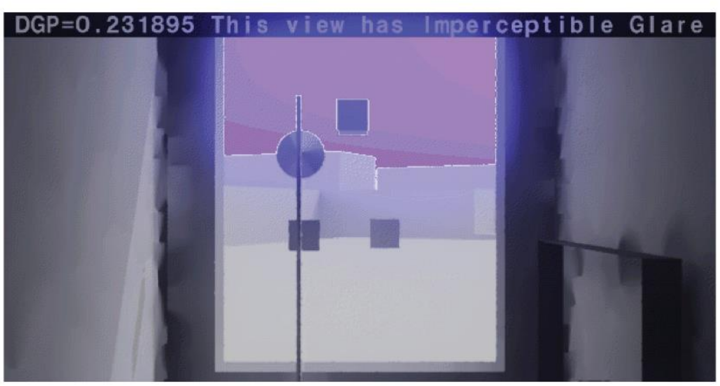

Simulation in Honeybee

Glare : 23%

Figure 20. Comparison of the results regarding DGP for HDR image and simulation at point B on May 14

Point B

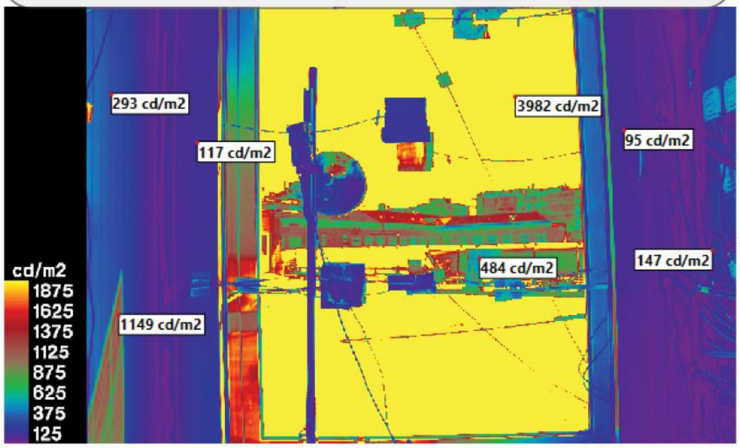

Falsecolor of captured by HDR camera 18.05.2021

Time: 14:37

Diffuse horizontal irradiance: 75 W/m2
Global horizontal irradiance: 1117 W/m2

Glare : 29%

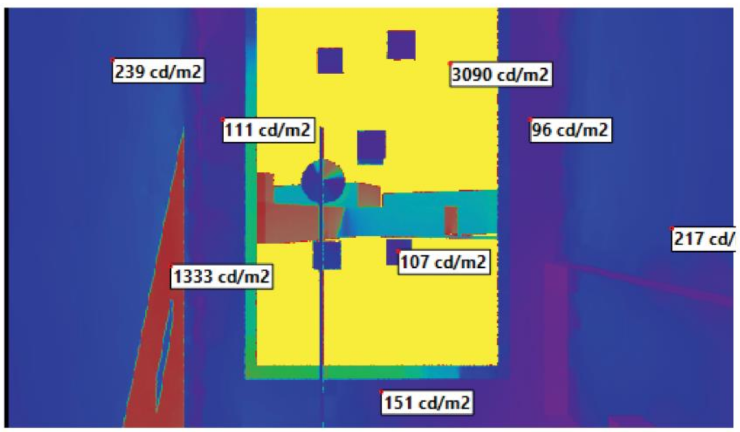

Falsecolor created by simulation in Honeybee

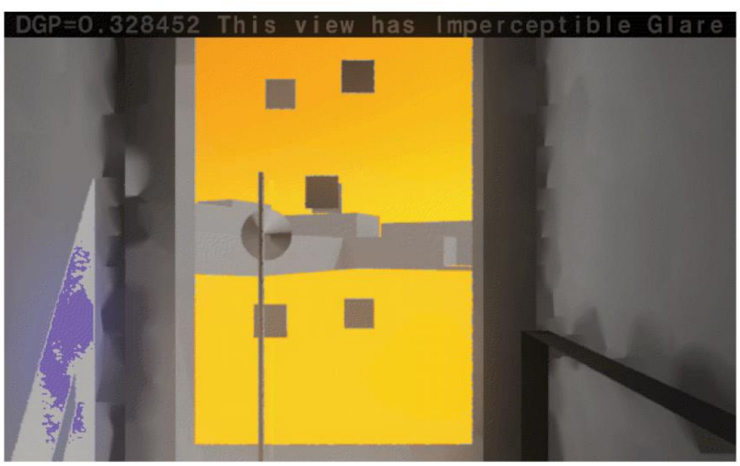

Simulation in Honeybee

Glare : 32%

Figure 21. Comparison of the results regarding DGP for HDR image and simulation at point B on May 18

Point C

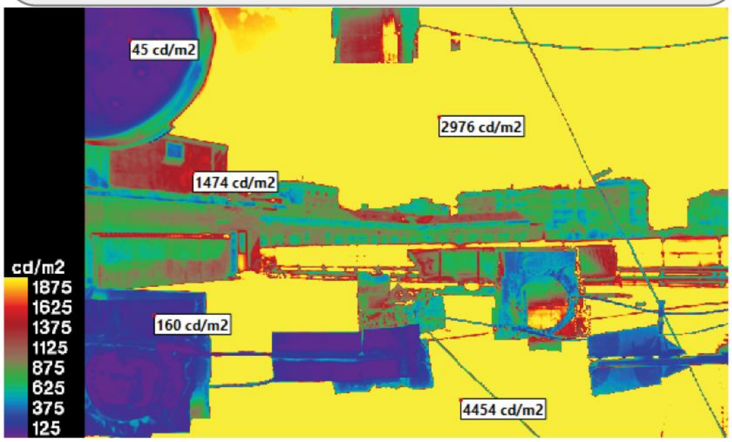

Falsecolor of captured by HDR camera 18.05.2021

Time: 14:45

Diffuse horizontal irradiance: 58 W/m2
Global horizontal irradiance: 1103 W/m2

Glare : 30%

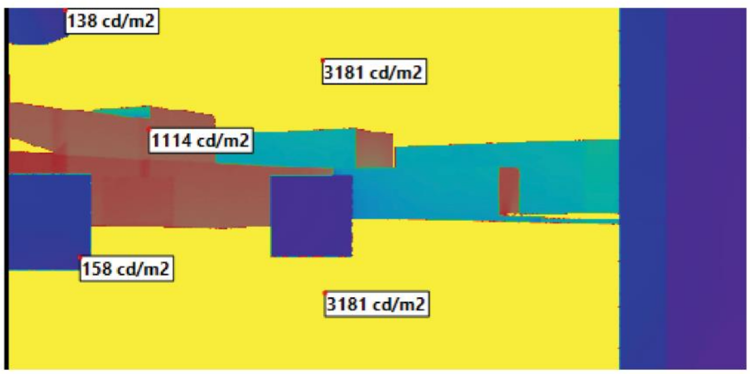

Falsecolor created by simulation in Honeybee

Simulation in Honeybee

Glare : 33%

Figure 22. Comparison of the results regarding DGP for HDR image and simulation at point C on May 18.

Comparing the results of simulation and HDR photography at point A is presented in Figure 19. The DHI and GHI values were 87 W/m^2 and 115 W/m^2, respectively, and the images were taken on May 14 at 14:31. The DGP value of the HDR image was 29% as the same as the simulation result. The luminance amounts were matched together at most of the labeled points. Only the outside (sky and the albedo) were in yellow, which means a high amount of luminance. However, the interior part of the DSF was mainly blue and green, which confirms the low amount of DGP.

Figure 20 presents the amount of DGP with HDR and simulation results at point B. It was taken on May 14 at 13:52 with DHI and GHI values of 65 W/m^2 and 85 W/m^2, respectively. As shown in Figure 20, the amount of DGP in HDR image was 20%, while the DGP of the simulation was 23%. It is worth mentioning that this image was taken under the overcast sky condition. Therefore, the low amount of DGP was not a surprise. The interior parts of DSF were dimmed, and the labels showed a low amount of luminance.

Figure 21 shows the HDR images of point B under the sunny sky taken at 14:37 on May 18. The GHI and DHI at the time of measurements were equal to 1117 W/m^2 and 75 W/m^2, respectively. The results show that the DGP value in the HDR image was 29%, while the simulation showed 32%. A higher amount of the DGP was observed in this image, while the glare condition was still imperceptible. Both simulation and HDR images show the high amount of luminance on the outside surfaces and sky. The labeled luminance points recorded similar values in simulation and HDR images.

The DGP value of HDR image and simulation at point C on May 18 shows in Figure 22. The measurements at this point have been done at 14:45 when the sky was sunny, and DHI and GHI were 58 W/m^2 and 1103 W/m^2, respectively. As the results presented, the DGP value in the HDR image was 30%, while in the simulation was 33%. The view shows mostly the outdoor environment, and a considerable part of the image was in yellow. It meant that the luminance amount was higher than 2000 cd/m^2 based on the presented legend.

Generally, the amount of the DGP at all of the measured points was similar or with 3% differences. The labeled points were also very closed. It seems that different luminance values between simulation and HDR images were because of different locations of the points. Comparing results showed the high amount of accuracy of the simulated model.

4. Results

4.1. Introduction

This chapter will present the results obtained by following the methodology explained in the previous chapter. According to the methodology, different indicators of daylight and glare are simulated. Simulations were used to perform generalizable results. The introduced DSF was modeled and simulated using Honeybee in Grasshopper and Diva for Rhino. The results of appropriate indicators for evaluating daylight and glare are prioritized and selected. Thus, the effect of the Venetian blind with different degree angles on the selected indicators was investigated. To explore the effect of Venetian blinds on daylighting and glare, three scenarios have been established. Scenarios one were done with the Venetian blind up, whereas scenarios two and three were performed with the Venetian blind drawn with slat tilt angles of 0° and 30°, respectively. Finally, the challenges and limitations of the study are introduced, and suggestions are made for future studies.

The results obtained from Diva and Honeybee software were compared, and the results showed that Diva software predicts the results up to twice more than real value. Therefore, after comparing the two software in this study, it was decided to use Honeybee software to perform point-in-time glare analysis to have more reliable results.

4.2. Comparison of glare analysis in Diva and Honeybee

The first question of this research was:

RQ1. Which simulation tools are more accurate and capable in terms of glare analysis?

A series of simulations have been done in Diva and Honeybee with the same parameters and boundary conditions to answer this question. The results have been compared to find the most suitable simulation tools in terms of calculating the glare.

4.2.1. Glare analysis with CIE sky models

Initially, the simulation was performed in two software, Diva and Honeybee. In order to analyze the glare condition in DSF, the amount of point-in-time glare was made in three main points, A, B, and C, so that their view directions were direct to the window. The simulation has been done for noon for 21 months: March, June, September, and December. It is worth mentioning that simulations for this comparison were conducted without consideration of Venetian blind. The Radiance parameters considered for the simulations in both software Diva and Honeybee are presented in Table 7.

Table 7. The radiance parameters used for the simulation with Diva and Honeybee

Parameter	Description	Value
-aa	Ambient accuracy	0.1
-ab	Ambient bounces	5
-ar	Ambient resolution	256
-ad	Ambient divisions	2048
-as	Ambient super-samples	1024
-dj	Direct jittering	0.5
-ds	Direct sampling ratio	0.25
-dc	Direct certainty	0.5
-dr	Direct relays	1
-dp	Direct- present density	256
-ps	Pixel sampling rate	4
-pt	Sampling threshold	0.1
-st	Specular sampling threshold	0.5
-lr	Limit reflections	6
-lw	Limit weight of each ray	0.01

These simulations were performed considering the CIE sky conditions in two modes: Clear Sky with the sun (CIE Clear Sky) and Overcast Sky (CIE overcast Sky). The false-color images and the amount of $DGP_{point\text{-}in\text{-}time}$ for each point have been shown in Figures 23-28.

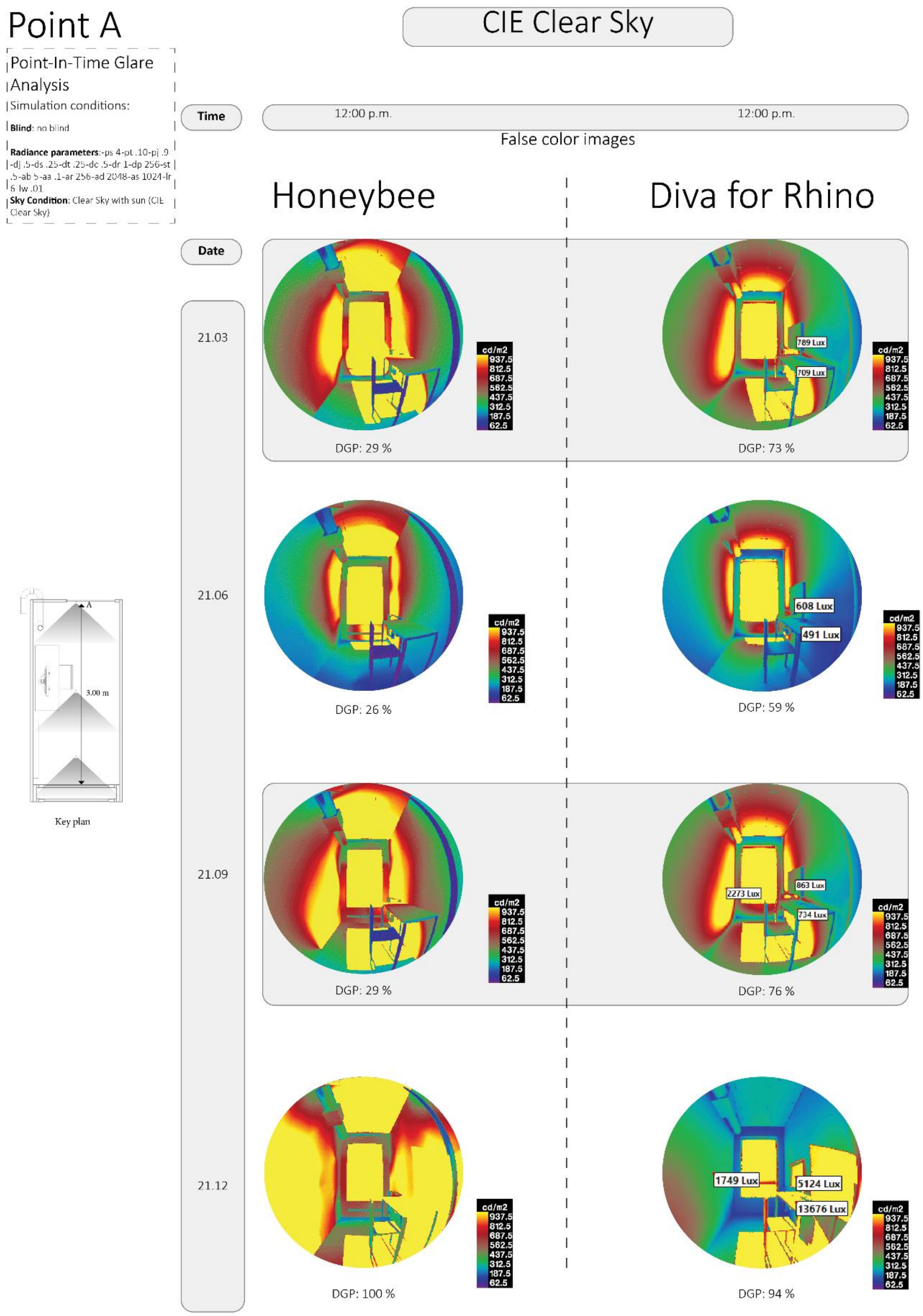

Figure 23. Results of point-in-time glare analysis at point A with CIE clear sky

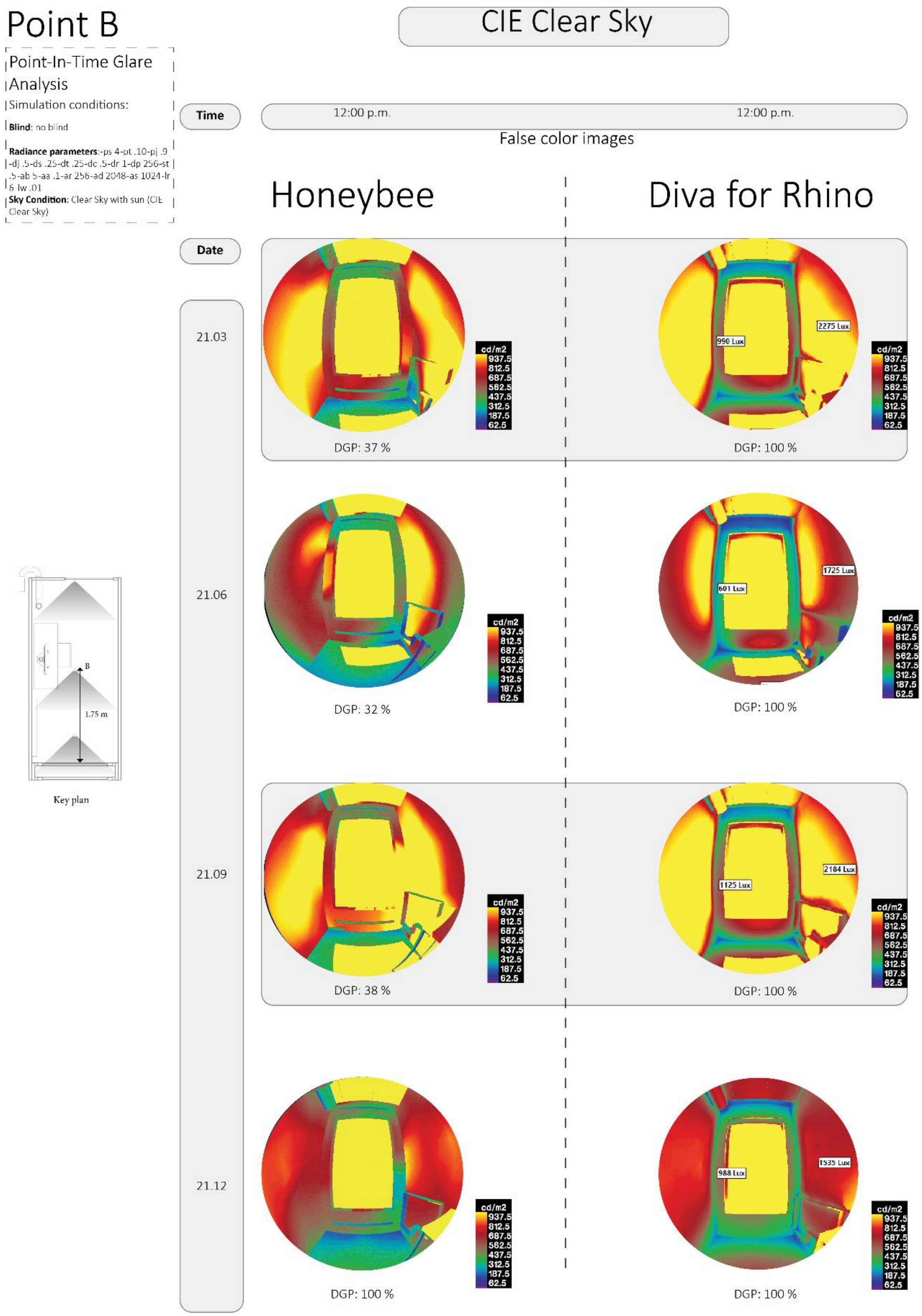

Figure 24. Results of point-in-time glare analysis at point B with CIE clear sky

Figure 25. Results of point-in-time glare analysis at point C with CIE clear sky

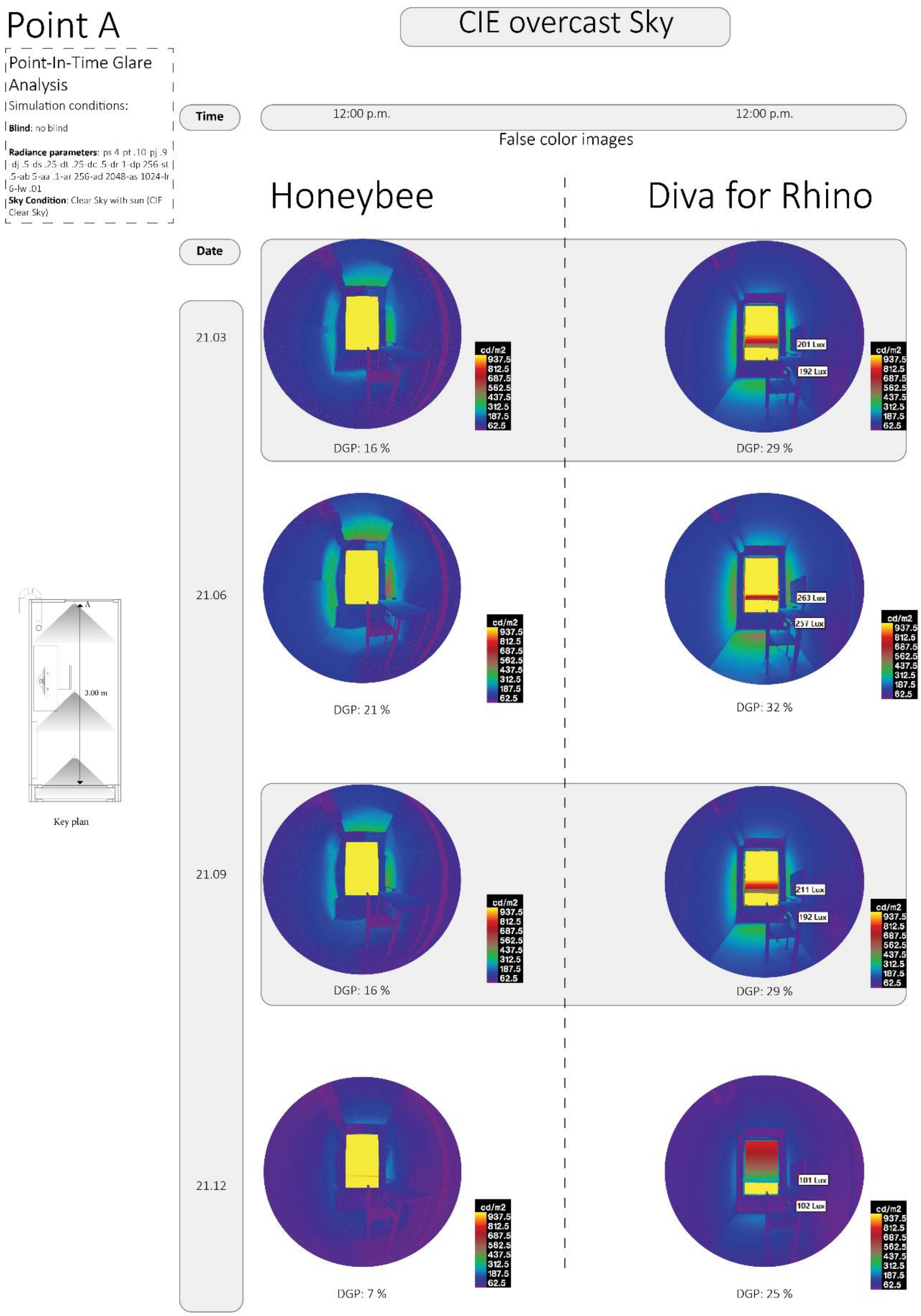

Figure 26. Results of point-in-time glare analysis at point A with CIE overcast sky

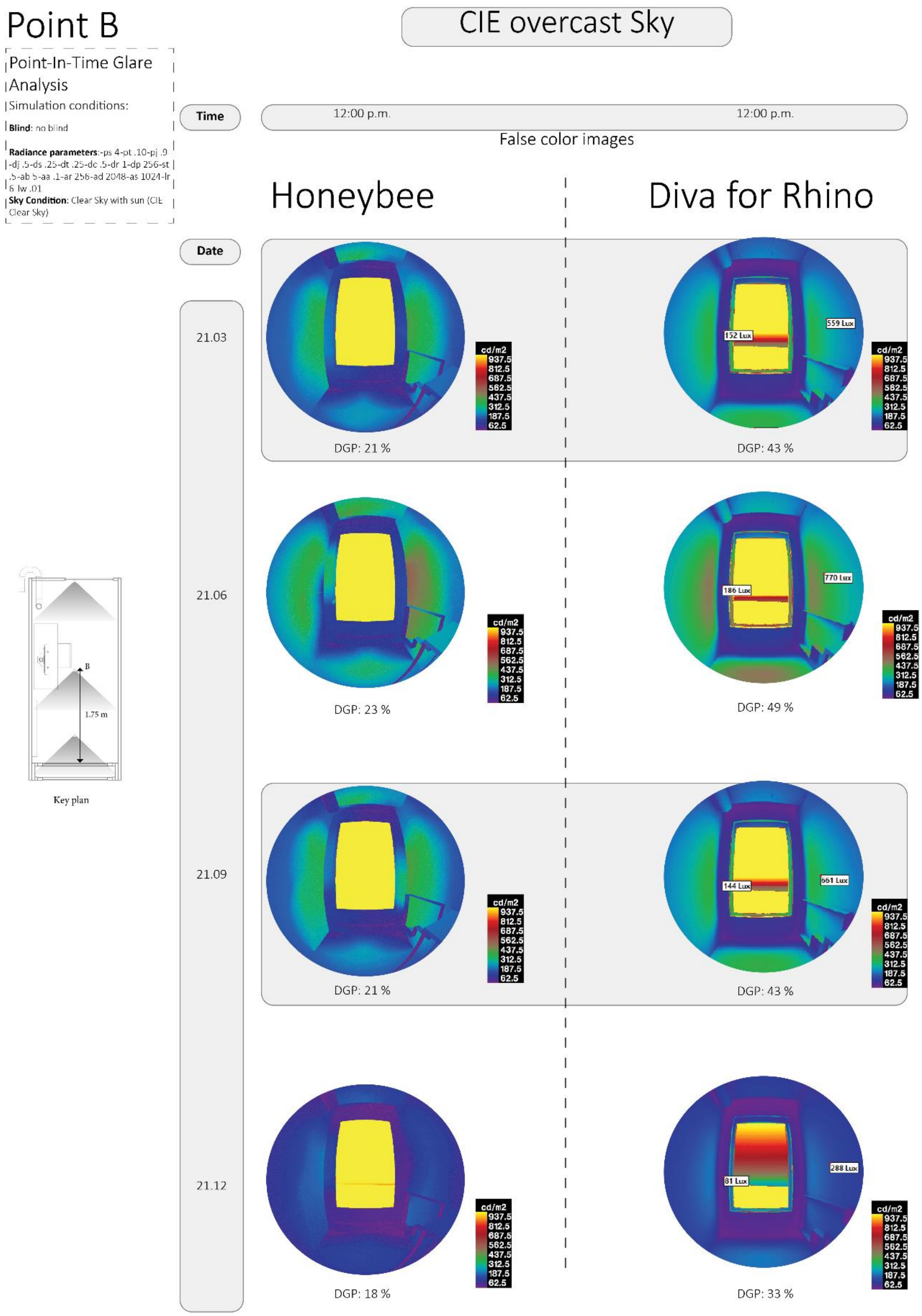

Figure 27. Results of point-in-time glare analysis at point B with CIE overcast sky

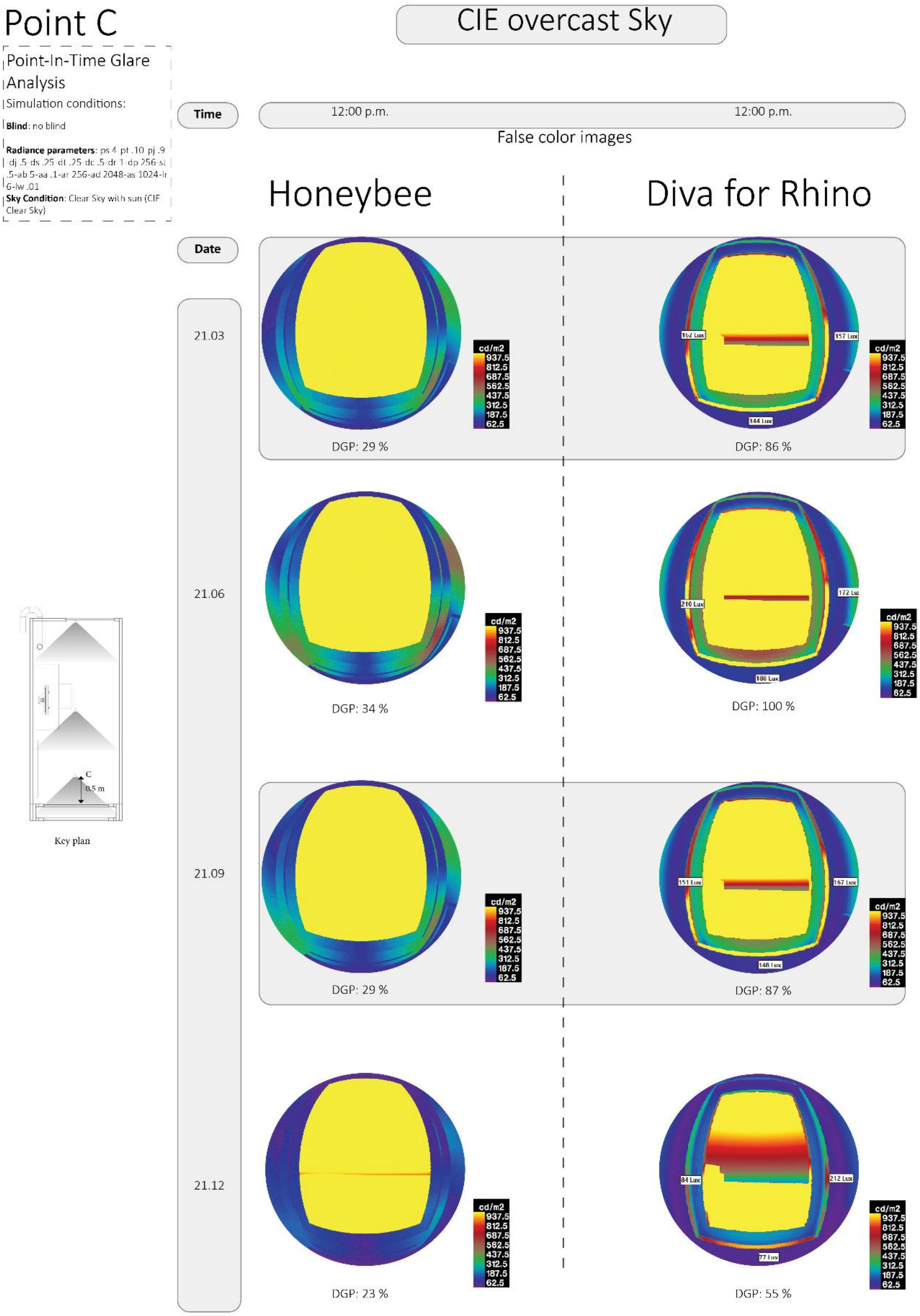

Figure 28. Results of point-in-time glare analysis at point C with CIE overcast sky

As shown in the results, for all the points, Diva for Rhino has overestimated the glare condition in the DSF. In general, under CIE clear sky for all points, Diva calculated the glare condition as intolerable. Diva's DGP amount for all points was more than 0.73 except for June 21 at point A where the DGP value was equal to 0.59. However, in Honeybee, the DGP amounts were between 0.26 to 0.29 for point A, and the intolerable glare has been observed just in December 21. For point B, the DGP values were 0.37, 0.32, 0.38, and 1 for March 21, June, September, and December, respectively. In point C, as the same with Diva, the glare condition was intolerable at all times.

The simulation results with CIE overcast sky for Honeybee were not observed glare even in point C, which is the closest to the window. The lowest DGP amount was 7% related to point A on December 21, and the highest amount of DGP was 29% C in June and September. In Diva, the glare condition in other than point A, which was recorded as the imperceptible glare, at points B and C, glare has occurred. At point B, perceptible glare and intolerable glare occurred, and only on December 21, there was imperceptible glare. However, at point C, all the simulated times, the intolerable glare condition was observed.

Generally, Diva overestimated the DGP about two times higher than Honeybee for all the periods and points. These differences sometimes reached three times, like in point B, where the DGP amounts under clear sky conditions were 32% in June, and this amount in Diva is 100%.

4.2.2. Glare analysis with Perez All-weather sky model

These results paved the way for conducting more simulations and comparisons of the DGP value between Honeybee and Diva with Perez All-weather sky. Therefore, the climate-based glare analysis has been done for points A, B, and C. The annual glare analysis was also conducted in this stage as both annual and climate-based glare analysis using the same sky condition. The same Radiance parameters utilized for both annual glare and point-in-time glare analysis were the same as the parameters in the previous section (Table 7). Figures 29-31 are shown the results of $DGP_{point\text{-}in\text{-}time}$ and DGP_{annual} of all points with the Perez All-weather sky model.

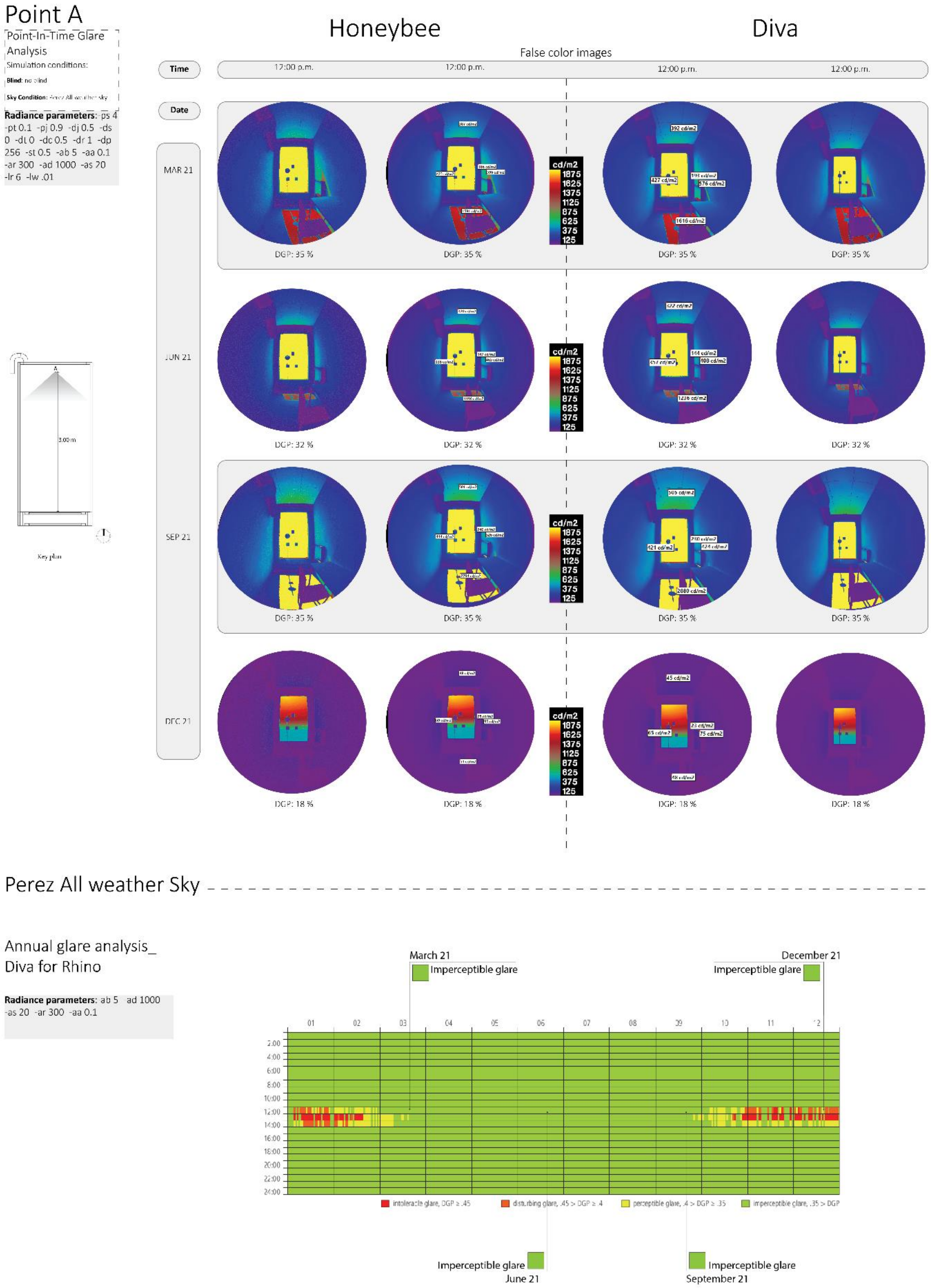

Figure 29. Results of point-in-time and annual glare analysis at point A with Perez all-weather sky

Point B

Point-In-Time Glare Analysis

Simulation conditions:

Blind: no blind

Sky Condition: Perez All weather sky

Radiance parameters:-ps 4 -pt 0.1 -pj 0.9 -dj 0.5 -ds 0 -dt 0 -dc 0.5 -dr 1 -dp 256 -st 0.5 -ab 5 -aa 0.1 -ar 300 -ad 1000 -as 20 -lr 6 -lw .01

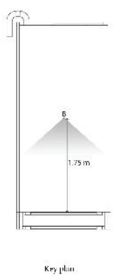

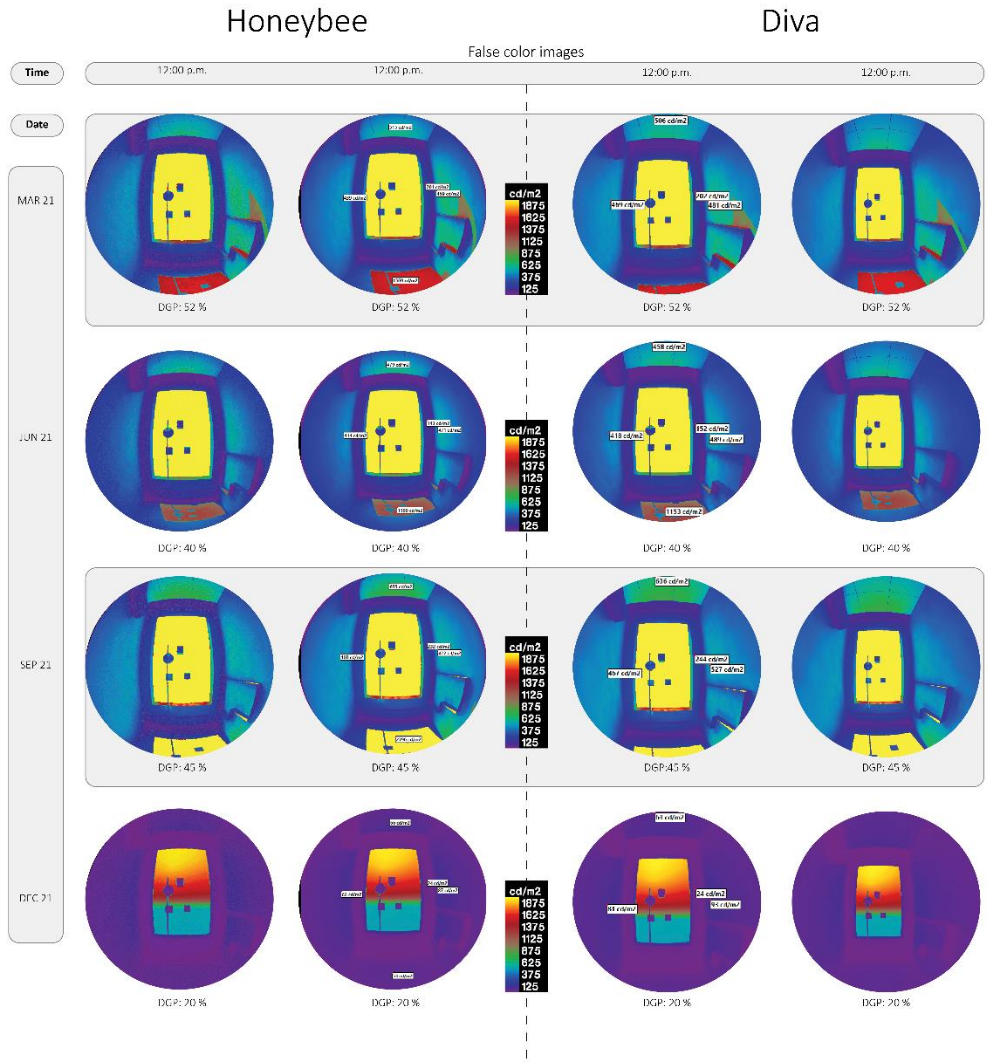

Perez All weather Sky

Annual glare analysis_ Diva for Rhino

Radiance parameters:-ab 5 -ad 1000 -as 20 -ar 300 -aa 0.1

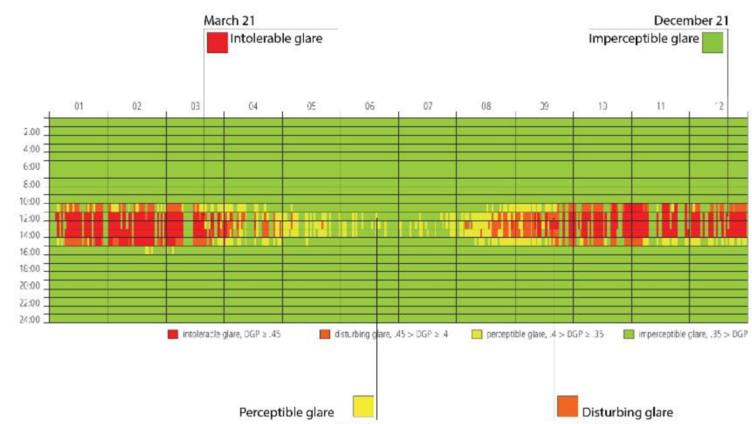

Figure 30. Results of point-in-time and annual glare analysis at point B with Perez all-weather sky

Figure 31. Results of point-in-time and annual glare analysis at point C with Perez all-weather sky

In these simulations, five same points were selected and labeled in both Diva and Honeybee to understand the luminance amount in each scene. The obtained results were different from the previous study which the CIE sky model conducted. The results of DGP for point A were obtained by DIVA software. The corresponding value was attained by Honeybee software, demonstrating nearly the same value given by DIVA software. For example, On March 21 and September 21, there was a perceptible glare condition with a DGP value of 35%. For two other months, the glare was evaluated as imperceptible. The luminance amounts for different times were nearly the same in both simulation tools. Although it is worth mentioning that the extracted DGP_{annual} were considered lower than 35% at all the selected simulation periods, the classifications were considered imperceptible glare class.

However, at point B for both Diva and Honeybee, the glare condition was disturbing and intolerable except on December 21 where the DGP amount was 20%. DGP amounts for March, June, and September were 52%, 40%, and 45%, respectively. The luminance amount for all simulation periods has shown very close surface luminance values. Although the DGP_{annual} results were classified March 21 as intolerable glare, June 21 as perceptible glare, September 21 as disturbing, and December 21 as imperceptible glare perception. Based on the achieved results, the classification of the annual glare was the same as the point-in-time glare analysis except on June 21. On June 21, the DGP point-in-time was 40%, disturbing glare class, while the DGP_{annual} was considered perceptible glare.

For point C, the DGP was 100% in all simulated months other than in December, with the DGP value of 27%. The luminance values have also shown the same in both Diva and Honeybee. The intolerable glare classes were achieved for months March, June, and September for annual glare analysis. However, this amount was classified as imperceptible glare perception for December.

The results of the glare analysis with the CIE sky model and Perez All-weather sky model demonstrated that Diva overestimates the glare condition at all studied points with the CIE sky model. The differences of $DGP_{point-in-time}$ in Diva were reached to more than three times more than the $DGP_{point-in-time}$ in Honeybee. However, the climate-based glare analysis using the Perez All-weather sky model has shown a similar $DGP_{point-in-time}$ at all studied points and the simulated days. Moreover, the extracted simulated hour from the DGP_{annual} results has revealed a strong correlation with the annual glare classifications.

4.3. Point-in-time glare analysis

For a detailed analysis of the glare condition in the DSF test cell, the simulations have been conducted by means of Honeybee in Grasshopper. Six points were selected in the test cell which A, B, and C were the same as the previous simulations. While three more points, namely A', B', and C' locating the exact distances from the window and 0.35 m from the right wall of DSF. These points looked at the window with a 45° view angle and elevated 1.20 m, the same height as A, B, and C. These spots were selected according to the experimental HDR capturing points and view directions presented in the previous section (Figure 10).

To vary the sun position and consequently different daylight conditions, different days in a year were selected. Winter solstice (December 21) and summer solstice (June 21), and Autumnal equinox (September 21), and vernal equinox (March 21) were selected for the glare analysis. The weather data file (.epw) was analyzed for each day to understand the sky condition during simulated days. Following the direct solar irradiance of Turin at previous days and having more comprehensive analysis and results, the opposite sky condition has been searched and selected close to these days. It means if the selected day, March 21, as an example, was sunny, another overcast day has been selected, March 24 in this case. Therefore, four more dates, March 24, June 19, September 24, and December 22, have been selected for the simulations. The Solar irradiance during the selected dates is shown in Figure 32.

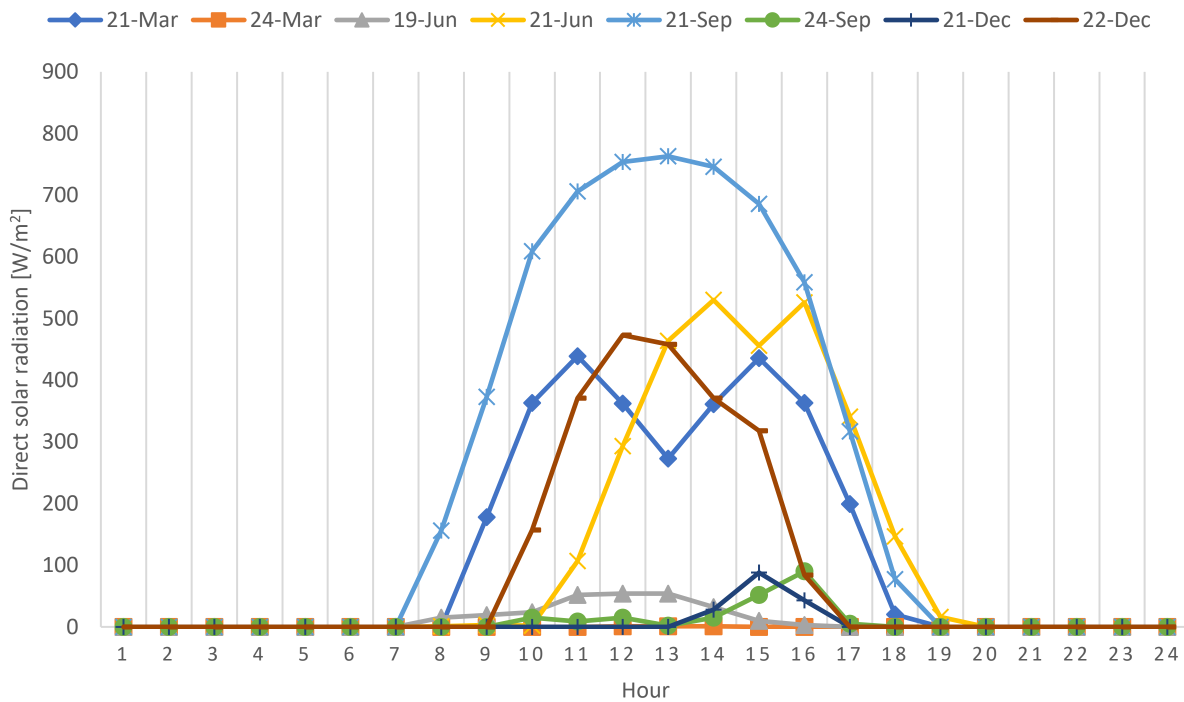

Figure 32. The direct solar radiation of the selected days

September 21 has the highest direct solar radiation among selected days, which reached about 770 W/m^2 in the noontime. While, on June 21, December 21, and March 21, the peak value were about 530 W/m^2, 473 W/m^2, 456 W/m^2, respectively.

Another difference with the previous simulation was simulation time. The simulations were conducted at four different times for each of the selected dates. The $DGP_{point\text{-}in\text{-}time}$ and DGP_{annual} were analyzed at 9.00 a.m, 12.00 p.m, 3.00 p.m, 6.00 p.m.

For this analysis, three conditions in terms of having shading devices were selected. The first scenario was the same as previous simulations, where the Venetian blind were pulled up. In two other scenarios, the Venetian blind was pulled down with different slat angles. The Venetian blind with 0° and 30° slat angle has been simulated, and glare conditions were analyzed in DSF.

4.3.1. Point-in-time glare analysis for scenario 1: Venetian blind up

As shown in Figures 33-35, the value of $DGP_{point\text{-}in\text{-}time}$ for points A, B, and C are presented for scenario one.

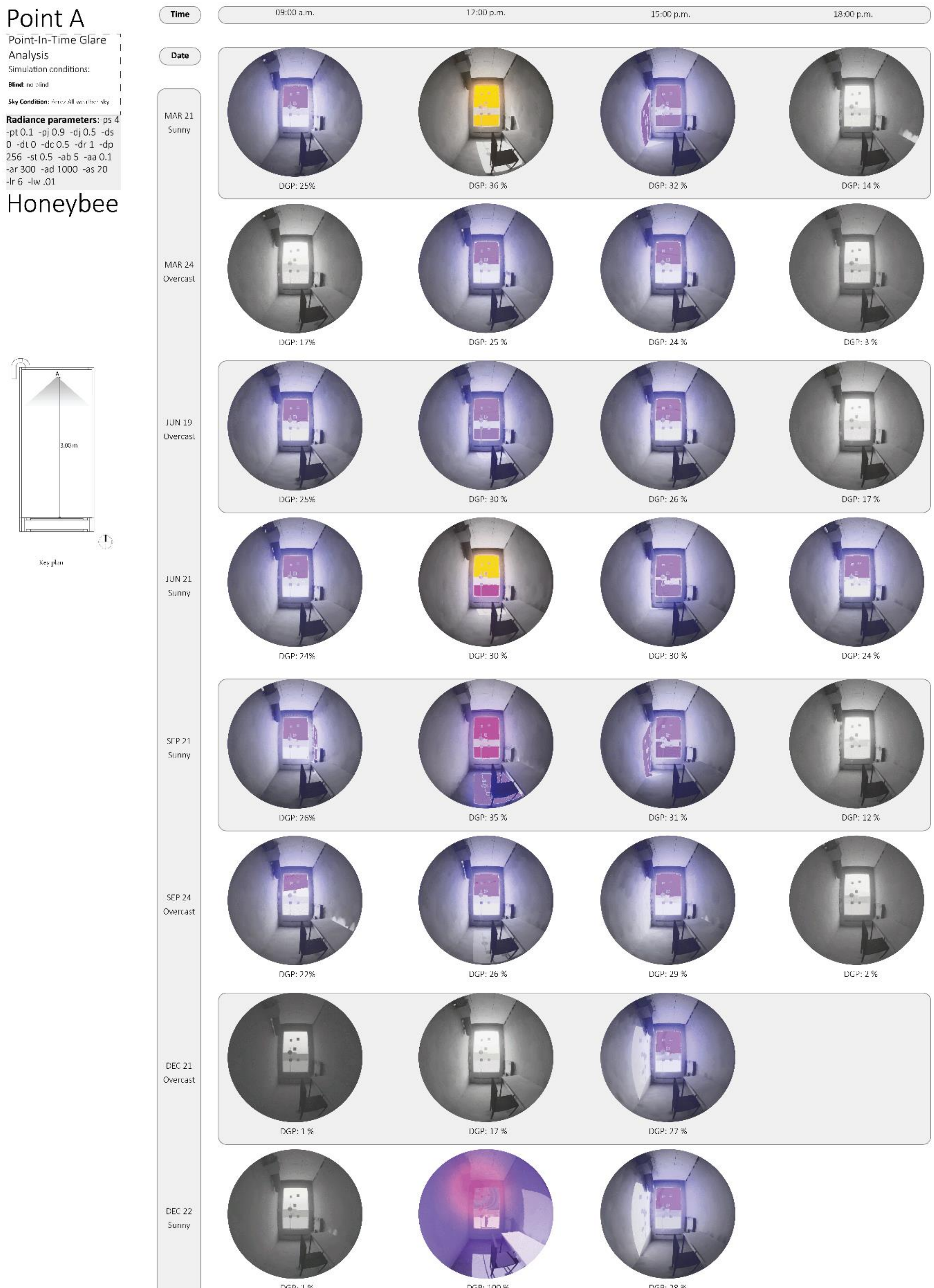

Figure 33. Results of $DGP_{point\text{-}in\text{-}time}$ and DGP_{annual} at point A with Perez all-weather sky

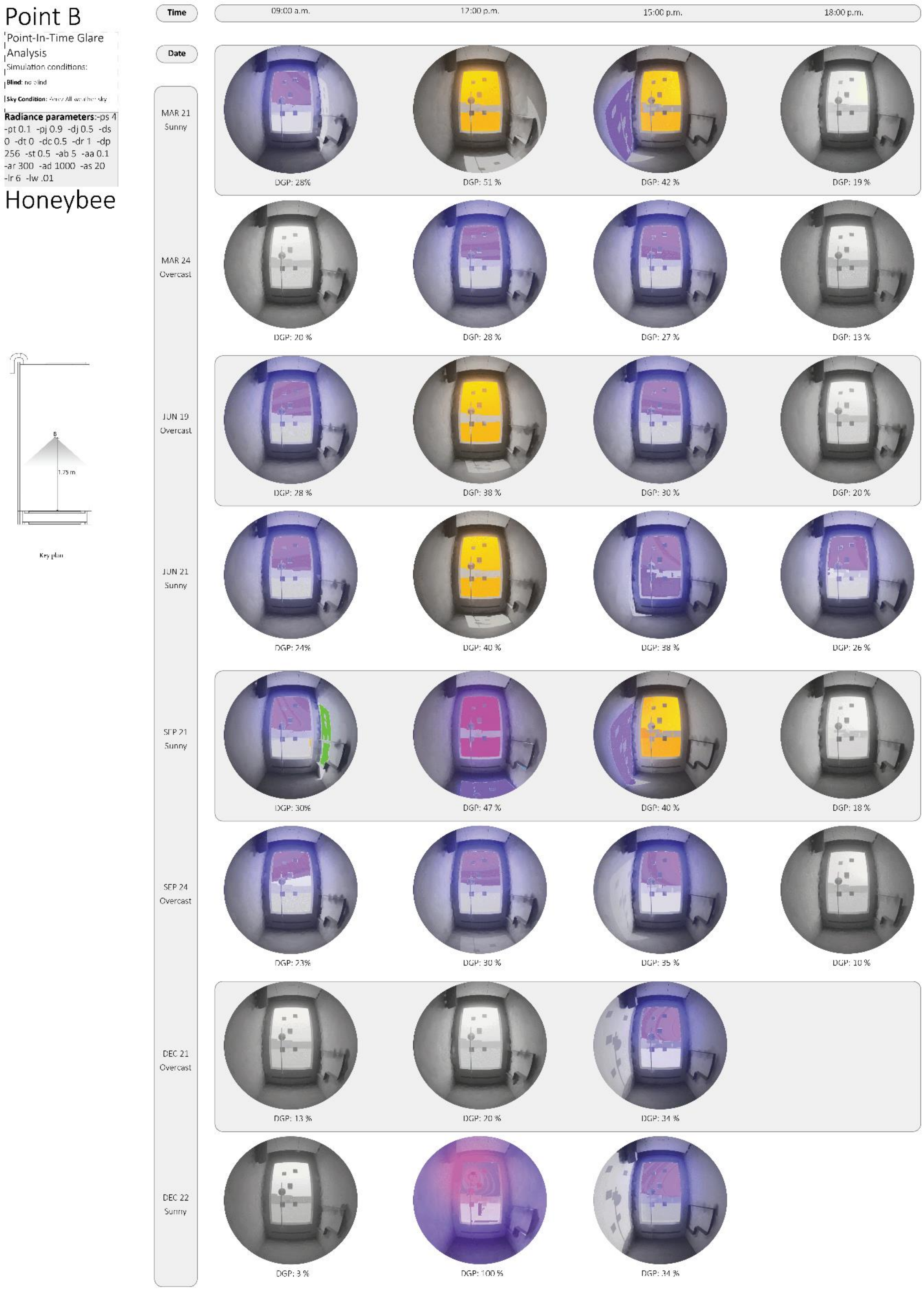

Figure 34. Results of $DGP_{point\text{-}in\text{-}time}$ and DGP_{annual} at point B with Perez all-weather sky

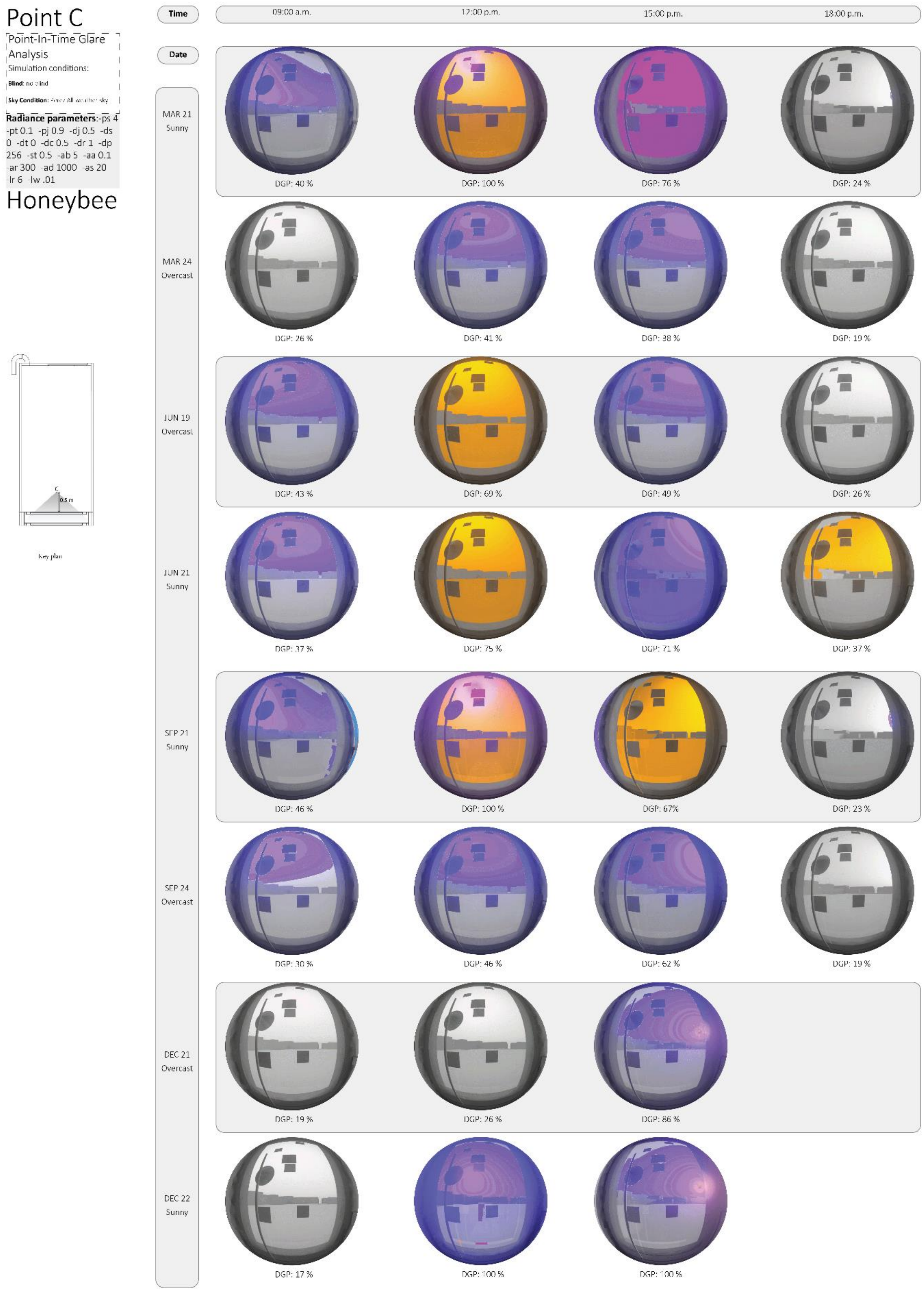

Figure 35. Results of $DGP_{point\text{-}in\text{-}time}$ and DGP_{annual} at point C with Perez all-weather sky

At point A, without Venetian blind, there was no glare condition observed except three simulated times. On December 22, the glare condition was intolerable at noontime, with a DGP value of 100%. The DGP value for the same time on March 21 and September 21 was 36% and 35%, respectively categorized as imperceptible glare. For point B, the intolerable glare happened during some sunny days. The highest DGP value was related to December 22 at noon. At 12:00 and 15:00 on March 21, DGP values were 51% and 42%, respectively. During June 21 and September 21 at noon, the glare was disturbing and intolerable, with DGP values of 40% and 47%. While these values at 15:00 decreased to 38% and 40%, respectively, for each of the dates above. At point C, the DGP amount was more than 45% between 12:00 and 15:00, which means the intolerable glare condition except for two simulated times. On March 24, which was an overcast at 15:00, the DGP value reached 38%, the highest amount on this day. The DGP value for December 21 at noon was 26% that was imperceptible glare condition.

For points A', B', and C' with a 45° angle view direction to the window surface, the DGP amounts were generally lower than previous points. The results of point-in-time glare analysis regarding these points are depicted in Figures 36-38.

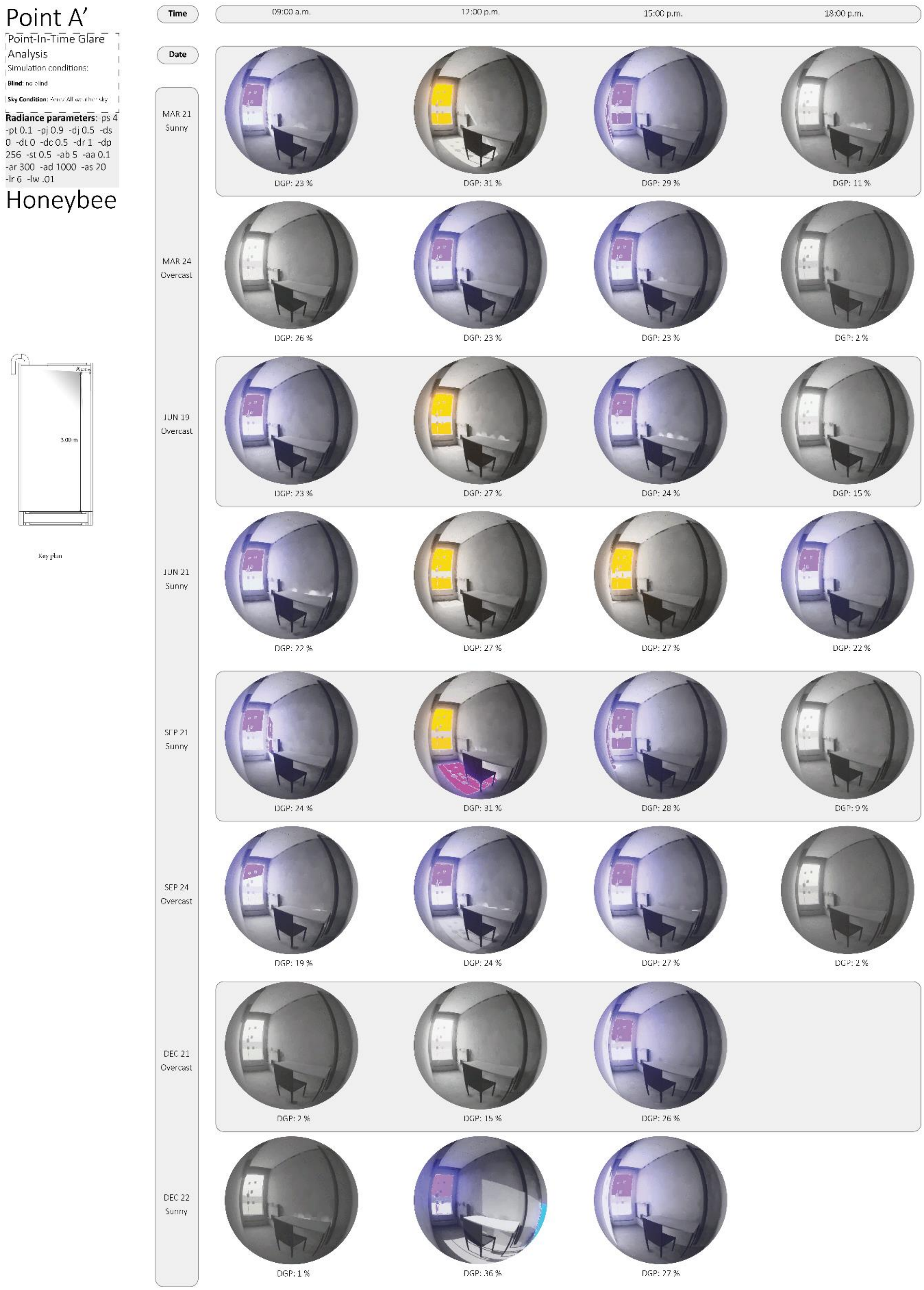

Figure 36. Results of $DGP_{point\text{-}in\text{-}time}$ and DGP_{annual} at point A' with Perez all-weather sky

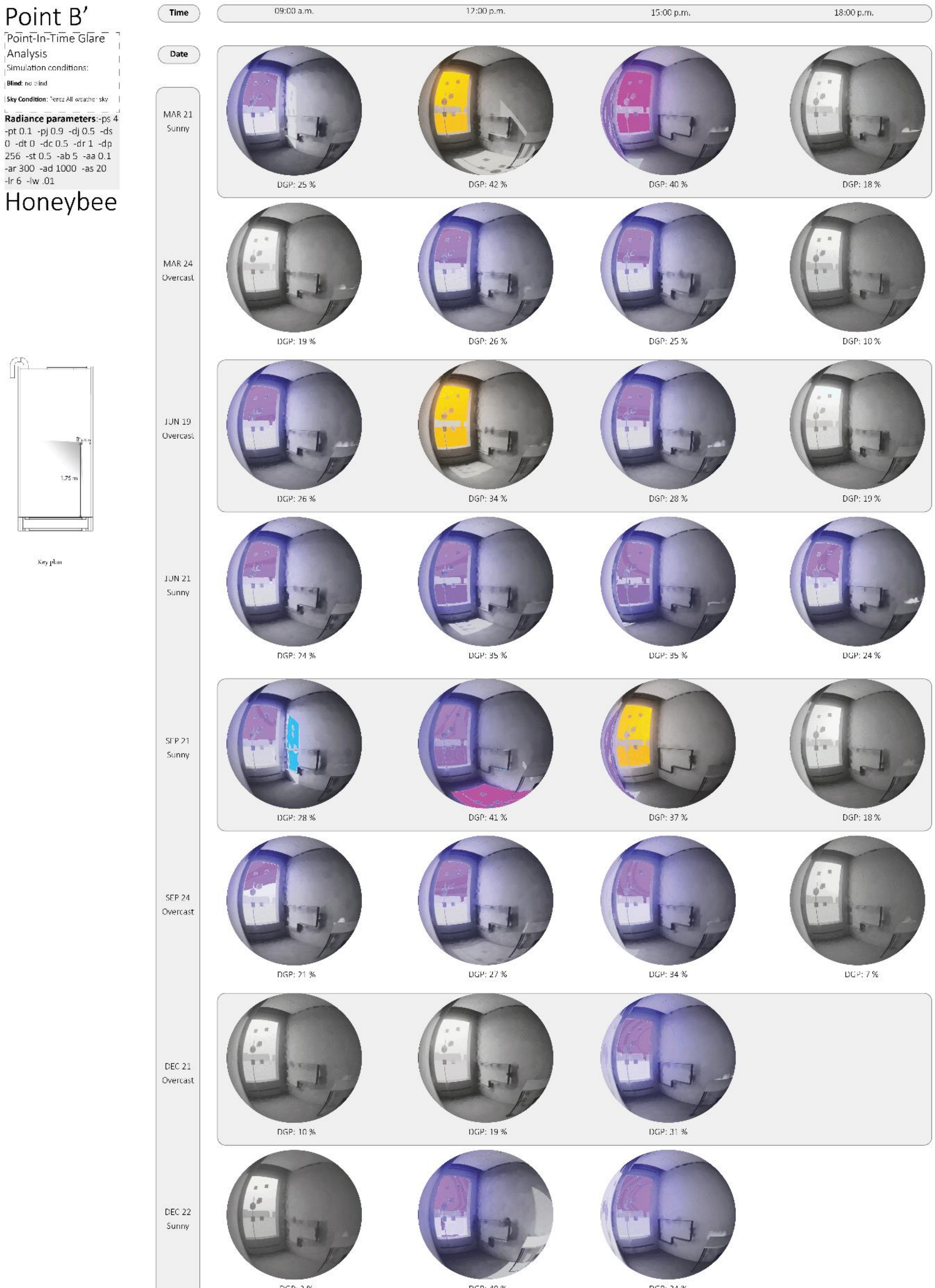

Figure 37. Results of DGP$_{point\text{-}in\text{-}time}$ and DGP$_{annual}$ at point B' with Perez all-weather sky

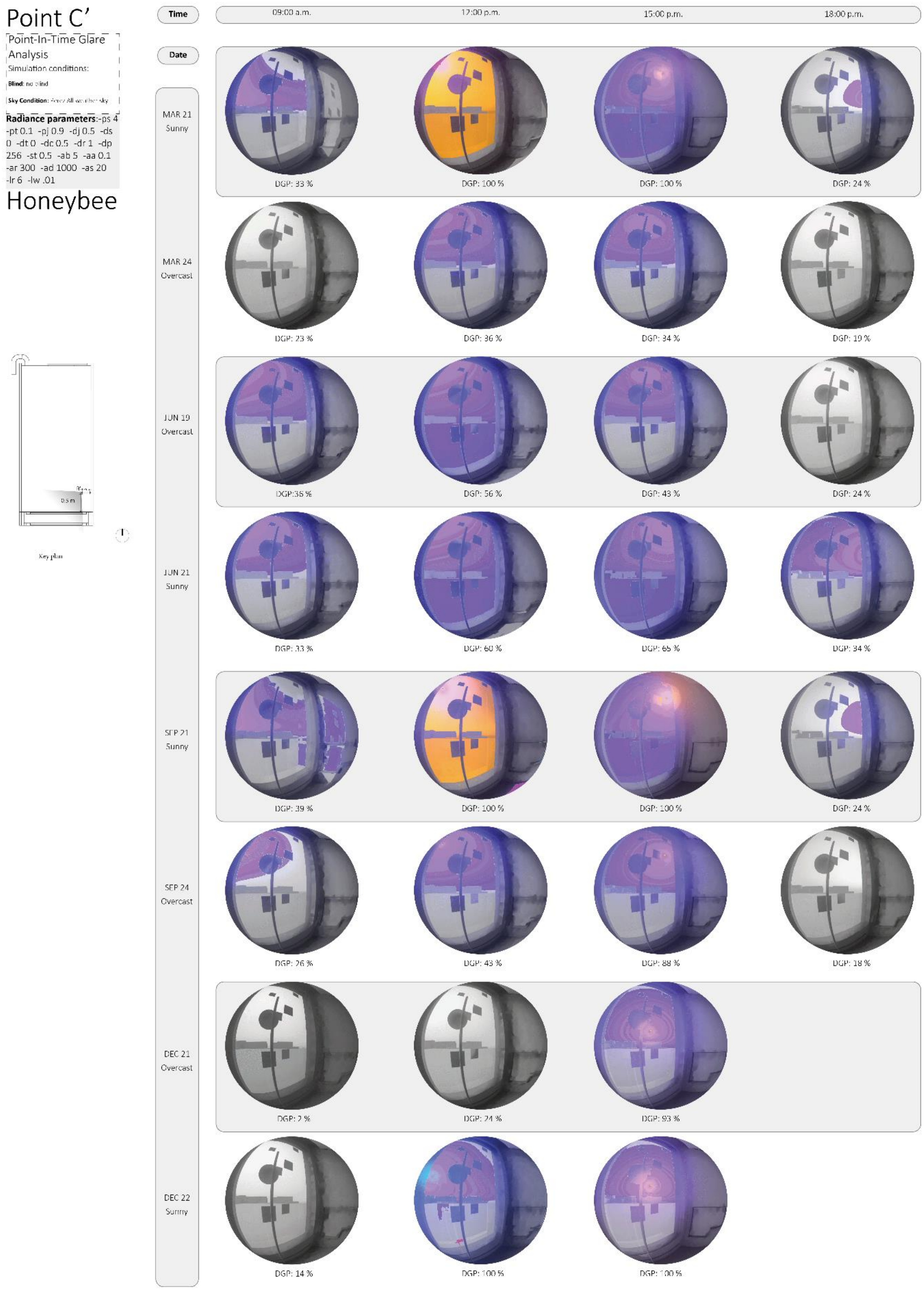

Figure 38. Results of $DGP_{point\text{-}in\text{-}time}$ and DGP_{annual} at point C' with Perez all-weather sky

At the point A', DGP values were lower than 30% at all simulated times. Only DGP reached 36% on December 22, which was the highest amount of DGP at this point. The second highest value of DGP for this point was related to September 21 at noontime with 31%. For point B', the highest amount of DGP happened at noon of March 21 with a value of 42%. September 21 with a DGP value equal to 41% and December 22 with 40% were other highest glare conditions at this point. Other than noontime and 15:00 at all the simulated dates, the glare condition was imperceptible. However, the DGP was different in point C'. At this point, the DGP was intolerable at noontime and 15:00 of all the sunny days. Although, during the afternoon and morning, the DGP was imperceptible with one exception: September 21. On September 21 at 9:00 in the morning, the DGP value was 39%, a perceptible glare condition.

Summary

In general, glare in DSF among simulated periods and hours happened significantly between noontime and 15:00. During morning and afternoon time for most of the points were glare-free conditions. The points were located far from the window like A and A', rarely experienced glare. On the other hand, at points B, B', C, and C', the glare happened potentially due to their distance to the window. The DGP value was higher at Points A, B, and C than points A', B', and C' were looking with 45° view direction. The simulation results demonstrated that DGP values were higher when the simulated day was sunny, and the DGP value decreased significantly when the weather condition was overcast. During December time, it should be noted that there was no sun in the sky due to the early sunset time (before 18:00). Consequently, there were no results of the DGP values for December 21 and 22 have been presented.

4.3.2. Point-in-time glare analysis for scenario 2: Venetian blind down, with the tilt angle of 0°

In order to analyze the effect of the Venetian blind on the glare circumstances of the DSF, two scenarios with the Venetian blind have been selected and analyzed. These scenarios have been considered scenario two (0° slat angle) and scenario three (30° slat angle). Scenario two was considered for the condition that the blind was pulled down and its slat has 0° angle. The DSF's motorized Venetian blind was placed between the cavities of the façade skins. The size of it is 3cm, and it is controlled automatically using the mechanism in the DSF. The number of selected dates and times was decreased based on the achieved glare analysis results in the previous section. For the analysis with Venetian blind, the dates and time capable for the glare situation have been selected. Therefore, the hour of 18:00 has been excluded since rarely glare happened at this time in the condition without a blind. The simulation dates selected for this analysis were as follow: March 21, June 21, September 21, and December 22 as sunny days and March 24, June 19, September 24, December 21 as days with overcast sky condition. Some days are the same as the previous simulations, but some have been changed to have fully overcast or sunny sky conditions. Moreover, the radiance parameters have been changed for the simulation with the Venetian blind. Based on the suggested in Mardaljevic [104], the simulation radiance parameters for the condition with blind was according to Table 8:

Table 8. The Radiance parameters for the simulation with Venetian blind

Parameter	Description	Value
-aa	Ambient accuracy	0.1
-ab	Ambient bounces	7
-ar	Ambient resolution	300
-ad	Ambient divisions	1500
-as	Ambient super-samples	1024
-dj	Direct jittering	0.5
-ds	Direct sampling ratio	0.25
-dc	Direct certainty	0.5
-dr	Direct relays	1
-dp	Direct- present density	256
-ps	Pixel sampling rate	4
-pt	Sampling threshold	0.1
-st	Specular sampling threshold	0.5
-lr	Limit reflections	6
-lw	Limit weight of each ray	0.01

The results of the simulations for scenario two are shown in Figures 39-44. According to the results at point A, the highest glare condition was back to December 21 at noontime. The DGP value for this time was 100%, while at other times, there was not any high amount of DGP at this point. For example, the second-highest amount of DGP was 35% which is perceptible glare relates to March 21 and December 19 at noon. For point B, the DGP amount was increased compared to point A. At the noontime of December 21 and March 21, the DGP amount was 100% and 40%, respectively. The glare condition was a perceptible class on September 21 and December 19 at noon with the DGP value of 39%. During all sunny days for point C, the glare condition in DSF was intolerable. However, on overcast days the peak of DGP value was 45% and 42% that happened on September 24 at 15:00 and December 19 at noon, respectively.

For the points A', B', and C', the DGP values were lower than the point looking directly to the window. So that, at point A' for all simulated times, the glare condition was imperceptible with the DGP value lower than 35%. While at point B’ except on noontime of December 22 with DGP value of 36% and march 21 with 35%, other hours were experienced imperceptible glare condition. On December 22, the DGP value was 100% at noon, and it was the highest amount at point C’. The glare was intolerable on 15:00 pf March 21 and September 21 with DGP values of 47% and 45%, respectively.

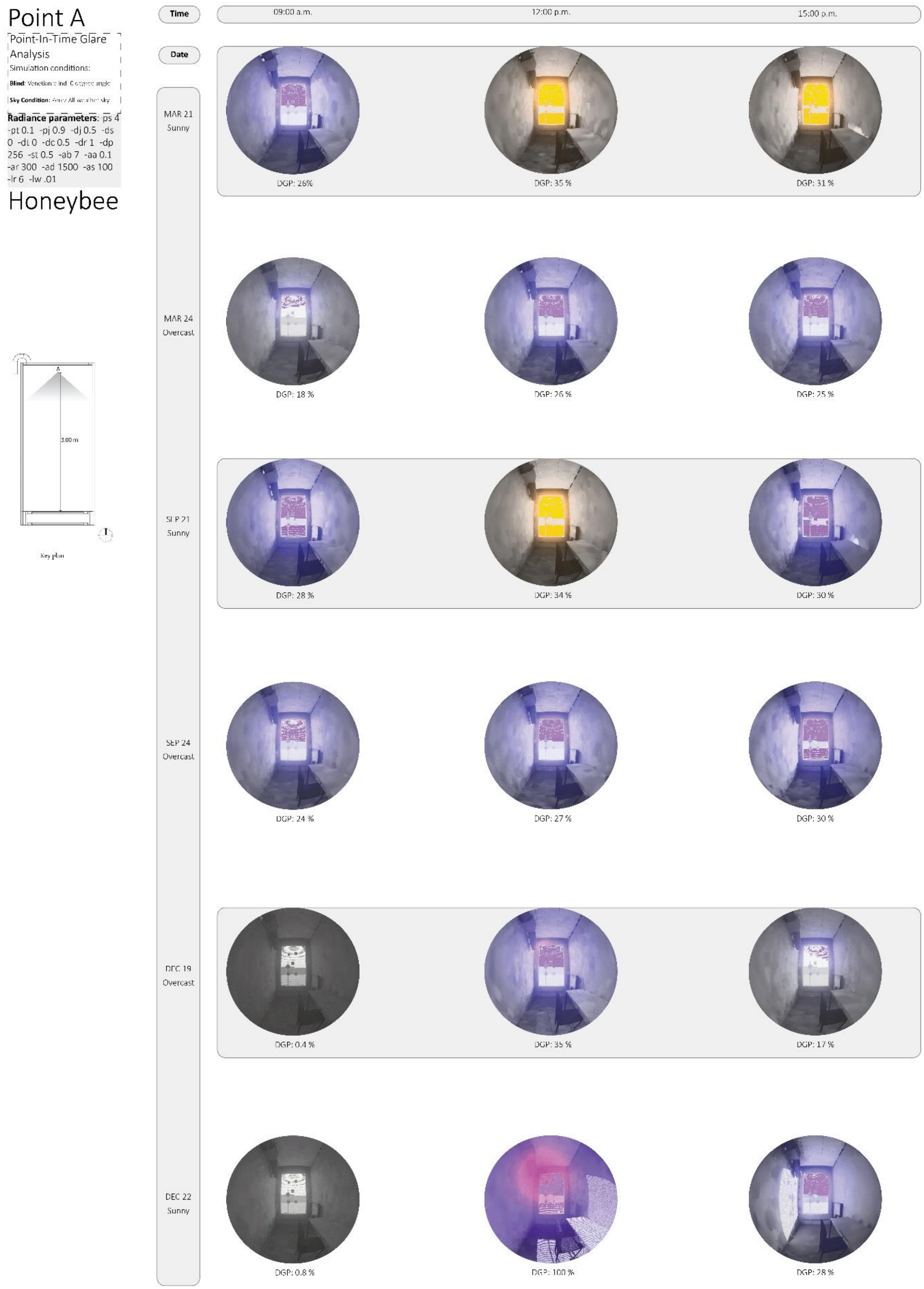

Figure 39. Results of scenario two; $DGP_{point\text{-}in\text{-}time}$ and DGP_{annual} at point A with Perez all-weather sky

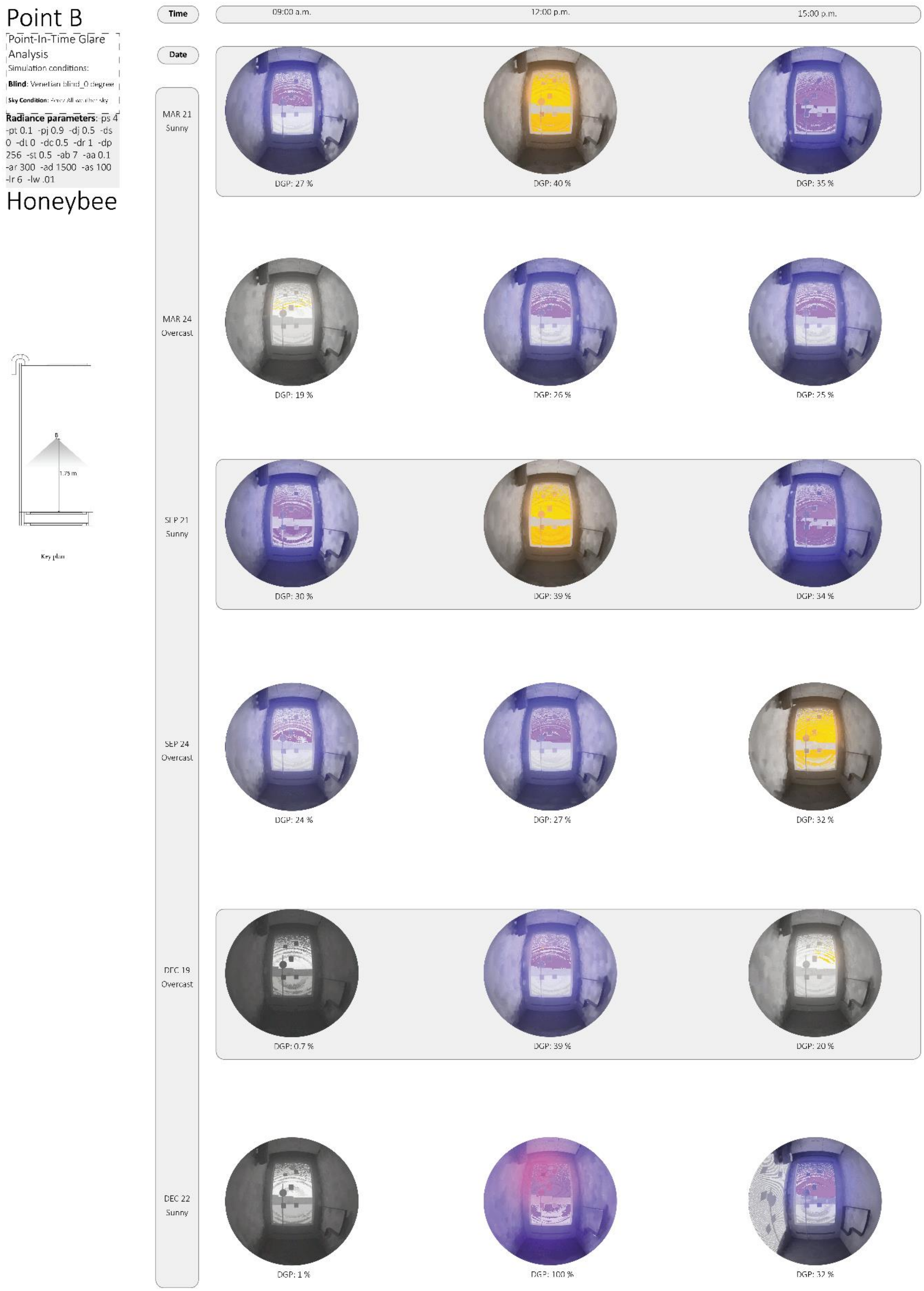

Figure 40. Results of scenario two; $DGP_{point\text{-}in\text{-}time}$ and DGP_{annual} at point B with Perez all-weather sky

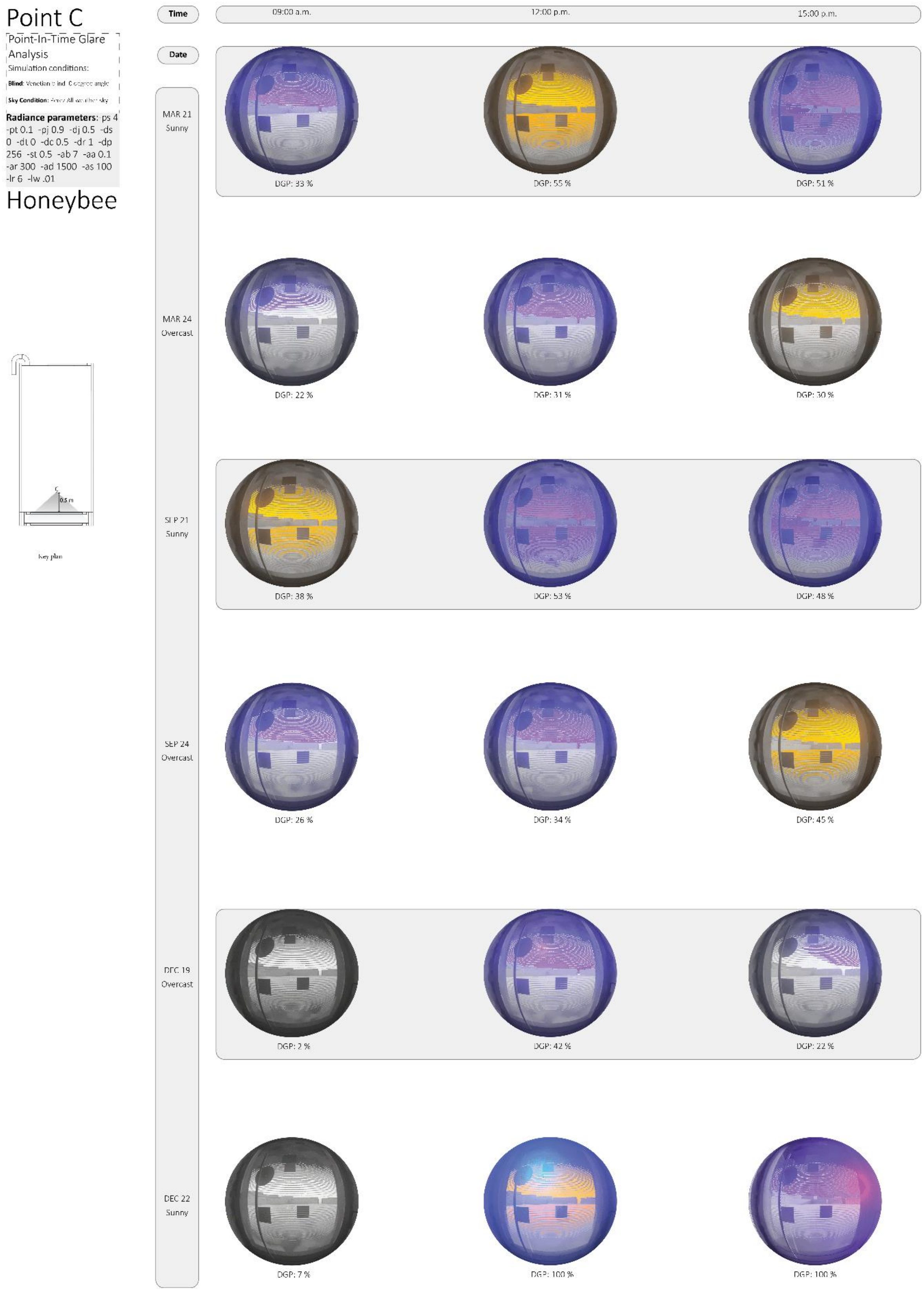

Figure 41. Results of scenario two; $DGP_{point\text{-}in\text{-}time}$ and DGP_{annual} at point C with Perez all-weather sky

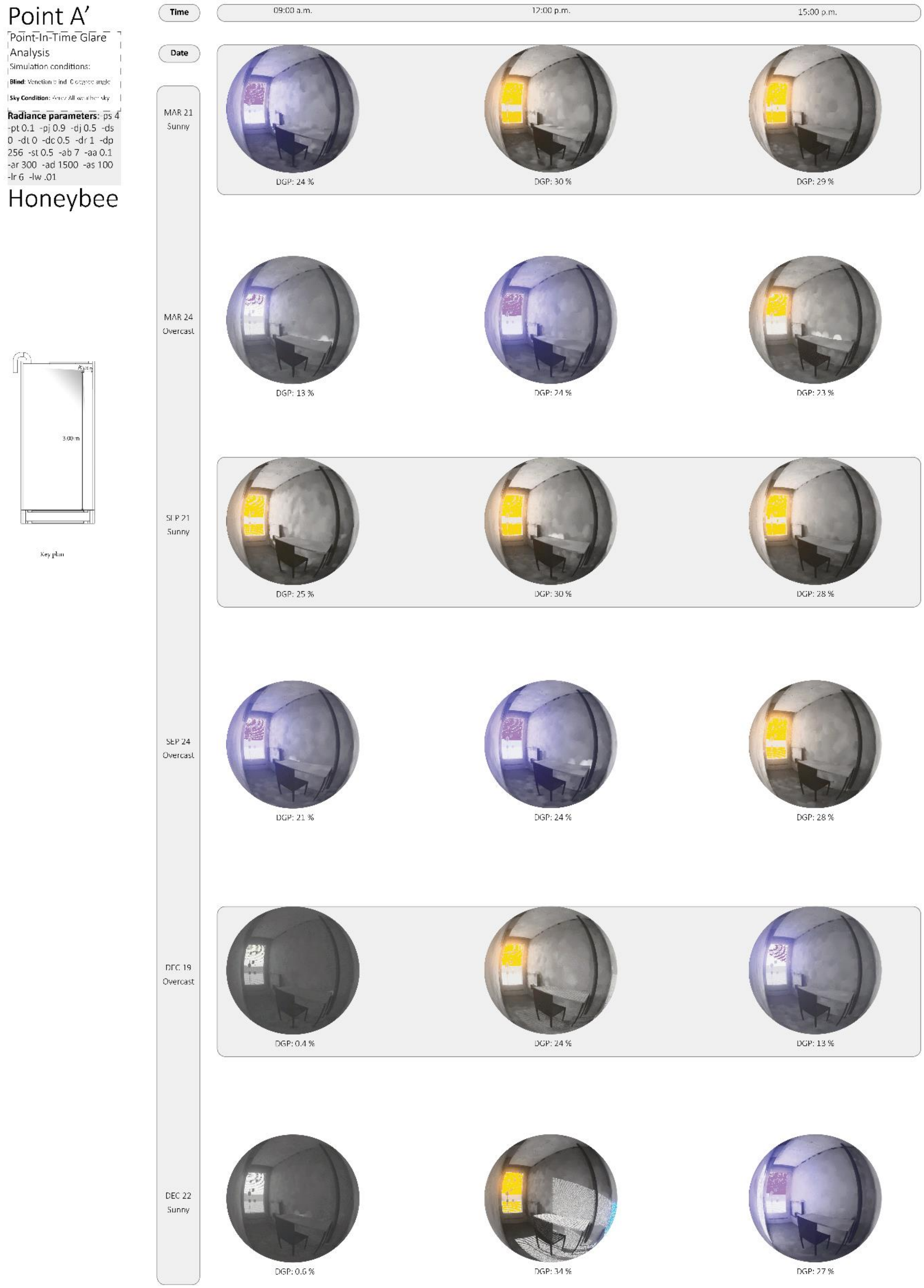

Figure 42. Results of scenario two; $DGP_{point\text{-}in\text{-}time}$ and DGP_{annual} at point A’ with Perez all-weather sky

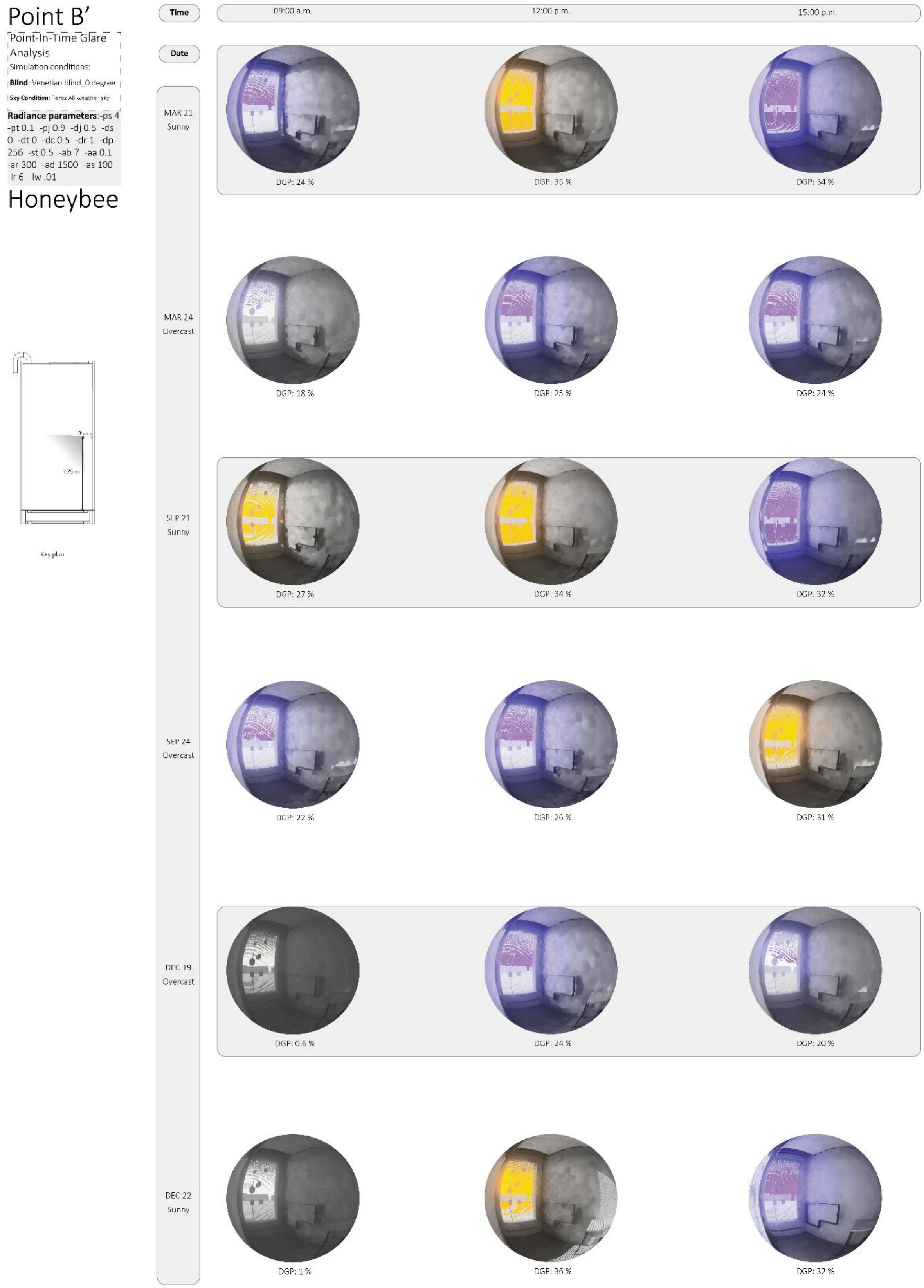

Figure 43. Results of scenario two; $DGP_{point\text{-}in\text{-}time}$ and DGP_{annual} at point B' with Perez all-weather sky

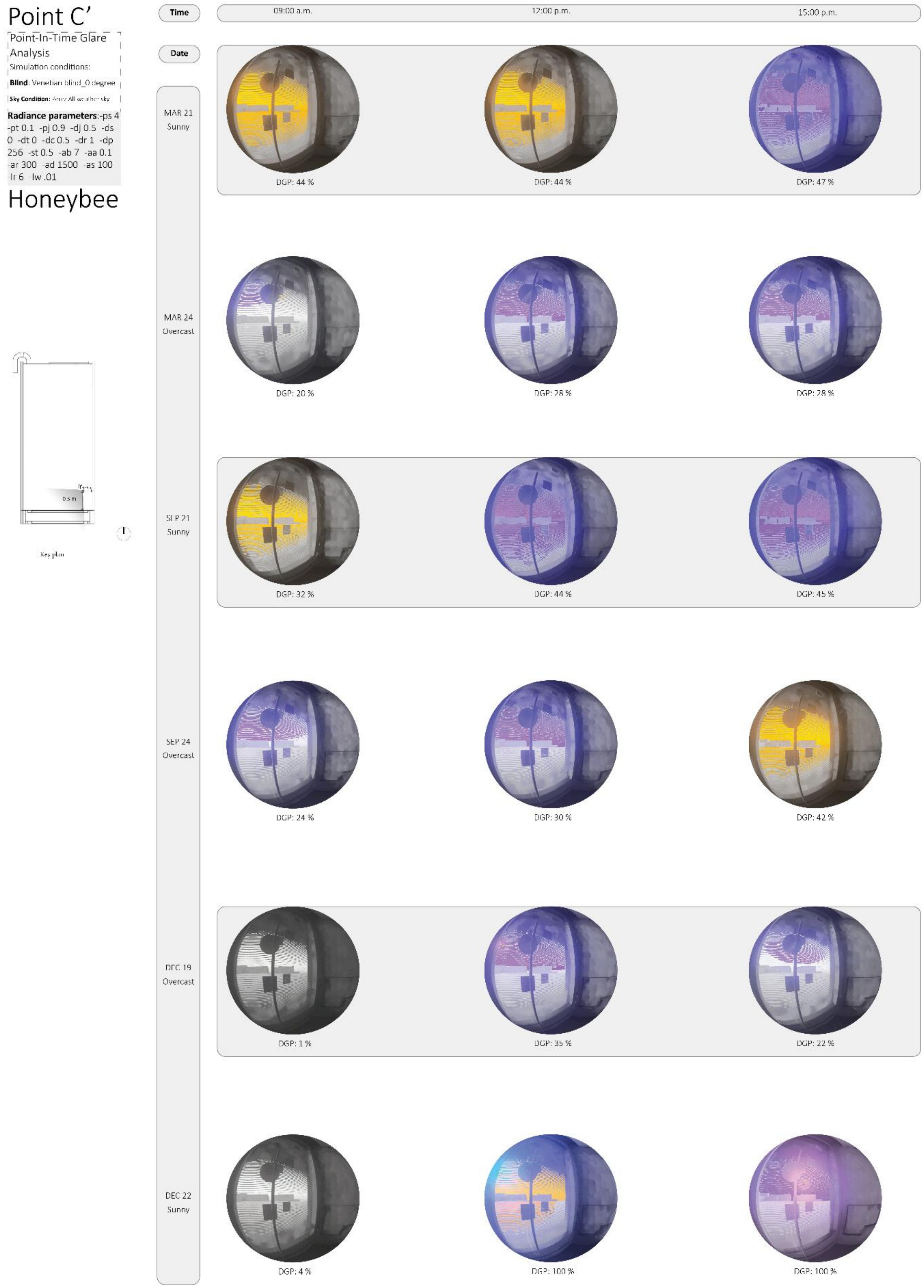

Figure 44. Results of scenario two; $DGP_{point\text{-}in\text{-}time}$ and DGP_{annual} at point C' with Perez all-weather sky

4.3.3. Point-in-time glare analysis for scenario 3: Venetian blind down, with the tilt angle of 30°

As mentioned before, for scenario three, the pulled-down Venetian blind with a 30° slat angle has been considered for glare investigation. In this scenario, the point-in-time glare analysis was conducted for the same month and time with scenario two. The corresponding results of simulations are presented in Figures 45-50.

Based on the results, there was no glare in the test cell with a 30° slat angle Venetian blind. Therefore, most of the simulated times, the glare condition was imperceptible. At point A, the highest DGP value was 27% which happened three times at noon on March 21, September 21, and December 21. Although the DGP value increased at point B, this increment was negligible. The highest DGP was related to the noontime of September 21, with a value of 28%. While at point C, the perceptible glare was observed. On September 21 at noon, the DGP value was 39%, the highest DGP among all the points and simulated times. The second highest DGP value was recoded at point C on March 21 at noon and point C' at noon of September 21 with 36%.

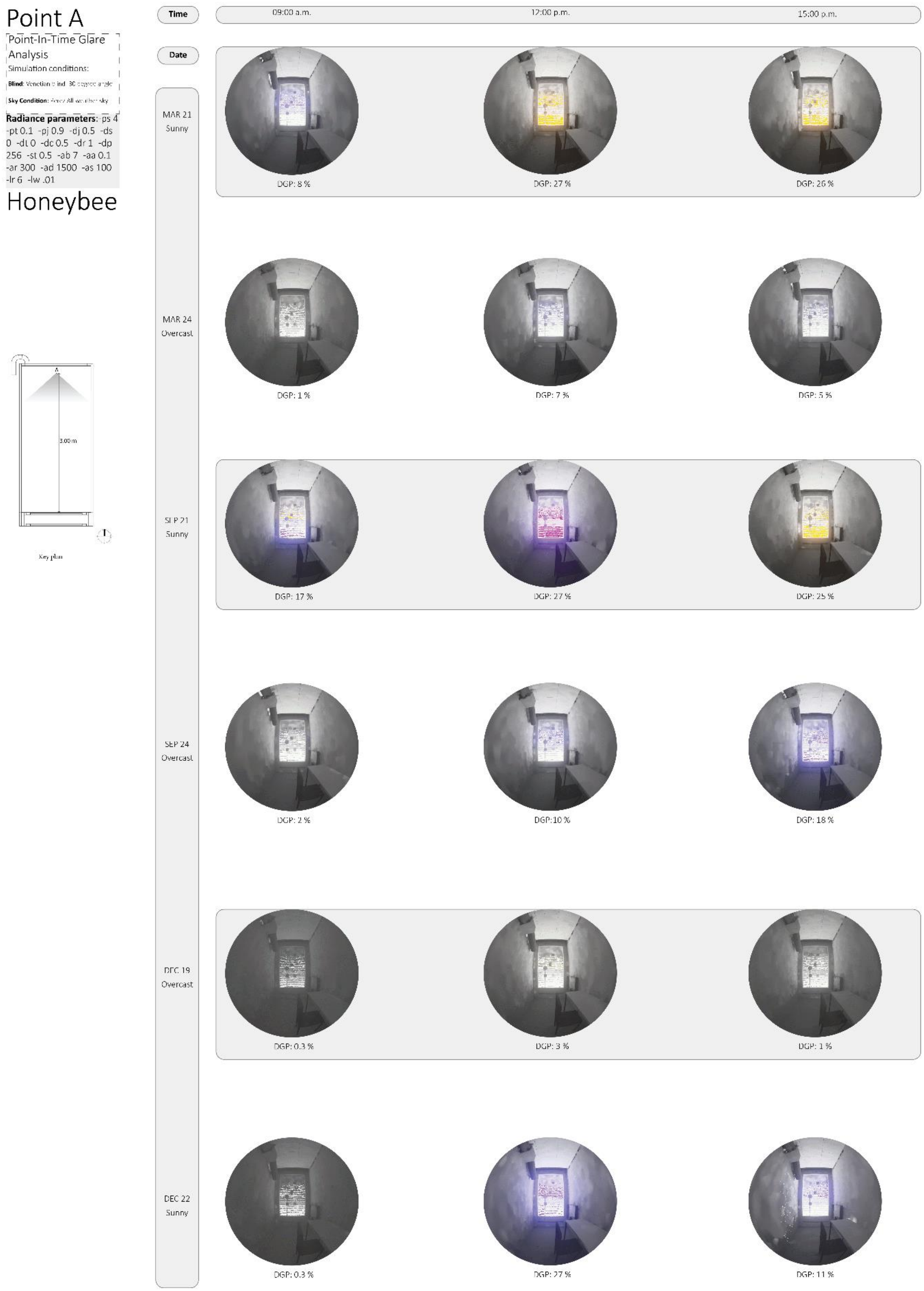

Figure 45. Results of scenario three; $DGP_{point\text{-}in\text{-}time}$ and DGP_{annual} at point A with Perez all-weather sky

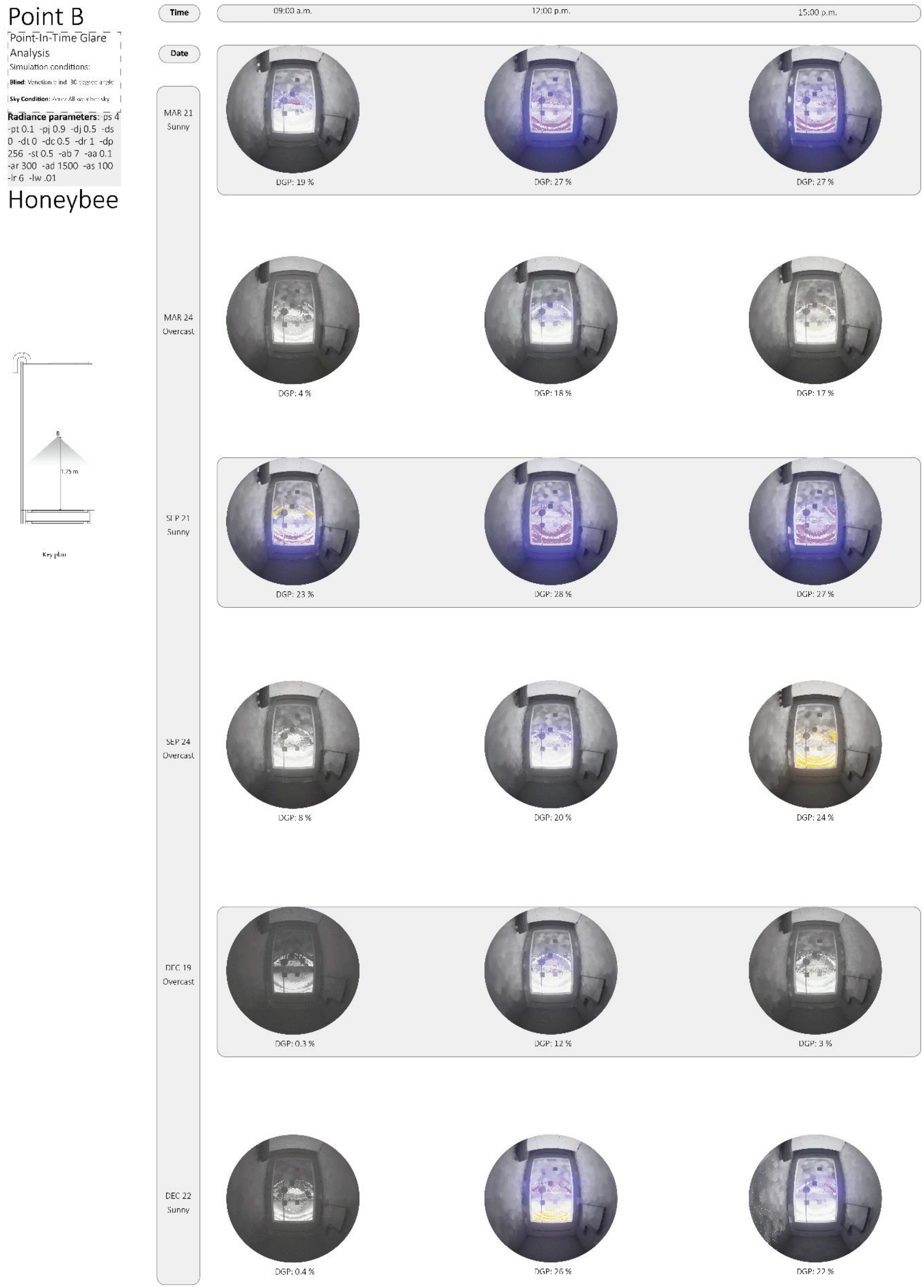

Figure 46. Results of scenario three; $DGP_{point\text{-}in\text{-}time}$ and DGP_{annual} at point B with Perez all-weather sky

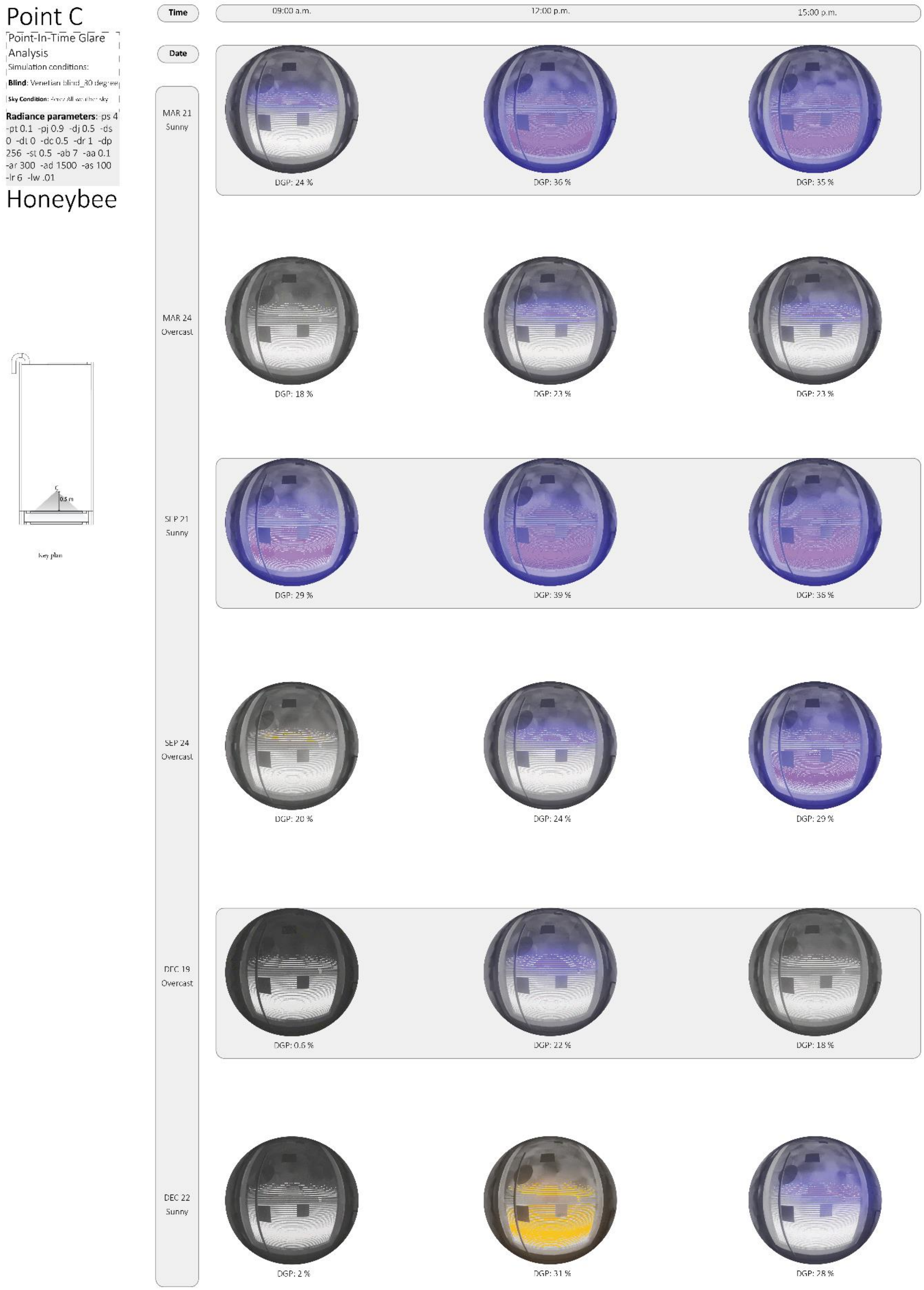

Figure 47. Results of scenario three; $DGP_{point\text{-}in\text{-}time}$ and DGP_{annual} at point C with Perez all-weather sky

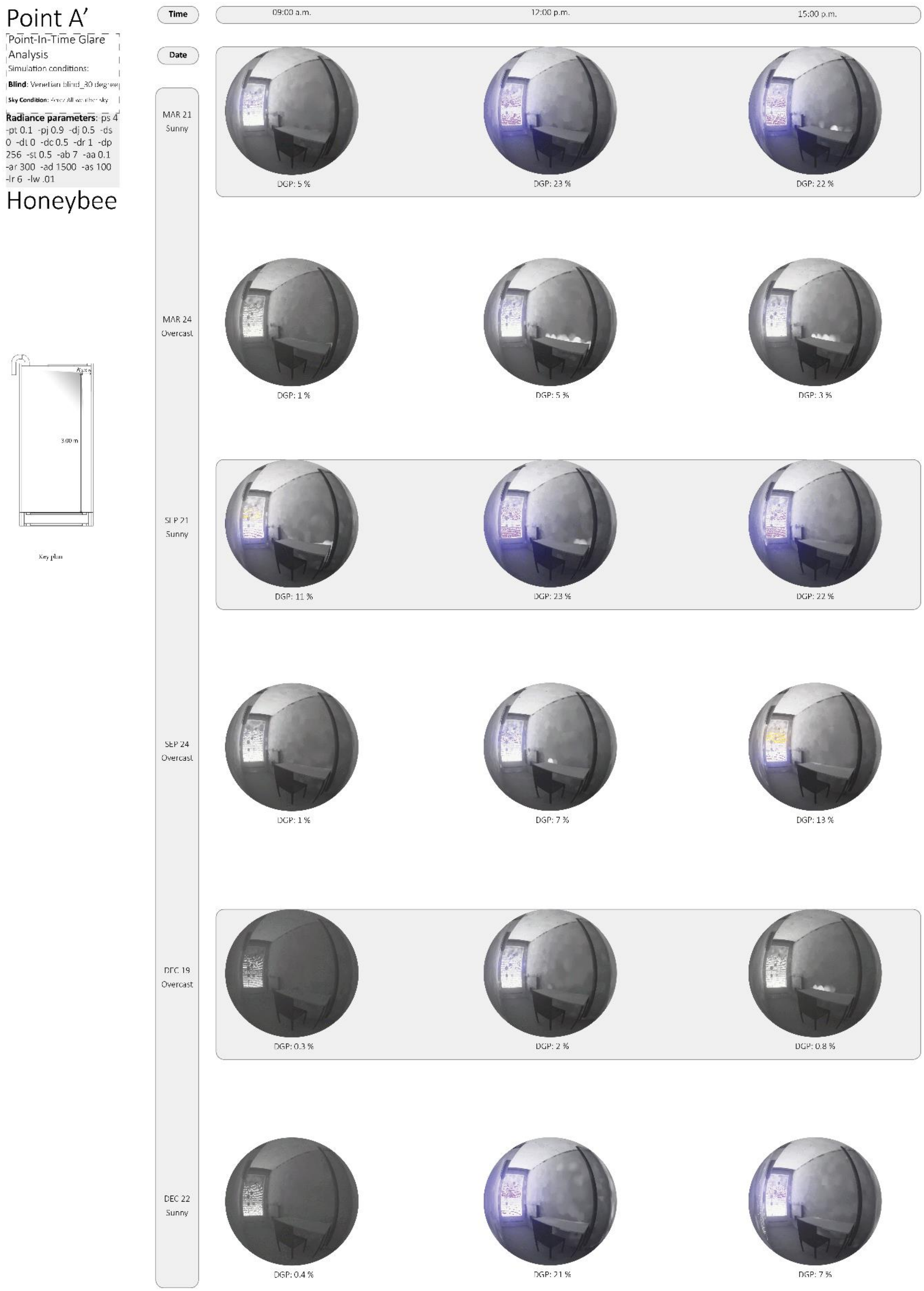

Figure 48. Results of scenario three; $DGP_{point\text{-}in\text{-}time}$ and DGP_{annual} at point A’ with Perez all-weather sky

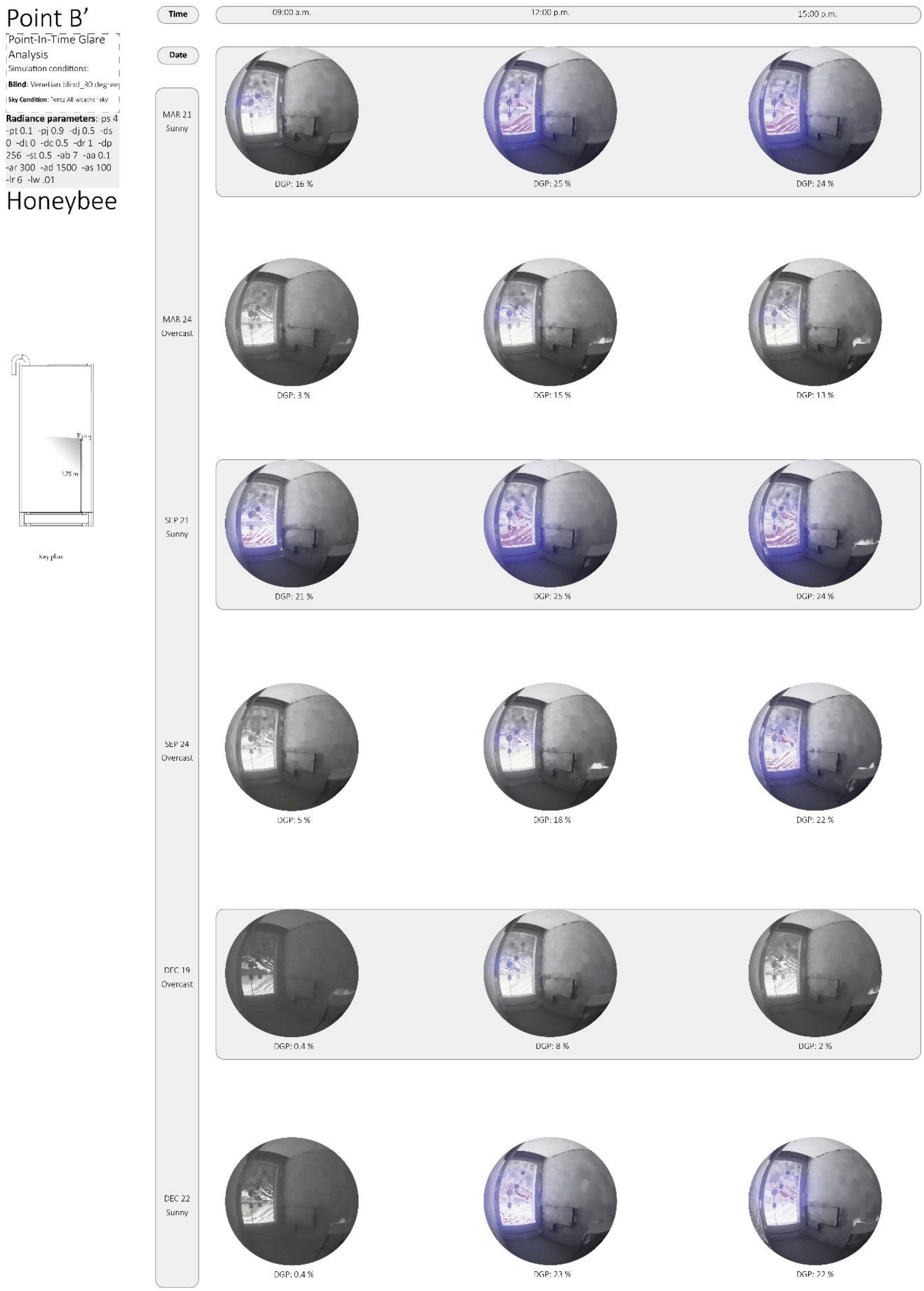

Figure 49. Results of scenario three; $DGP_{point\text{-}in\text{-}time}$ and DGP_{annual} at point B’ with Perez all-weather sky

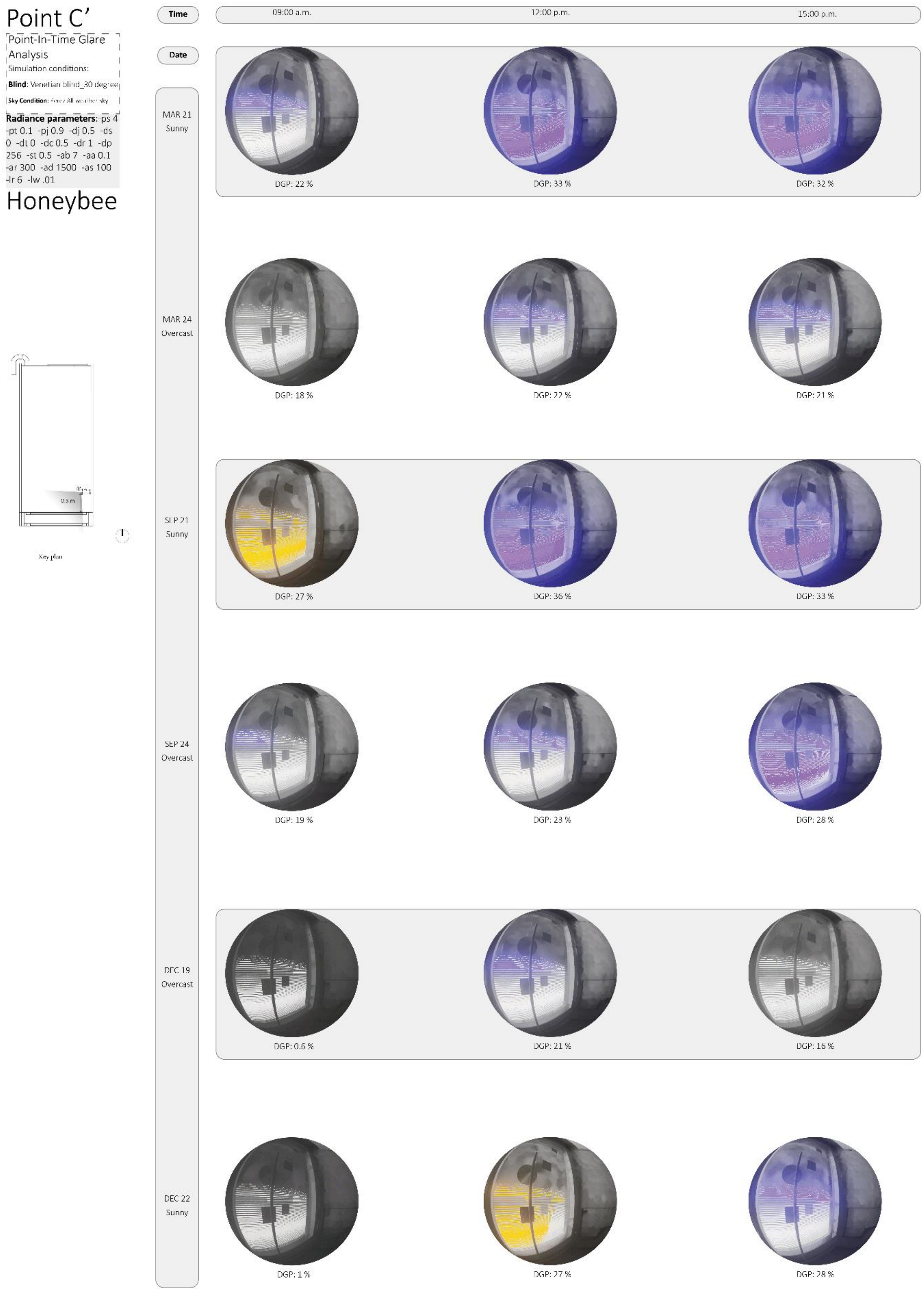

Figure 50. Results of scenario three; $DGP_{point\text{-}in\text{-}time}$ and DGP_{annual} at point C' with Perez all-weather sky

4.4. Annual glare analysis

The Annual DGP calculations were conducted with the "Annual Glare" simulation option on DIVA-for-Rhino for the same points. The occupancy schedule considering for these simulations was from 8 a.m. to 6 p.m., the usual working period and potential period for daylighting. The sky model for annual glare analysis was the same as the previous section (point-in-time glare analysis), the Perez All-Weather sky model generated from the Torino weather file. The Radiance parameters inserted in Diva for conducting annual glare analysis are shown in Table 9.

Table 9. The Radiance parameters of the DGPannual simulation

Parameter	Description	Value
-aa	Ambient accuracy	0.1
-ab	Ambient bounces	5
-ar	Ambient resolution	300
-ad	Ambient divisions	1000
-as	Ambient super-samples	20
-dj	Direct jittering	0.5
-ds	Direct sampling ratio	0.25
-dc	Direct certainty	0.5
-dr	Direct relays	1
-dp	Direct- present density	256
-ps	Pixel sampling rate	4
-pt	Sampling threshold	0.1
-st	Specular sampling threshold	0.5
-lr	Limit reflections	6
-lw	Limit weight of each ray	0.01

4.4.1. Annual glare analysis for scenario one

The Annual DGP calculations have been done separately for each scenario. In Figure 51 the results of annual glare at points A, B, and C have been illustrated.

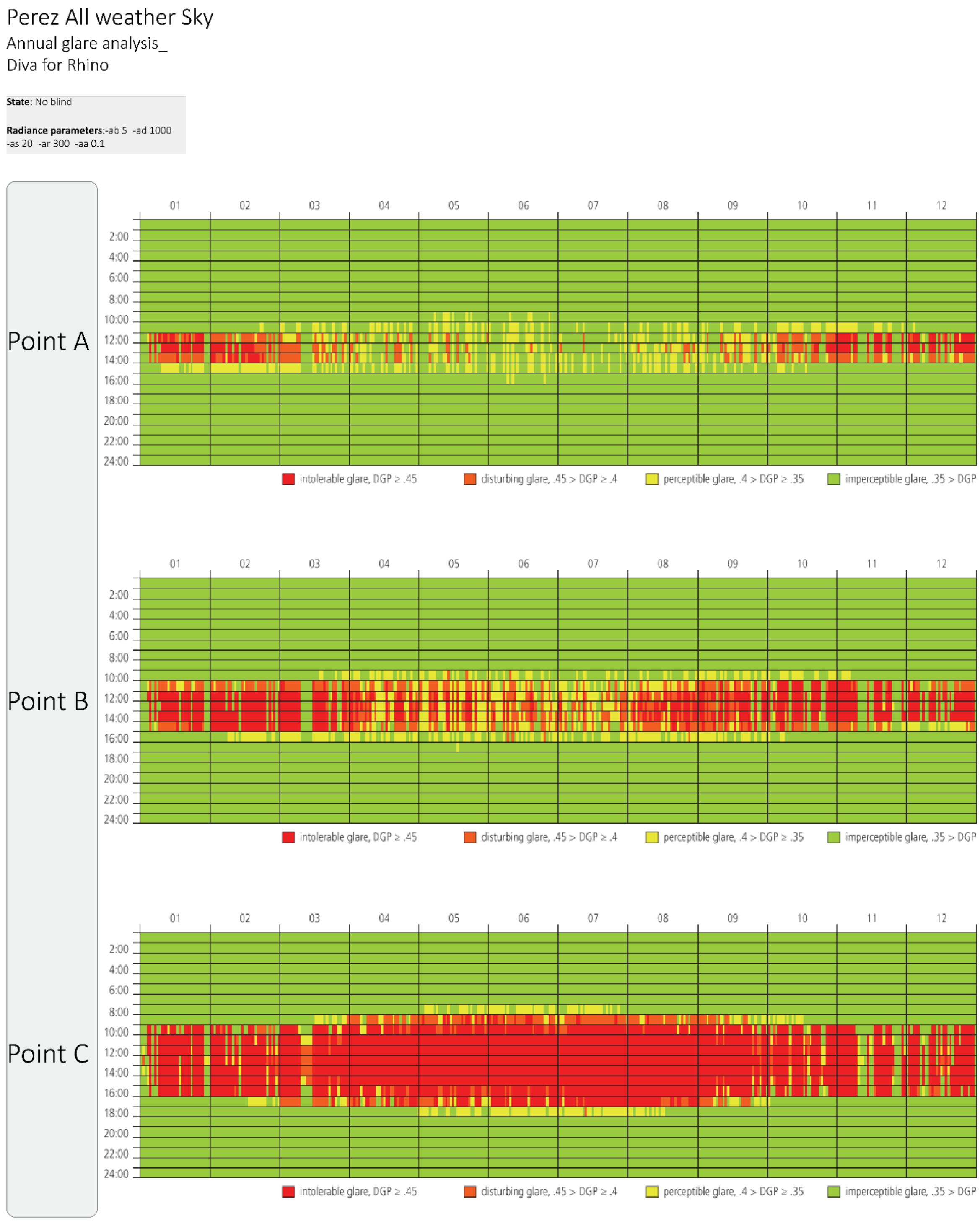

Figure 51. Results of DGP_{annual} for points A, B, C in scenario one

The annual DGP for points A resulted in an "imperceptible" glare for most of the hours in a year. The intolerable glare happened during January, February, and the first days of

March between 12:00 to 14:00. The same situation (intolerable glare) was also observed during the winter months, from mid-October to the end of December. For other months, there were imperceptible glare or, in the worth situation, perceptible glare conditions. The result was not a surprise, once the preliminary point-in-time showed low illuminance levels on the office's interior, indicating that the space has low brightness. At point B, the annual DGP showed more hours with intolerable glare. January to March and September to October, the intolerable glare happened from 11:00 to 15:00. From April to July, the annual DGP were either perceptible or disturbing glare condition. However, in point C, the annual glare during the whole year was mainly intolerable between 9:00 to 17:00. The imperceptible glare was only observed before 9:00 in the morning and after 17:00.

Comparison the results for points A', B', and C' demonstrated that the glare hours were decreased compared with points A, B, and C. As can be seen in Figure 52, in point A' the hours with imperceptible glare were increased in compared with the point A.

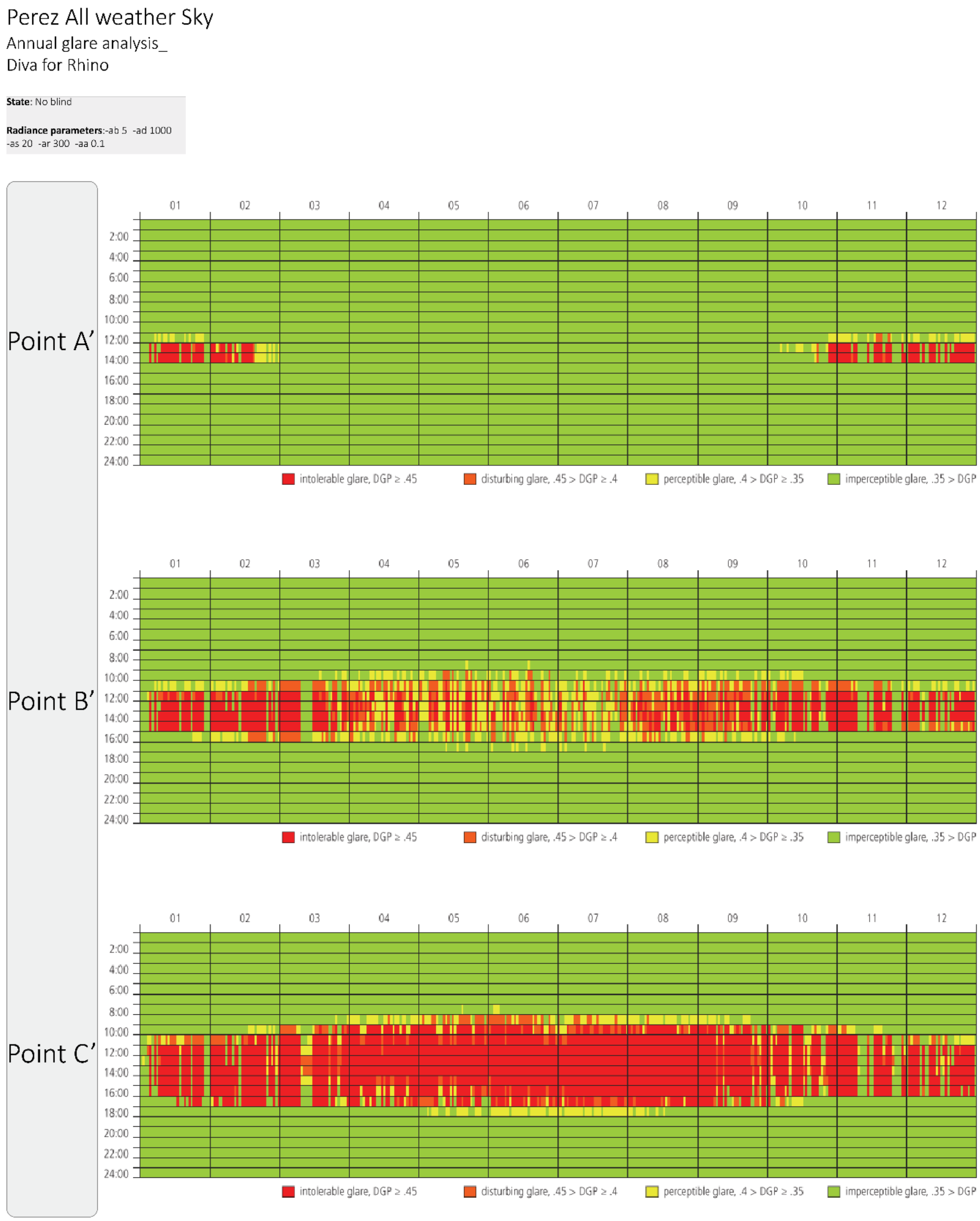

Figure 52. Results of DGP_{annual} for points A', B', C' in scenario one

From March to the end of September, the DGP annual showed imperceptible glare potentially for all the hours at point A'. the intolerable glare happened during January, February, November, and December at noon and 14:00. For point B', the DGP values were utterly different from point A'. The DGP values were higher than 35% for most of the year between 10:00 and 16:00. In comparison with point B, at this point, the DGP values were similar however the hours with perceptible and disturbing glare increased in the summertime. The simulation results showed DGP values higher than 45% for most times of the year at point C'. The annual DGP values at this point were very similar to the annual results of point C. The hours with an intolerable glare at point C' started from 9:00 morning during summer months while the DGP values for point C started from 8:00. During summer months, some hours, especially in the morning, were perceptible and disturbing glare while the similar hours at point C were intolerable.

4.4.2. Annual glare analysis for scenario two

The annual DGP values were calculated for scenario one in case of the existence of Venetian blind with 0° angle. The corresponding results have been presented in Figures 53-54.

The simulation results showed that the DGP values were lower than 35% for most of the year at points A and B. The perceptible glare happened between 12:00 to 14:00 in January, February, November, and December at point A. At this point, the disturbing glare condition only happened around 13:00 during mentioned months (Figure 53). For point B, the hours with disturbing glare were observed between 12:00 to 15:00 during February to March and October to December. A few hours in April, May, and September with the perceptible glare condition were detected. On point C, however, the glare conditions were higher and happened most of the year. The DGP values were higher than 40% from 10:00 to 16:00 during months January to march and October to December. For other months the DGP value mainly was between 35% and 40% (perceptible glare).

On the other hand, the glare at point A’ decreased compared to point A, and the disturbing glare was limited to the hour of 13:00 in January, part of February, and November. Figure 54 shows that in December, the glare was disturbing around 13:00 and 14:00. At point B’, the hours with glary condition increased compared to point A’ but was lower than point B. The glare happened during January, February, March, and October to December between 13:00 to 15:00. The duration of the disturbing and intolerable glare was increased in point C’ in comparison with point C, and it occurred between 12:00 to 17:00 of January to March. However, during summertime, the glare was mainly perceptible in the DSF at point C’, and from August to the end of the year, the DGP values were higher than 45%.

Perez All weather Sky

Annual glare analysis_

Diva for Rhino

State: Venetian blind_0 degree angle

Radiance parameters:-ab 7 -ad 1500 -as 100 -ar 300 -aa 0.1

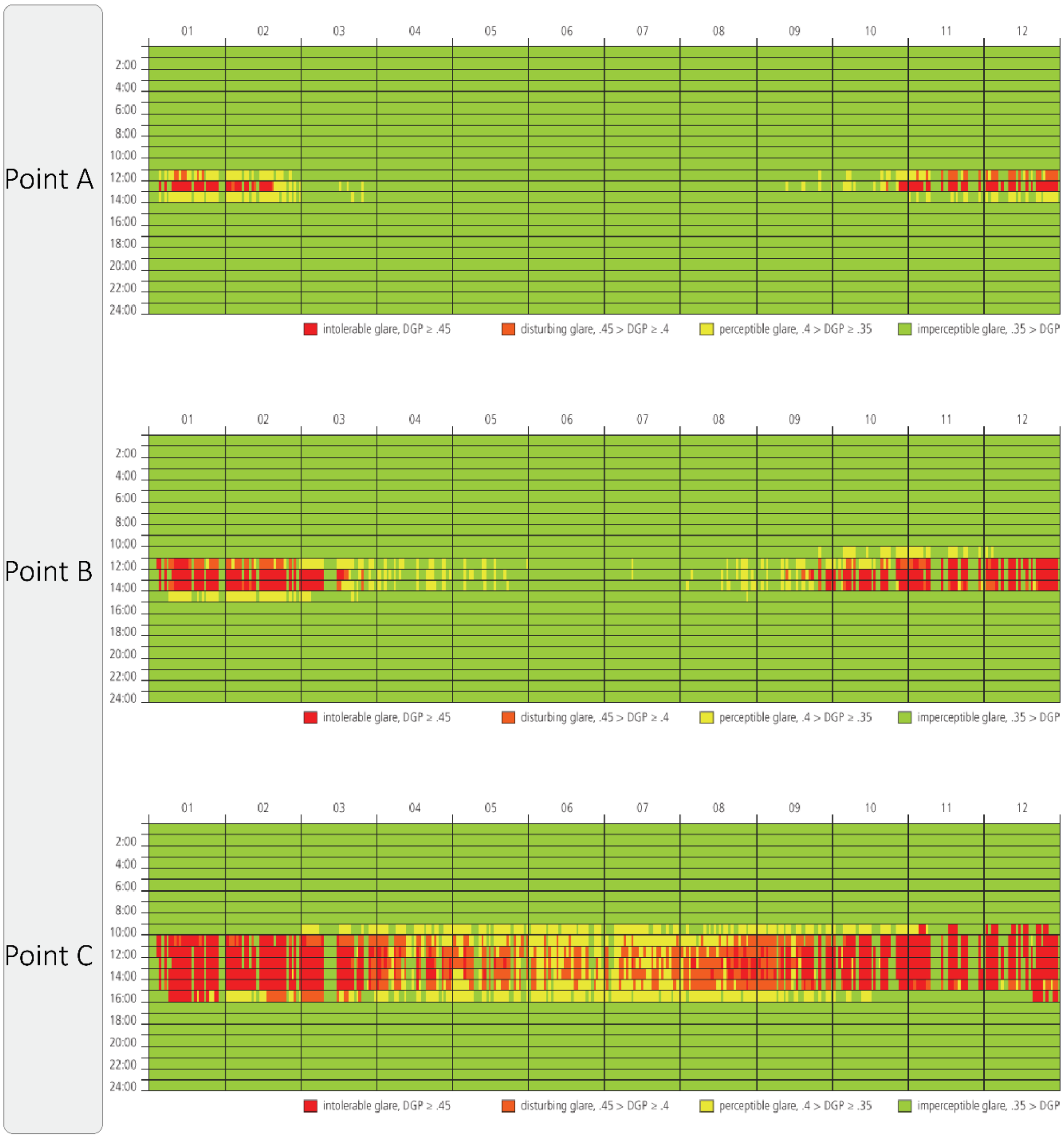

Figure 53. Results of DGP_{annual} for points A, B, C in scenario two

Perez All weather Sky

Annual glare analysis_

Diva for Rhino

State: Venetian blind_0 degree angle

Radiance parameters:-ab 7 -ad 1500 -as 100 -ar 300 -aa 0.1

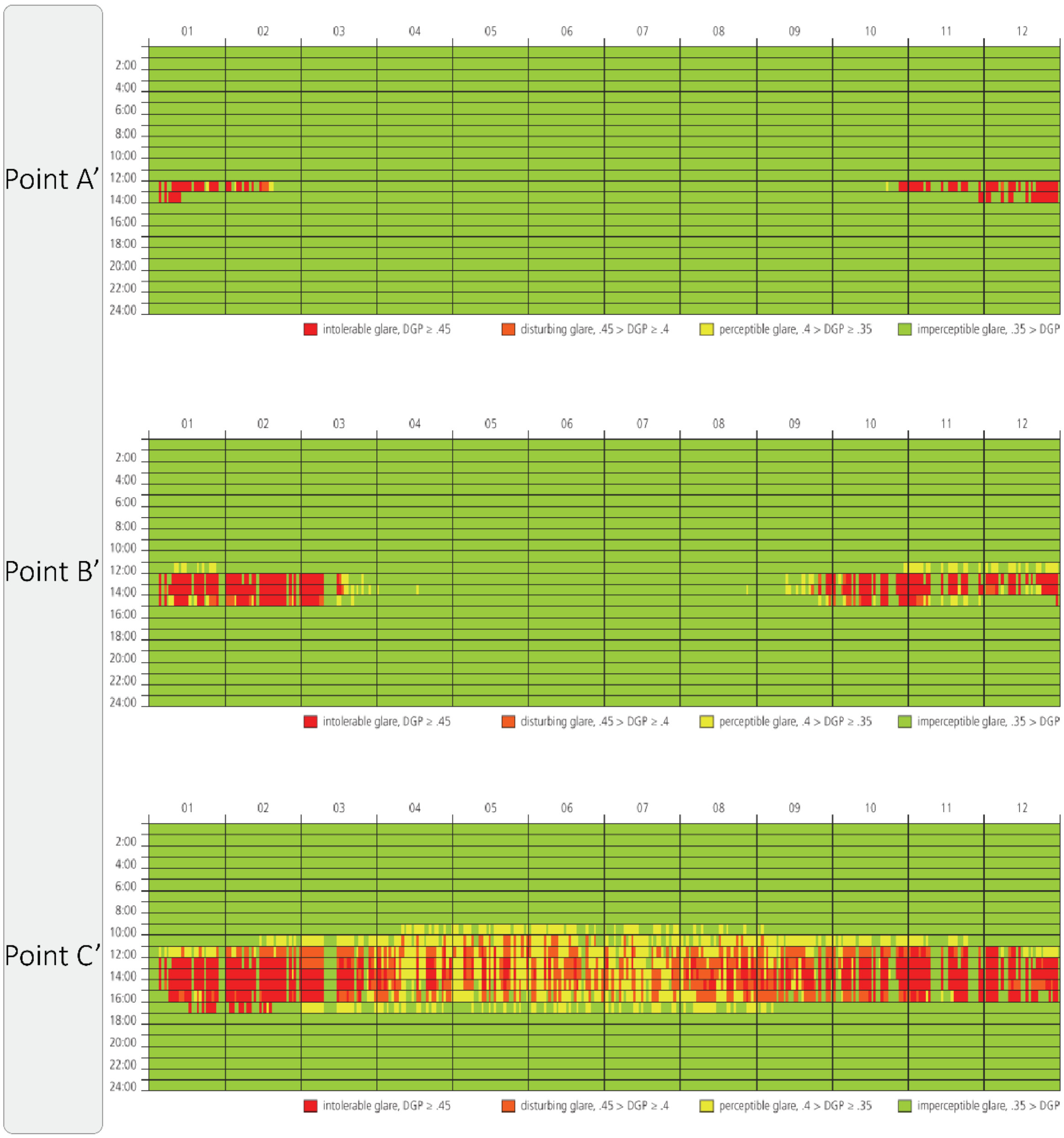

Figure 54. Results of DGP_{annual} for points A’, B’, C’ in scenario two

4.4.3. Annual glare analysis for scenario three

The annual DGP values for scenario three have been depicted in Figures 55-56. As it is clear from the graph, at points A and B, there was only a glare-free condition all-around a year when the Venetian blind with 30° angle was considered. The same condition happened for the points A' and B' in the test cell. A few hours at points C and C' during April, June, and July, the perceptible glare has been observed. The results of this analysis were not surprising since, in the previous section (point-in-time analysis), it was shown that in the presence of Venetian blind with 30° slat angle, the glare condition in the DSF was solved entirely.

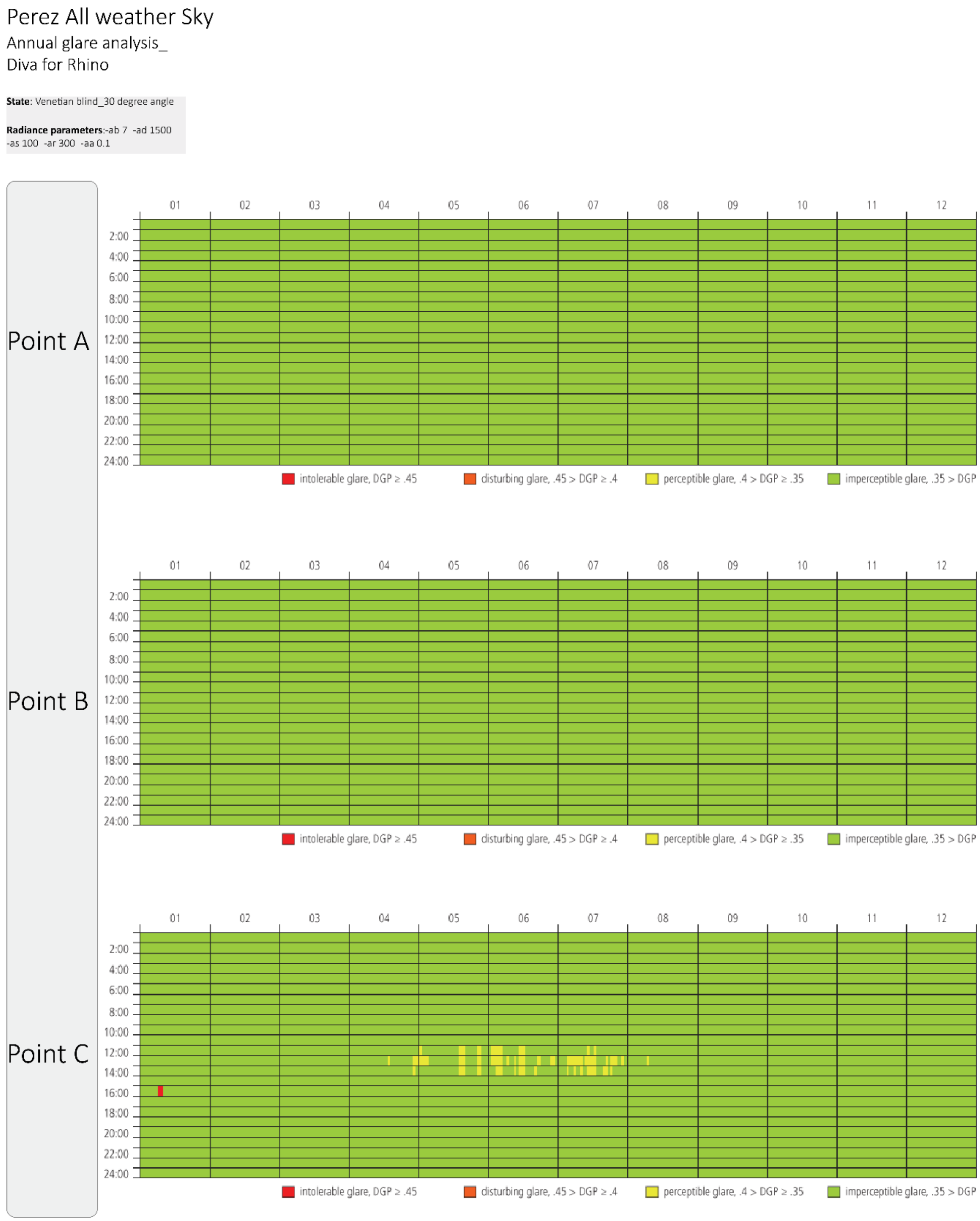

Figure 55. Results of DGP_{annual} for points A, B, C in scenario three

Perez All weather Sky

Annual glare analysis_

Diva for Rhino

State: Venetian blind_30 degree angle

Radiance parameters:-ab 7 -ad 1500 -as 100 -ar 300 -aa 0.1

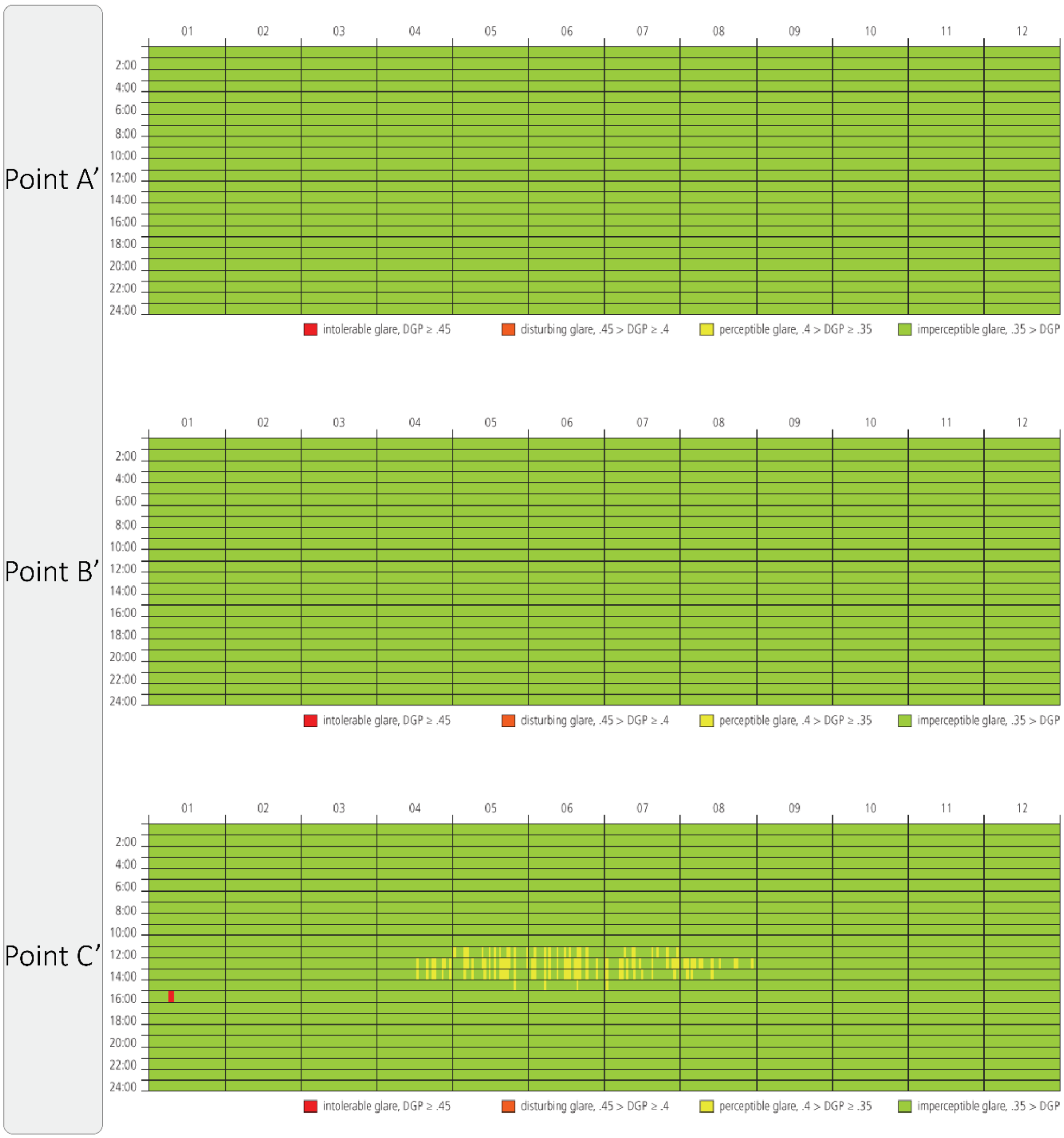

Figure 56. Results of DGP_{annual} for points A', B', C' in scenario three

Summary

Comparing the annual glare and point-in-time analysis results in this study revealed that the DGP amount in conditions without blinds (scenario one) is much more significant than in conditions with blinds (scenarios two and three). In scenario two, the glare was still happened at some hours of the year and on the simulated points. While in the third scenario, the glare has wholly disappeared at all points and all hours. Therefore, it indicates the effect of the blind slat angle on the glare condition of the environment. One of the most important results obtained from the above simulations is that it is enough to achieve visual comfort in DSF to change the angle of the Venetian blind up to 30 degrees. Hence, the analysis of more angles such as 60° and 75° has been excluded in the simulations; however, these angles were measured with HDR images. The results showed that the DGP amount at points A', B', and C' was lower than points A, B, and C. It reveals the relation of the view direction and DGP in the spaces. As a rule, the closer the points got to the window, which was the primary source of entering light in this DSF, the DGP value increased. According to the results obtained in the above simulations, it can be concluded that the DGP_{annual} and the $DGP_{point\text{-}in\text{-}time}$ have provided similar values. However, numerical analysis and comparisons have been carried out to ascertain the correlation between DGP_{annual} and the $DGP_{point\text{-}in\text{-}time}$, and the results are reported in the following sections.

4.5. Comparison of the discomfort glare classes in DGP_{annual} and $DGP_{point\text{-}in\text{-}time}$

The second and third question of this research were:

RQ2. How can glare analyses be simplified through doing annual glare analysis instead of point-in-time glare analysis?

RQ3. What is the correspondence degree between the annual glare analysis and point-in-time analysis?

In order to find the answer to these questions, the results of DGP_{annual} and $DGP_{point-in-time}$ has been analyzed in detail. The results have been categorized based on the discomfort glare classes, and then their classes have been matched. To this end, firstly, the exact amount of each simulated time for each point was extracted and placed in a table. After that, the DGP_{annual} and $DGP_{point-in-time}$ were categorized according to the DGP value in discomfort glare classes. The corresponding color for each discomfort class has been assigned to the DGP values. These colors will help visually comprehend how much the DGP_{annual} and $DGP_{point-in-time}$ were in the same classes at each simulated time. Horizontal illuminance and vertical illuminance values for each point and simulated time has been extracted and presented in the Table.

4.5.1. Discomfort glare classes DGP_{annual} and $DGP_{point-in-time}$ for scenario one

The results regarding the DGP_{annual} and $DGP_{point-in-time}$ for points A, B, C, A', B', and C' have been presented in Tables 11-16.

Table 10. Summary of the results for scenario one at point A

Date	Time	DGP_Annual [-]	DGP_Annual class [-]	DGP_point-in-time class [-]	DGP_point-in-time [-]	Vertical illuminance [lux]	Horizontal illuminance [lux]
21.03	9:00	0.3			0.25	741	368
	12:00	0.44			0.36	2459	1207
	15:00	0.32			0.32	1651	824
	18:00	0.015			0.14	238	113
24.03	9:00	0.26			0.17	306	150
	12:00	0.31			0.25	730	359
	15:00	0.26			0.25	603	313
	18:00	0.006			0.027	111	52
19.06	9:00	0.36			0.25	762	382
	12:00	0.38			0.3	1289	664
	15:00	0.3			0.26	917	479
	18:00	0.21			0.17	296	167
21.06	9:00	0.3			0.24	552	302
	12:00	0.38			0.3	1454	785
	15:00	0.32			0.3	1403	718
	18:00	0.24			0.24	602	316
21.09	9:00	0.28			0.26	903	449
	12:00	0.39			0.35	2306	1095
	15:00	0.29			0.31	1491	711
	18:00	0.01			0.12	208	107
24.09	9:00	0.3			0.22	402	200
	12:00	0.3			0.26	809	428
	15:00	0.29			0.29	1285	654
	18:00	0.003			0.02	82	42
21.12	9:00	0.19			0.004	16	10
	12:00	0.23			0.17	298	157
	15:00	0.21			0.27	978	496
	18:00	0.003			0	0	0
22.12	9:00	0.22			0.009	51	33
	12:00	1			1	29916	10926
	15:00	0.22			0.28	1314	661
	18:00	0.003			0	0	0
A							

Table 11. Summary of the results for scenario one at point B

Date	Time	DGP_Annual [-]	DGP_Annual class [-]	DGP_point-in-time class [-]	DGP_point-in-time [-]	Vertical illuminance [lux]	Horizontal illuminance [lux]
21.03	9:00	0.35			0.28	1608	698
	12:00	0.58			0.51	5367	2726
	15:00	0.4			0.42	4016	1720
	18:00	0.022			0.19	502	230
24.03	9:00	0.27			0.2	678	313
	12:00	0.34			0.28	1574	772
	15:00	0.28			0.27	1374	662
	18:00	0.008			0.13	226	110
19.06	9:00	0.39			0.28	1688	791
	12:00	0.44			0.38	2961	1558
	15:00	0.32			0.31	2206	1023
	18:00	0.21			0.2	718	352
21.06	9:00	0.32			0.26	1327	638
	12:00	0.46			0.4	3415	1616
	15:00	0.36			0.38	3088	1349
	18:00	0.24			0.25	1339	573
21.09	9:00	0.35			0.3	2148	871
	12:00	0.49			0.47	4966	2104
	15:00	0.36			0.39	3707	1423
	18:00	0.013			0.018	476	207
24.09	9:00	0.33			0.23	896	399
	12:00	0.33			0.3	2027	722
	15:00	0.33			0.35	2760	1348
	18:00	0.003			0.099	194	88
21.12	9:00	0.2			0.14	41	23
	12:00	0.25			0.2	694	320
	15:00	0.24			0.27	2312	1002
	18:00	0.003			0	0	0
22.12	9:00	0.26			0.033	124	67
	12:00	1			1	31753	2293
	15:00	0.25			0.34	2978	1414
	18:00	0.003			0	0	0
B							

Table 12. Summary of the results for scenario one at point C

Date	Time	DGP_Annual [-]	DGP_Annual class [-]	DGP_point-in-time class [-]	DGP_point-in-time [-]	Vertical illuminance [lux]	Horizontal illuminance [lux]
21.03	9:00	0.51			0.4	4457	2215
	12:00	1			1	30127	20864
	15:00	0.7			0.75	10986	6281
	18:00	0.07			0.23	1519	754
24.03	9:00	0.34			0.26	2043	1018
	12:00	0.46			0.41	4818	2498
	15:00	0.36			0.38	4222	2239
	18:00	0.015			0.19	660	350
19.06	9:00	0.55			0.43	5102	2722
	12:00	0.69			0.69	9529	7623
	15:00	0.43			0.49	6626	3526
	18:00	0.24			0.26	2056	1140
21.06	9:00	0.43			0.37	4075	2148
	12:00	0.77			0.75	11180	15853
	15:00	0.57			0.7	10223	5160
	18:00	0.29			0.36	3987	1737
21.09	9:00	0.51			0.46	5479	2592
	12:00	1			1	46446	34454
	15:00	0.67			0.66	8856	4791
	18:00	0.03			0.23	1385	676
24.09	9:00	0.45			0.3	2679	1373
	12:00	0.45			0.45	5786	3455
	15:00	0.54			0.62	8867	4898
	18:00	0.003			0.19	585	294
21.12	9:00	0.22			0.19	119	76
	12:00	0.3			0.26	1995	1042
	15:00	0.65			0.86	9673	3599
	18:00	0.003			0	0	0
22.12	9:00	0.23			0.17	347	221
	12:00	1			1	36348	12394
	15:00	0.95			1	18556	6097
	18:00	0.003			0	0	0
C							

Table 13. Summary of the results for scenario one at point A'

Date	Time	DGP_Annual [-]	DGP_Annual class [-]	DGP_point-in-time class [-]	DGP_point-in-time [-]	Vertical illuminance [lux]	Horizontal illuminance [lux]
21.03	9:00	0.23			0.23	573	346
	12:00	0.33			0.31	1725	1081
	15:00	0.25			0.29	1229	879
	18:00	0.006			0.1	162	114
24.03	9:00	0.22			0.14	189	145
	12:00	0.24			0.23	448	334
	15:00	0.22			0.23	491	300
	18:00	0.004			0.018	77	48
19.06	9:00	0.26			0.23	580	376
	12:00	0.26			0.27	930	670
	15:00	0.24			0.24	626	467
	18:00	0.12			0.15	237	163
21.06	9:00	0.23			0.22	462	301
	12:00	0.27			0.27	1088	735
	15:00	0.24			0.27	1005	717
	18:00	0.21			0.22	485	294
21.09	9:00	0.23			0.24	710	429
	12:00	0.32			0.31	1925	1031
	15:00	0.23			0.28	1199	730
	18:00	0.005			0.08	167	111
24.09	9:00	0.24			0.2	276	192
	12:00	0.24			0.24	629	417
	15:00	0.23			0.27	1019	672
	18:00	0.003			0.014	68	42
21.12	9:00	0.05			0.018	14	10
	12:00	0.21			0.15	230	148
	15:00	0.19			0.26	873	526
	18:00	0.003			0	0	0
22.12	9:00	0.2			0.007	40	30
	12:00	0.38			0.37	2908	1684
	15:00	0.2			0.27	1058	712
	18:00	0.003			0	0	
A'							

Table 14. Summary of the results for scenario one at point B'

Date	Time	DGP_Annual [-]	DGP_Annual class [-]	DGP_point-in-time class [-]	DGP_point-in-time [-]	Vertical illuminance [lux]	Horizontal illuminance [lux]
21.03	9:00	0.35			0.25	1341	611
	12:00	0.54			0.42	4214	2240
	15:00	0.41			0.4	3598	2010
	18:00	0.023			0.18	462	223
24.03	9:00	0.28			0.19	510	289
	12:00	0.34			0.26	1283	699
	15:00	0.29			0.25	1119	676
	18:00	0.008			0.09	189	106
19.06	9:00	0.41			0.26	1335	728
	12:00	0.45			0.34	2359	1458
	15:00	0.34			0.28	1772	996
	18:00	0.22			0.19	593	343
21.06	9:00	0.33			0.25	1158	596
	12:00	0.46			0.35	2806	1480
	15:00	0.38			0.35	2651	1476
	18:00	0.25			0.25	1083	573
21.09	9:00	0.35			0.28	1707	788
	12:00	0.46			0.41	4049	1826
	15:00	0.36			0.36	3222	1538
	18:00	0.014			0.18	414	220
24.09	9:00	0.34			0.21	700	384
	12:00	0.34			0.28	1590	860
	15:00	0.34			0.34	2729	1534
	18:00	0.003			0.07	165	87
21.12	9:00	0.2			0.1	35	21
	12:00	0.25			0.19	573	305
	15:00	0.25			0.31	2292	1243
	18:00	0.003			0	0	0
22.12	9:00	0.25			0.02	95	66
	12:00	0.47			0.4	3788	1879
	15:00	0.27			0.34	2924	1855
	18:00	0.003			0	0	0
B'							

Table 15. Summary of the results for scenario one at point C'

Date	Time	DGP_Annual [-]	DGP_Annual class [-]	DGP_point-in-time class [-]	DGP_point-in-time [-]	Vertical illuminance [lux]	Horizontal illuminance [lux]
21.03	9:00	0.45			0.33	3190	1417
	12:00	1			1	18047	18887
	15:00	1			1	10545	18882
	18:00	0.053			0.24	1386	711
24.03	9:00	0.32			0.23	1514	852
	12:00	0.42			0.36	3677	2073
	15:00	0.34			0.34	3352	1923
	18:00	0.01			0.19	548	304
19.06	9:00	0.5			0.36	3787	2131
	12:00	0.61			0.56	7028	4561
	15:00	0.41			0.43	5091	3019
	18:00	0.23			0.24	1700	1006
21.06	9:00	0.4			0.33	2931	1746
	12:00	0.67			0.6	7786	4895
	15:00	0.65			0.65	9135	5290
	18:00	0.28			0.34	3365	1656
21.09	9:00	0.47			0.39	4158	1766
	12:00	1			1	29492	33420
	15:00	1			1	42416	23848
	18:00	0.02			0.24	1374	663
24.09	9:00	0.33			0.26	1956	1123
	12:00	0.41			0.43	3595	2903
	15:00	0.99			0.88	11950	6540
	18:00	0.003			0.18	490	265
21.12	9:00	0.22			0.019	96	64
	12:00	0.29			0.24	1519	836
	15:00	0.77			0.93	10193	3603
	18:00	0.003			0	0	0
22.12	9:00	0.28			0.14	262	184
	12:00	1			1	23120	11583
	15:00	0.88			1	20800	6325
	18:00	0.003			0	0	
C'							

The green, yellow, orange, and red corresponds to the imperceptible glare, perceptible glare, disturbing glare, and intolerable glare, respectively. By analyzing and comparing the results of DGP_{annual} and $DGP_{point\text{-}in\text{-}time}$, there were matched in most simulated time and points. For points A, B, and C, the DGP_{annual} and $DGP_{point\text{-}in\text{-}time}$ have less match than points A', B', C' having a 45° view angle. For the points far from windows, such as A and A', the same classes were more observed than the points located near the window. For example, at point, A' on all 32 simulated hours, DGP_{annual} and $DGP_{point\text{-}in\text{-}time}$ were assigned in the same discomfort classes.

As can be seen in the results, the horizontal illuminance and vertical illuminance showed a significant relation with the DGP values. The DGP values showed the intolerable glare condition, the vertical illuminance received a high amount of light. For example, at point C on September 21 at noontime, the DGP_{annual} and $DGP_{point\text{-}in\text{-}time}$ values were equal to 1, and the vertical illuminance and horizontal illuminance values were 46446 lux and 34454 lux at that time, respectively. However, at the same time but on December 21, DGP_{annual} and $DGP_{point\text{-}in\text{-}time}$ were imperceptible glare, and vertical illuminance received 1995 lux, and horizontal illuminance received 1042 lux.

Another interesting point that can be highlighted was about the DGP_{annual} values and $DGP_{point\text{-}in\text{-}time}$ values. Almost at all the simulated time and points, the DGP_{annual} overestimated the glare condition during the morning while underestimated in the afternoon compared to $DGP_{point\text{-}in\text{-}time}$. As an example, at point B, the DGP_{annual} value was 0.35, and $DGP_{point\text{-}in\text{-}time}$ was 0.28 at 9:00 in the morning while at 18:00 DGP_{annual} was 0.02 and $DGP_{point\text{-}in\text{-}time}$ reached 0.19. furthermore, for point A the DGP_{annual} and $DGP_{point\text{-}in\text{-}time}$ in the morning on September 21 were 0.28 and 0.26 respectively, while these amounts were 0.01 and 0.12 at 18:00.

4.5.2. Discomfort glare classes DGP_{annual} and $DGP_{point\text{-}in\text{-}time}$ for scenario two

By adding the Venetian blind in the simulation, the amounts of DGP values, horizontal and vertical illuminance have changed accordingly. The results of the simulation of scenario two are presented in Tables 17-22.

Table 16. Summary of the results for scenario two at point A

Date	Time	DGP_Annual [-]	DGP_Annual class [-]	DGP_point-in-time class [-]	DGP_point-in-time [-]	Vertical illuminance [lux]	Horizontal illuminance [lux]
21.03	9:00	0.25			0.26	563	256
	12:00	0.36			0.35	1638	554
	15:00	0.26			0.31	1045	470
24.03	9:00	0.23			0.18	254	109
	12:00	0.27			0.26	566	297
	15:00	0.24			0.25	516	247
21.09	9:00	0.24			0.28	739	300
	12:00	0.32			0.34	1353	625
	15:00	0.24			0.30	984	472
24.09	9:00	0.26			0.24	310	113
	12:00	0.26			0.27	601	273
	15:00	0.24			0.30	986	391
21.12	9:00	0.20			0.00	14	5
	12:00	0.28			0.34	263	135
	15:00	0.10			0.17	868	340
22.12	9:00	0.21			0.01	36	16
	12:00	1.00			1.00	31360	1683
	15:00	0.20			0.28	1079	544
A							

Table 17. Summary of the results for scenario two at point B

Date	Time	DGP_Annual [-]	DGP_Annual class [-]	DGP_point-in-time class [-]	DGP_point-in-time [-]	Vertical illuminance [lux]	Horizontal illuminance [lux]
21.03	9:00	0.27			0.27	1109	306
	12:00	0.42			0.40	2842	723
	15:00	0.29			0.35	1916	741
24.03	9:00	0.24			0.19	416	148
	12:00	0.28			0.26	1013	262
	15:00	0.24			0.25	801	329
21.09	9:00	0.26			0.30	1463	485
	12:00	0.36			0.39	2737	967
	15:00	0.27			0.34	1840	591
24.09	9:00	0.28			0.23	568	189
	12:00	0.28			0.27	1342	334
	15:00	0.26			0.32	1804	587
21.12	9:00	0.21			0.01	27	10
	12:00	0.39			0.39	472	127
	15:00	0.12			0.20	1486	588
22.12	9:00	0.23			0.02	78	20
	12:00	1.00			1.00	3195	1397
	15:00	0.22			0.32	2003	912
B							

Table 18. Summary of the results for scenario two at point C

Date	Time	DGP_Annual [-]	DGP_Annual class [-]	DGP_point-in-time class [-]	DGP_point-in-time [-]	Vertical illuminance [lux]	Horizontal illuminance [lux]
21.03	9:00	0.36			0.33	2252	723
	12:00	0.53			0.55	5616	1507
	15:00	0.46			0.51	4963	1413
24.03	9:00	0.26			0.22	857	225
	12:00	0.32			0.31	2081	500
	15:00	0.27			0.30	1787	509
21.09	9:00	0.36			0.38	3058	945
	12:00	0.48			0.53	5150	1449
	15:00	0.38			0.48	4765	1005
24.09	9:00	0.32			0.26	1212	354
	12:00	0.31			0.34	2500	735
	15:00	0.35			0.44	3926	896
21.12	9:00	0.22			0.02	50	15
	12:00	0.39			0.42	3286	2461
	15:00	0.18			0.22	940	238
22.12	9:00	0.26			0.07	164	38
	12:00	1.00			1.00	34515	1672
	15:00	0.96			1.00	16538	5577
C							

Table 19. Summary of the results for scenario two at point A'

Date	Time	DGP_Annual [-]	DGP_Annual class [-]	DGP_point-in-time class [-]	DGP_point-in-time [-]	Vertical illuminance [lux]	Horizontal illuminance [lux]
21.03	9:00	0.20			0.24	470	221
	12:00	0.30			0.30	922	675
	15:00	0.23			0.28	885	520
24.03	9:00	0.21			0.13	185	108
	12:00	0.22			0.24	398	264
	15:00	0.21			0.23	413	210
21.09	9:00	0.20			0.25	510	323
	12:00	0.27			0.30	1135	645
	15:00	0.21			0.28	773	441
24.09	9:00	0.22			0.21	253	130
	12:00	0.22			0.24	443	333
	15:00	0.21			0.28	614	421
21.12	9:00	0.09			0.00	10	6
	12:00	0.24			0.24	158	105
	15:00	0.02			0.13	751	340
22.12	9:00	0.19			0.01	33	16
	12:00	0.46			0.32	2138	1331
	15:00	0.19			0.27	954	538
A'							

Table 20. Summary of the results for scenario two at point B'

Date	Time	DGP_Annual [-]	DGP_Annual class [-]	DGP_point-in-time class [-]	DGP_point-in-time [-]	Vertical illuminance [lux]	Horizontal illuminance [lux]
21.03	9:00	0.25			0.24	950	322
	12:00	0.36			0.35	2257	919
	15:00	0.30			0.34	2230	853
24.03	9:00	0.23			0.18	370	121
	12:00	0.26			0.25	806	307
	15:00	0.24			0.24	665	381
21.09	9:00	0.24			0.27	1064	368
	12:00	0.32			0.34	2132	880
	15:00	0.27			0.32	1746	704
24.09	9:00	0.26			0.22	485	185
	12:00	0.26			0.26	1149	340
	15:00	0.27			0.31	1801	558
21.12	9:00	0.20			0.01	22	9
	12:00	0.27			0.24	334	150
	15:00	0.09			0.20	1557	750
22.12	9:00	0.21			0.01	64	22
	12:00	0.48			0.36	2760	1334
	15:00	0.23			0.32	2108	1364
B'							

Table 21. Summary of the results for scenario two at point C'

Date	Time	DGP_Annual [-]	DGP_Annual class [-]	DGP_point-in-time class [-]	DGP_point-in-time [-]	Vertical illuminance [lux]	Horizontal illuminance [lux]
21.03	9:00	0.33			0.44	1552	490
	12:00	0.49			0.44	3869	1116
	15:00	0.46			0.47	4414	1274
24.03	9:00	0.27			0.20	707	207
	12:00	0.33			0.28	1467	489
	15:00	0.28			0.28	1481	459
21.09	9:00	0.32			0.32	1848	516
	12:00	0.43			0.44	3876	1000
	15:00	0.42			0.45	4165	1195
24.09	9:00	0.33			0.24	827	251
	12:00	0.33			0.30	1899	684
	15:00	0.41			0.42	3395	1070
21.12	9:00	0.22			0.01	39	10
	12:00	0.30			0.35	654	224
	15:00	0.20			0.22	8185	2655
22.12	9:00	0.24			0.04	119	40
	12:00	0.98			1.00	3768	1382
	15:00	0.96			1.00	18838	5846
C'							

Analyzing the results regarding glare analysis in scenario two has shown that the DGP_{annual} has been able to predict the glare condition of the space with a high amount of accuracy. For example, at points A and A' for all simulated time, the glare was imperceptible with exceptions on December 22 and March 21 at noon. On December 22 at 12:00, the DGP_{annual} has estimated the glare as intolerable with the exact value of 46%, while $DGP_{point\text{-}in\text{-}time}$ is considered imperceptible glare. The only incorrect estimation of the glare classes by DGP_{annual} at point B happened on March 21. At that time (15:00), the value of DGP_{annual} was 29%, and $DGP_{point\text{-}in\text{-}time}$ was 35%.

On the other hand, at point B', the glare was classified as imperceptible for all simulation times with two exceptions. On March 21 at noontime, the glare was calculated as perceptible by using DGP_{annual} and $DGP_{point\text{-}in\text{-}time}$ with the value of 36% and 35%, respectively. The error on glare class estimation utilizing DGP_{annual} happened on December 21 at noon, where the DGP_{annual} estimated intolerable condition while $DGP_{point\text{-}in\text{-}time}$ showed perceptible glare. Comparing the results at points C and C' revealed the most inconsistent glare classes happened at these points. These inconsistencies mainly occurred during the morning and afternoon. As an example, at point C on March 21 at 9:00, the DGP_{annual} value was 36%, and $DGP_{point\text{-}in\text{-}time}$ was 33%. On September 21 and September 24 at 15:00, DGP_{annual} were perceptible with 38% and 35%; however, $DGP_{point\text{-}in\text{-}time}$ was 48% and 45%, respectively. For point C' three times were not matched together on March 21 at 9:00 and 12:00, and on September 21 at 15:00.

4.5.3. Discomfort glare classes DGP_{annual} and $DGP_{point\text{-}in\text{-}time}$ for scenario three

The results of the simulation for scenario three are shown in Tables 22-26. In this case, the lower amount of light was entered into the space. The results of vertical and horizontal illuminances confirm this idea. Consequently, the lower glare values have been recorded in this scenario compared to the previous scenarios.

Table 22. Summary of the results for scenario three at point A

Date	Time	DGP_Annual [-]	DGP_Annual class [-]	DGP_point-in-time class [-]	DGP_point-in-time [-]	Vertical illuminance [lux]	Horizontal illuminance [lux]
21.03	9:00	0.218			0.08	138	83
	12:00	0.283			0.27	328	214
	15:00	0.226			0.26	310	181
24.03	9:00	0.219			0.01	78	36
	12:00	0.245			0.07	123	77
	15:00	0.222			0.05	123	67
21.09	9:00	0.209			0.17	214	117
	12:00	0.26			0.27	447	255
	15:00	0.211			0.25	325	194
24.09	9:00	0.242			0.02	72	55
	12:00	0.242			0.10	154	88
	15:00	0.217			0.19	217	122
21.12	9:00	0.159			0.00	4	2
	12:00	0.223			0.03	49	37
	15:00	0.048			0.01	129	67
22.12	9:00	0.179			0.00	14	7
	12:00	0.304			0.27	303	130
	15:00	0.179			0.11	196	82
A							

Table 23. Summary of the results for scenario three at point B

Date	Time	DGP_Annual [-]	DGP_Annual class [-]	DGP_point-in-time class [-]	DGP_point-in-time [-]	Vertical illuminance [lux]	Horizontal illuminance [lux]
21.03	9:00	0.24			0.19	304	116
	12:00	0.30			0.27	723	293
	15:00	0.25			0.27	687	275
24.03	9:00	0.23			0.04	115	50
	12:00	0.26			0.18	308	111
	15:00	0.23			0.17	249	97
21.09	9:00	0.23			0.23	401	172
	12:00	0.27			0.28	816	365
	15:00	0.23			0.27	695	296
24.09	9:00	0.26			0.08	191	70
	12:00	0.26			0.20	301	132
	15:00	0.23			0.24	381	170
21.12	9:00	0.19			0.00	8	3
	12:00	0.23			0.12	118	52
	15:00	0.08			0.03	221	110
22.12	9:00	0.19			0.00	24	9
	12:00	0.30			0.26	463	213
	15:00	0.19			0.22	363	120
B							

Table 24. Summary of the results for scenario three at point C

Date	Time	DGP_Annual [-]	DGP_Annual class [-]	DGP_point-in-time class [-]	DGP_point-in-time [-]	Vertical illuminance [lux]	Horizontal illuminance [lux]
21.03	9:00	0.26			0.24	1092	167
	12:00	0.35			0.36	2677	377
	15:00	0.28			0.35	2189	405
24.03	9:00	0.22			0.18	443	65
	12:00	0.25			0.23	933	141
	15:00	0.23			0.23	962	138
21.09	9:00	0.27			0.29	1440	253
	12:00	0.35			0.39	3129	520
	15:00	0.35			0.36	2419	431
24.09	9:00	0.25			0.20	567	99
	12:00	0.25			0.24	1217	178
	15:00	0.24			0.29	1612	235
21.12	9:00	0.18			0.01	27	4
	12:00	0.23			0.22	412	74
	15:00	0.06			0.18	898	136
22.12	9:00	0.22			0.02	78	13
	12:00	0.32			0.31	1683	264
	15:00	0.22			0.28	1013	181
C							

Table 25. Summary of the results for scenario three at point A'

Date	Time	DGP_Annual [-]	DGP_Annual class [-]	DGP_point-in-time class [-]	DGP_point-in-time [-]	Vertical illuminance [lux]	Horizontal illuminance [lux]
21.03	9:00	0.18			0.05	93	80
	12:00	0.23			0.23	346	198
	15:00	0.19			0.22	228	182
24.03	9:00	0.13			0.01	50	33
	12:00	0.20			0.05	105	86
	15:00	0.15			0.03	97	63
21.09	9:00	0.18			0.11	158	118
	12:00	0.23			0.23	383	240
	15:00	0.18			0.22	250	185
24.09	9:00	0.20			0.01	67	49
	12:00	0.20			0.07	155	87
	15:00	0.18			0.13	126	122
21.12	9:00	0.02			0.00	3	2
	12:00	0.16			0.02	30	35
	15:00	0.01			0.01	109	63
22.12	9:00	0.06			0.00	7	6
	12:00	0.28			0.21	153	136
	15:00	0.06			0.07	121	87
A'							

Table 26. Summary of the results for scenario three at point B'

Date	Time	DGP_Annual [-]	DGP_Annual class [-]	DGP_point-in-time class [-]	DGP_point-in-time [-]	Vertical illuminance [lux]	Horizontal illuminance [lux]
21.03	9:00	0.21			0.16	245	113
	12:00	0.26			0.25	620	282
	15:00	0.23			0.24	602	263
24.03	9:00	0.21			0.03	90	45
	12:00	0.24			0.15	194	101
	15:00	0.22			0.13	189	93
21.09	9:00	0.21			0.21	337	160
	12:00	0.24			0.25	832	344
	15:00	0.22			0.24	639	278
24.09	9:00	0.23			0.05	154	65
	12:00	0.23			0.18	253	118
	15:00	0.21			0.22	344	171
21.12	9:00	0.13			0.00	6	3
	12:00	0.22			0.08	81	48
	15:00	0.03			0.02	191	113
22.12	9:00	0.18			0.00	17	9
	12:00	0.27			0.23	363	184
	15:00	0.19			0.22	227	133
B'							

Table 27. Summary of the results for scenario three at point C'

Date	Time	DGP_Annual [-]	DGP_Annual class [-]	DGP_point-in-time class [-]	DGP_point-in-time [-]	Vertical illuminance [lux]	Horizontal illuminance [lux]
21.03	9:00	0.27			0.22	784	154
	12:00	0.33			0.33	1976	381
	15:00	0.30			0.32	1932	383
24.03	9:00	0.24			0.18	351	72
	12:00	0.27			0.22	769	134
	15:00	0.24			0.21	671	119
21.09	9:00	0.27			0.27	1185	248
	12:00	0.35			0.36	2508	482
	15:00	0.30			0.33	1824	389
24.09	9:00	0.27			0.19	418	89
	12:00	0.27			0.23	889	185
	15:00	0.27			0.28	1255	209
21.12	9:00	0.20			0.01	23	4
	12:00	0.24			0.21	327	62
	15:00	0.11			0.16	766	139
22.12	9:00	0.19			0.01	58	12
	12:00	0.29			0.27	1456	249
	15:00	0.25			0.28	1052	214
C'							

By comparing the results of this scenario, the DGP_{annual} predicted the same discomfort glare classes as $DGP_{point\text{-}in\text{-}time}$ at all the simulated times and points. Almost most of the results were correctly estimated the glare classes by DGP_{annual}. The discomfort glare classes at this scenario were either imperceptible or perceptible. Therefore in case of having Venetian blind with 30° results in a glare-free space. The perceptible glare relates to points C on March 21 at noon and September 21 at noon and 15:00. Although, at C' was only happened on September 21 at noontime with DGP_{annual} value was 35% and $DGP_{point\text{-}in\text{-}time}$ was 36%.

The highest captured vertical illuminance value was 3129 lux at noon of September 21 at point C. The horizontal value was 520 lux at this point which was also the highest amount among all simulations. It confirms the consistency of the DGP values and the vertical illuminance since the vertical illuminances are used to calculate the DGP values.

Summary of findings

Comparing the results of scenarios, it can be concluded that the closer the examined points to the window, the greater the amount of glare classes inconsistency. The highest estimation of glare classes employing DGP_{annual} was related to scenarios three, two, and one. It means that by having the Venetian blind, the estimation accuracy of the glare classes will be increased. The mismatch of DGP_{annual} and $DGP_{point\text{-}in\text{-}time}$ potentially occurred on sunny days, and overcast days, DGP_{annual} and $DGP_{point\text{-}in\text{-}time}$ were entirely consistent. Therefore, it seems that the highest amount of light led to a higher amount of error in estimating the glare values. The morning's overestimation and afternoon underestimation of DGP_{annual} have been observed in all scenarios at most simulated times and points.

4.6. Correlation of DGP_{annual} and $DGP_{point\text{-}in\text{-}time}$

These simulated results in the previous section need to be analyzed more in detail to find and understand the correlation between DGP_{annual} and $DGP_{point\text{-}in\text{-}time}$. Therefore, calculating the correlation of DGP_{annual} and $DGP_{point\text{-}in\text{-}time}$ was necessary to find how accurate was DGP_{annual} in predicting the glare. These correlations not only help to comprehend the accuracy of predicting the discomfort glare classes but also show the exact amount of glare estimated by DGP_{annual} compared to the $DGP_{point\text{-}in\text{-}time}$. Hence, the correlation for each scenario was calculated and analyzed separately in the following subsections.

4.6.1. Correlation of DGP_{annual} and $DGP_{point-in-time}$ for scenario one

The scatter plot of DGP_{annual} and $DGP_{point-in-time}$ was presented in Figure 57.

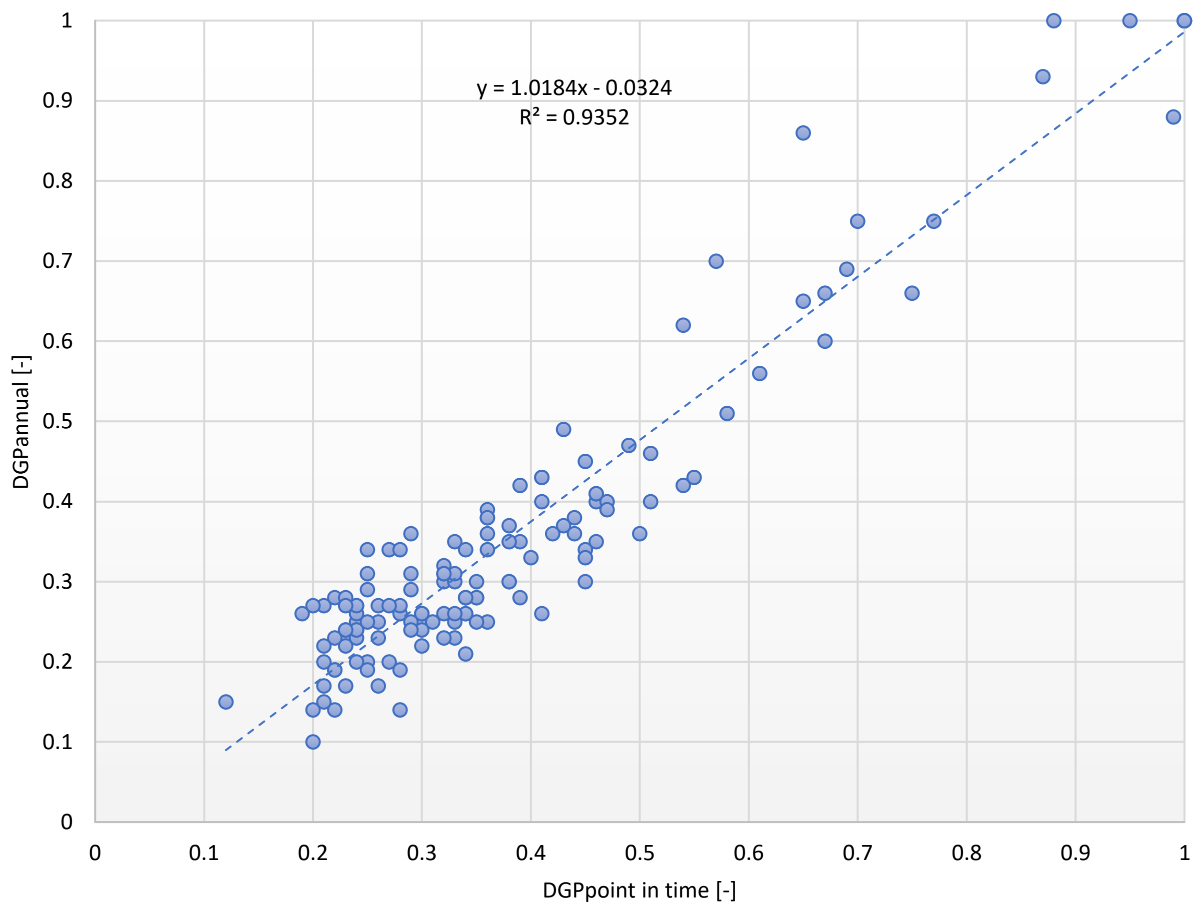

Figure 57. The scatter plot of DGP_{annual} and $DGP_{point-in-time}$ in scenario one

The X-axis represents values of a $DGP_{point-in-time}$, which was considered the independent variable, and the Y-axis represents values of a DGP_{annual} considered the dependent variable. Since the reliable DGP values based on the study of Wienold [40] are between 0.2 to 0.8. Therefore, It needs to be mentioned that results relative to DGP_{annual} and $DGP_{point-in-time}$ lower than 0.18 were filtered. The scatter plot showed a high correlation between DGP_{annual} and $DGP_{point-in-time}$. The figure represents a linear and positive relationship between two variables. As can be seen, all points were around the trendline, and there was a slight oscillation or deviation between the points. The R2 of these variables was equal to 0.93, which means a high correlation between the variables. Analyzing this scatter plot showed that DGP_{annual} predicted the DGP value with high accuracy and its results were very close to the $DGP_{point\text{-}in\text{-}time}$.

4.6.2. Correlation of DGP_{annual} and $DGP_{point\text{-}in\text{-}time}$ for scenario two

The correlation of the DGP_{annual} and $DGP_{point\text{-}in\text{-}time}$ values for scenario two has been compared, and its results are depicted in the following scatter plot (Figure 58).

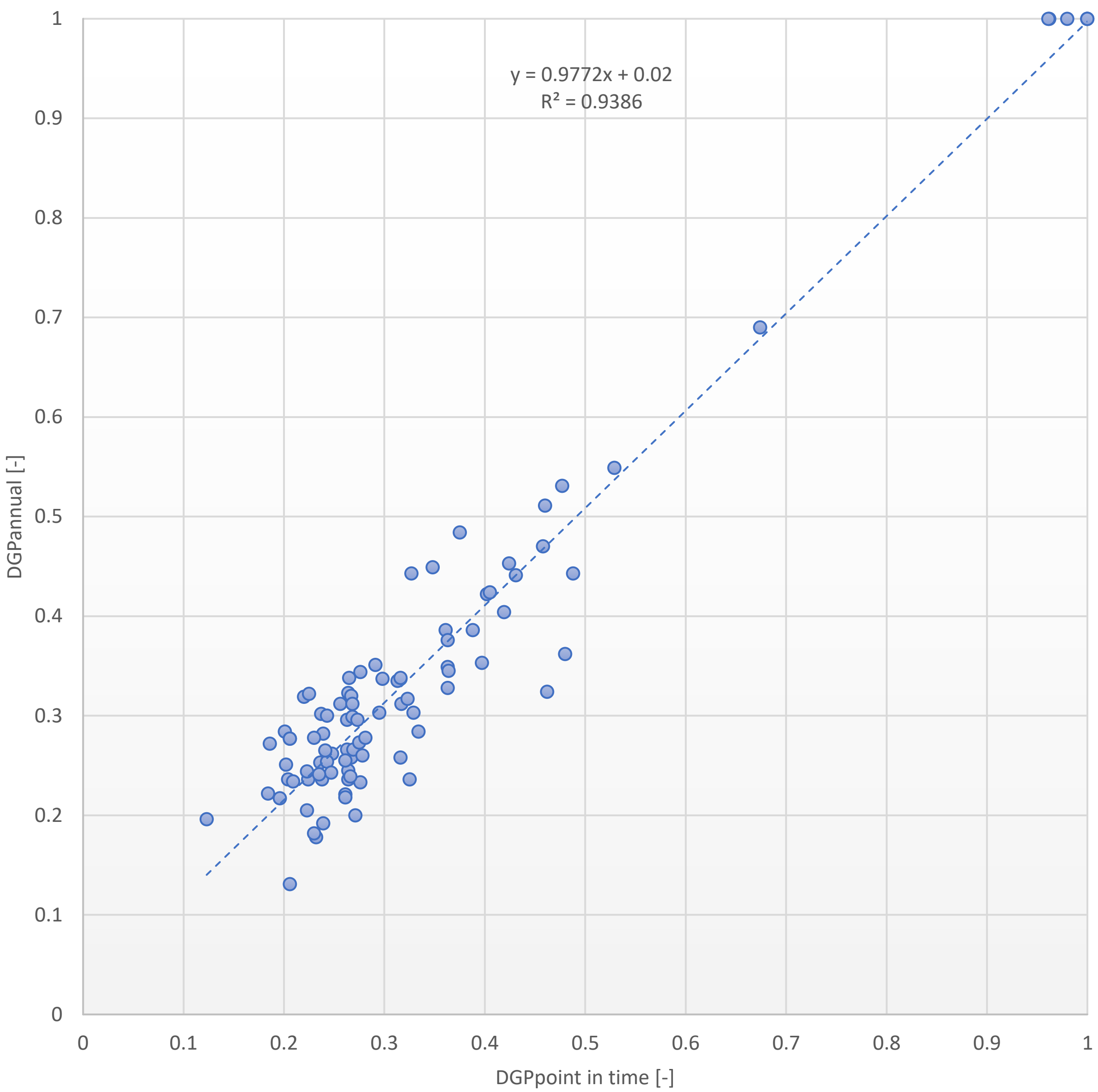

Figure 58. The scatter plot of DGP_{annual} and $DGP_{point-in-time}$ in scenario two

Figure 58 showed a very good correlation in the estimation of the glare in scenario two. The R^2 = 0. 94 confirm that the high accuracy between the DGP_{annual} and $DGP_{point-in-time}$ existed in this scenario. Therefore, the $DGP_{annual,}$ in addition to predicting the discomfort glare classes, it can estimate the very close amount of $DGP_{point-in-time}$.

4.6.3. Correlation of DGP_{annual} and $DGP_{point-in-time}$ for scenario three

The following scatter plot presents the correlation of DGP_{annual} and $DGP_{point-in-time}$ of scenario three. The R^2 for this correlation was equal to 0.63, and it shows a good correlation but not as much as the previous scenarios.

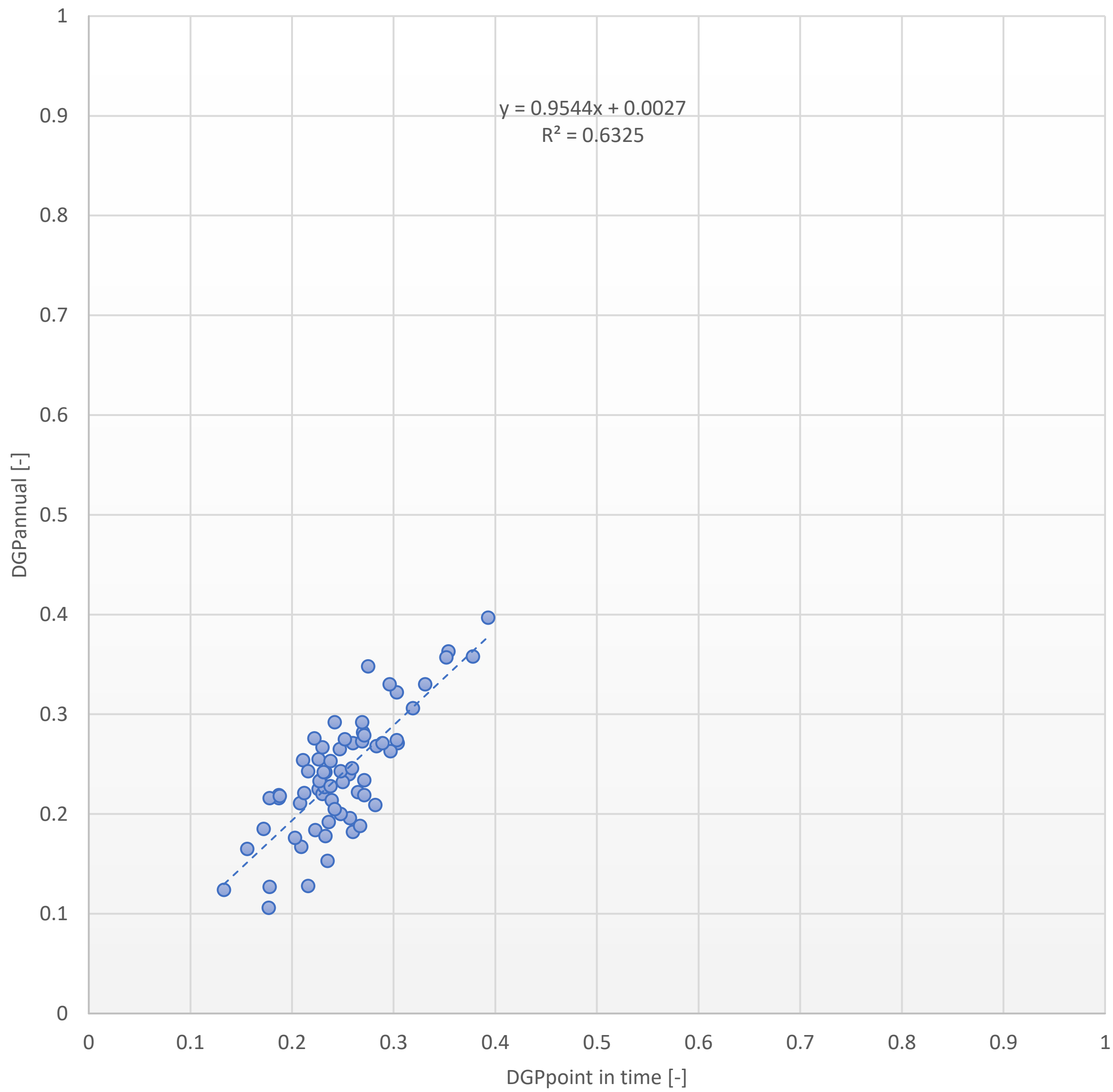

Figure 59. The scatter plot of DGP_{annual} and $DGP_{point-in-time}$ in scenario three

More precisely, it was noticeable that DGP_{annual} did not accurately estimate the $DGP_{point-in-time}$ values based on the R^2. However, it should be noted that according to the previous sections, the DGP_{annual} predicted the discomfort glare classes without any error.

Therefore, even if the high R^2 was not achieved for this scenario, the DGP_{annual} and $DGP_{point\text{-}in\text{-}time}$ fit well when discomfort glare classes are concerned.

4.7. Multivariate linear regression

In order to understand the exact amount of data variances around the trendline and correlation of DGP_{annual} and $DGP_{point\text{-}in\text{-}time}$ with each other multivariate linear regression was conducted. The obtained results were entered into Excel. The data output was presented in tables format introducing the most relevant statistical parameters in order to discuss the efficiency of the predicted model. According to the Anova Fisher test, it is possible to conclude that the F value is immense, so we can determine that the variability between the two groups, which are DGP_{annual} and $DGP_{point\text{-}in\text{-}time}$, is more significant than the variabilities of the observations within the two groups.

The greater the F value, the stronger the correlation between the two groups. So, the comparison of Fisher test values for the three different scenarios is crucial to determine which is the most accurate one for model prediction.

Otherwise, the means of the two groups are different, but they show a high correlation between them, so the estimation model for the glare through DGP annual is reliable.

4.7.1. Multivariate linear regression of DGP_{annual} and $DGP_{point\text{-}in\text{-}time}$ for scenario one

According to the obtained results in Table 28. Summary results of multivariate linear regression for scenario one found that DGP_{annual} was predicting with very high accuracy the glare condition in the DSF. As results illustrated, the R Square is equal to 0.89, and the standard error was 0.08, which is standing in the optimal range; this value showed that the simulated values of DGP_{annual} were reliable and acceptable. High R square indicated some predictive power of the multiple regression model, which was DGP_{annual} in our study. The Observation was represented by the number of samples used for this regression analysis, where 191 equals the simulation results. The F value is equal to

1575.9701, which is a considerable value showing that even the means of the two groups are not the same for scenario one, but the variance is suitable in order to estimate the glare for scenario one.

Table 28. Summary results of multivariate linear regression for scenario one

SUMMARY OUTPUT

Regression Statistics	
Multiple R	0.944942344
R Square	0.892916033
Adjusted R Square	0.892349451
Standard Error	0.080431627
Observations	191

ANOVA

	df	*SS*	*MS*	*F*	*Significance F*
Regression	1	10.19533919	10.19534	1575.9701	1.24858E-93
Residual	189	1.222687603	0.006469		
Total	190	11.4180268			

4.7.2. Multivariate linear regression of DGP_{annual} and $DGP_{point\text{-}in\text{-}time}$ for scenario two

The results of multivariate linear regression for scenario two are shown in Table 29.

Table 29. Summary results of multivariate linear regression for scenario two

SUMMARY OUTPUT

Regression Statistics	
Multiple R	0.927588945
R Square	0.860421251
Adjusted R Square	0.85910447
Standard Error	0.078297644
Observations	108

ANOVA

	df	*SS*	*MS*	*F*	*Significance F*
Regression	1	4.005853681	4.005853681	653.4279	3.94167E-47
Residual	106	0.649835236	0.006130521		
Total	107	4.655688917			

The R square at this statistical report for scenario two was 0.86, which shows a high correlation between DGP_{annual} and $DGP_{point\text{-}in\text{-}time}$. The standard error for this model was deficient, with a value of 0.078. It represented the high quality of the predictive model when the DGP_{annual} was used to predict the $DGP_{point\text{-}in\text{-}time}$. Furthermore, the R square and standard error values in this scenario were very similar to scenario one.

According to the Anova test, the F value (653.4279) was still significant, and it showed a good correlation between the two groups for scenario two. The difference between the two F values between the first and second scenarios can be explained by the difference in the sample size. In other words, the sample size is a critical factor for multivariate regression between the two compared groups: the larger the sample size, the more accurate the correlation.

4.7.3. Multivariate linear regression of DGP_{annual} and $DGP_{point\text{-}in\text{-}time}$ for scenario three

The statistical summary regarding the regression of DGP_{annual} and $DGP_{point\text{-}in\text{-}time}$ for the scenario is presented below.

Table 30. Summary results of multivariate linear regression for scenario three

SUMMARY OUTPUT

Regression Statistics	
Multiple R	0.772215893
R Square	0.596317386
Adjusted R Square	0.59250906
Standard Error	0.070436185
Observations	108

ANOVA

	df	*SS*	*MS*	*F*	*Significance F*
Regression	1	0.776846026	0.776846	156.582525	1.31209E-22
Residual	106	0.525893159	0.004961		
Total	107	1.302739185			

As can be seen from Table 30, the R square was about 0.6, which was the lowest amount among all scenarios, and the F factor is lower than the previous scenarios proving that the correlation between the two groups was not considered under scenario three conditions. However, the standard error in this scenario was 0.07 lower than in previous scenarios and showed the high reliability of this predictive model.

Analyzing and comparing the results of the scenarios indicated that scenarios one, two, and three had the highest prediction accuracy when the DGP_{annual} was considered to estimate the $DGP_{point\text{-}in\text{-}time}$, respectively. It can be concluded that under the dimmed condition with lower light entrance because of Venetian blind, the exact value predicted by DGP_{annual} was not highly correlated with $DGP_{point\text{-}in\text{-}time}$ values.

4.8. Diagnostic analysis

This section used the GLANCE methodology presented by Giovannini to understand the accuracy in predicting glare employing DGP_{annual}. The DGP_{annual} and $DGP_{point\text{-}in\text{-}time}$ values were found for the reference viewpoints in DSF. Therefore, three DGP threshold values have been considered in correspondence with the DGP threshold values defined by Wienold for the four glare comfort classes, as shown in Table 31.

Table 31. The glare comfort classes and DGP thresholds

Glare Comfort Class	**DGP Threshold (DGP_{thr})**
Imperceptible glare	$0.00 \leq DGP < 0.35$
Perceptible glare	$0.35 \leq DGP < 0.40$
Disturbing glare	$0.40 \leq DGP < 0.45$
Intolerable glare	$0.45 \leq DGP < 1.00$

The DGP_{thr} values are identified by means of a diagnostic analysis applied to the time series of the DGP_{annual} and $DGP_{point\text{-}in\text{-}time}$ values, extracted from each simulated point. This technique estimated the DGP value when the DGP_{annual} was used instead of the $DGP_{point\text{-}in\text{-}time}$. In more detail, comparing the estimation of a given glare comfort classes through an DGP_{annual} that obtained through the DGP_{thr} may result in one of the four different conditions:

- True Positive (TP): when $DGP_{annual} > DGP_{thr}$ and $DGP_{point\text{-}in\text{-}time} > DGP_{thr}$
- False Negative (FN): when $DGP_{annual} > DGP_{thr}$ and $DGP_{point\text{-}in\text{-}time} < DGP_{thr}$
- True Negative (TN): when $DGP_{annual} < DGP_{thr}$ and $DGP_{point\text{-}in\text{-}time} < DGP_{thr}$ and
- False Positive (FP): when $DGP_{annual} < DGP_{thr}$ and $DGP_{point\text{-}in\text{-}time} > DGP_{thr}$

TP and TN represent a correct ("True") estimation of the glare comfort classes, as both metrics are consistent in the calculation of a glare condition. Conversely, FN and FP scenarios indicate an incorrect ("False") estimation since there is a discordance between the glare estimation of DGP_{thr} and $DGP_{point\text{-}in\text{-}time}$. Especially, FP represents an overestimation of the glare condition, as the glare classes estimated by DGPannual show a glare condition, contrary to what happens using the $DGP_{point\text{-}in\text{-}time}$. On the other hand, an FN led to underestimating the glare comfort class, as the estimated glare class using the DGP_{annual} shows a glare-free condition, in contrast with $DGP_{point-in-time}$ estimation. However, both quadrants of FP and FN determine a "false" estimation of the glare condition, FN appears to be the most dangerous situation since the GLANCE method does not detect a discomfort glare condition, unlike the DGP. Furthermore, FN and TP are the most relevant cases (according to the epidemiological approach), as it represents an unfavorable misclassification of a glare condition. In fact, because the goal of forecasting glare is to prevent it from happening, a good FN prediction is crucial.

4.8.1. Diagnostic analysis for scenario one

The diagnostic analysis has been done for each scenario (without blind and with blind) with three glare comfort classes. Perceptible glare with DGP_{thr} value of 0.35, disturbing glare class with DGP_{thr} value of 0.4, and intolerable glare class with the DGP_{thr} equal to 0.45. Figure 60 presented a glare classification based on the GLANCE methodology for scenario one (without a blind).

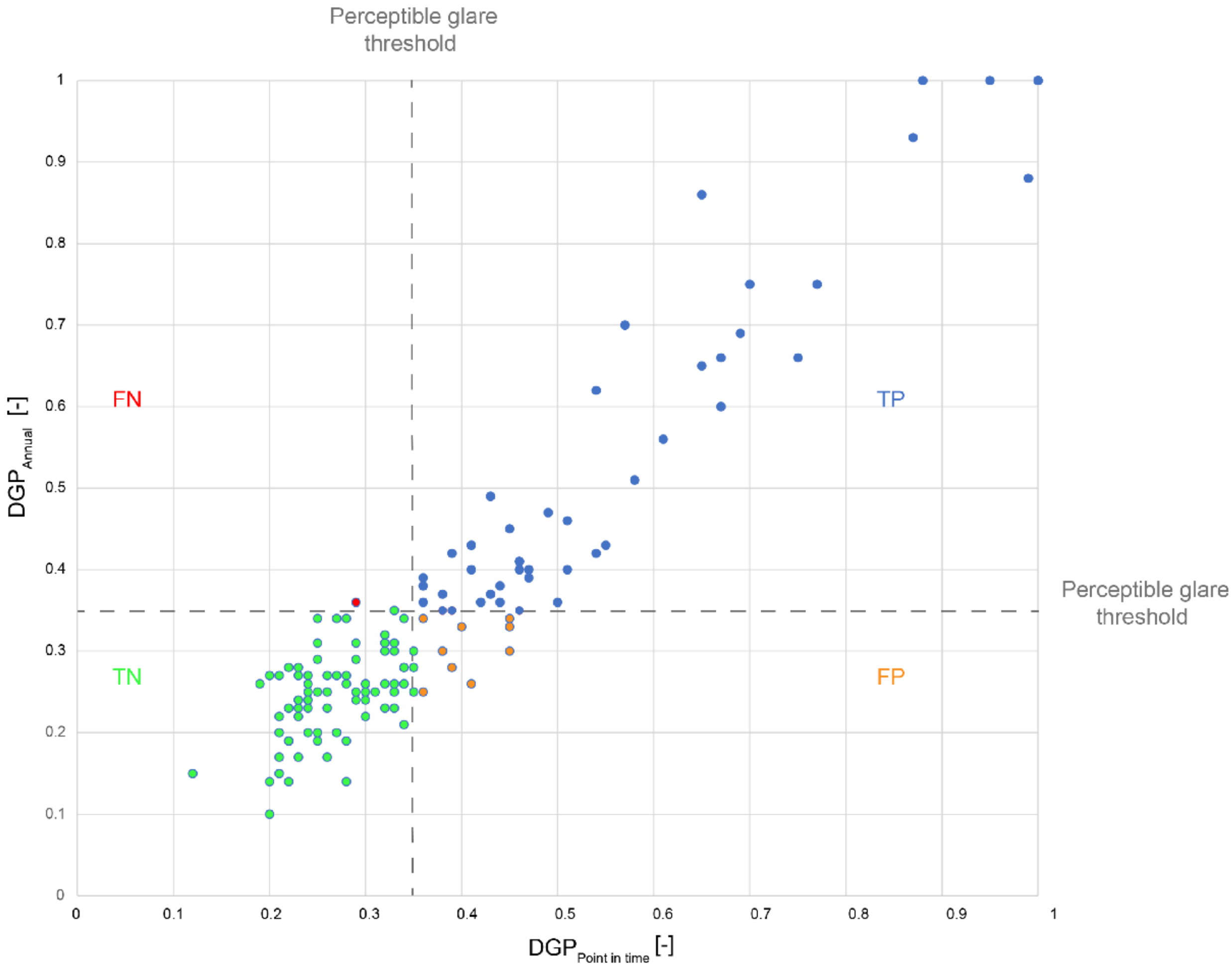

Figure 60. The binary classification of DGP$_{point-in-time}$ -DGP$_{annual}$ calculated for scenario one with perceptible glare threshold

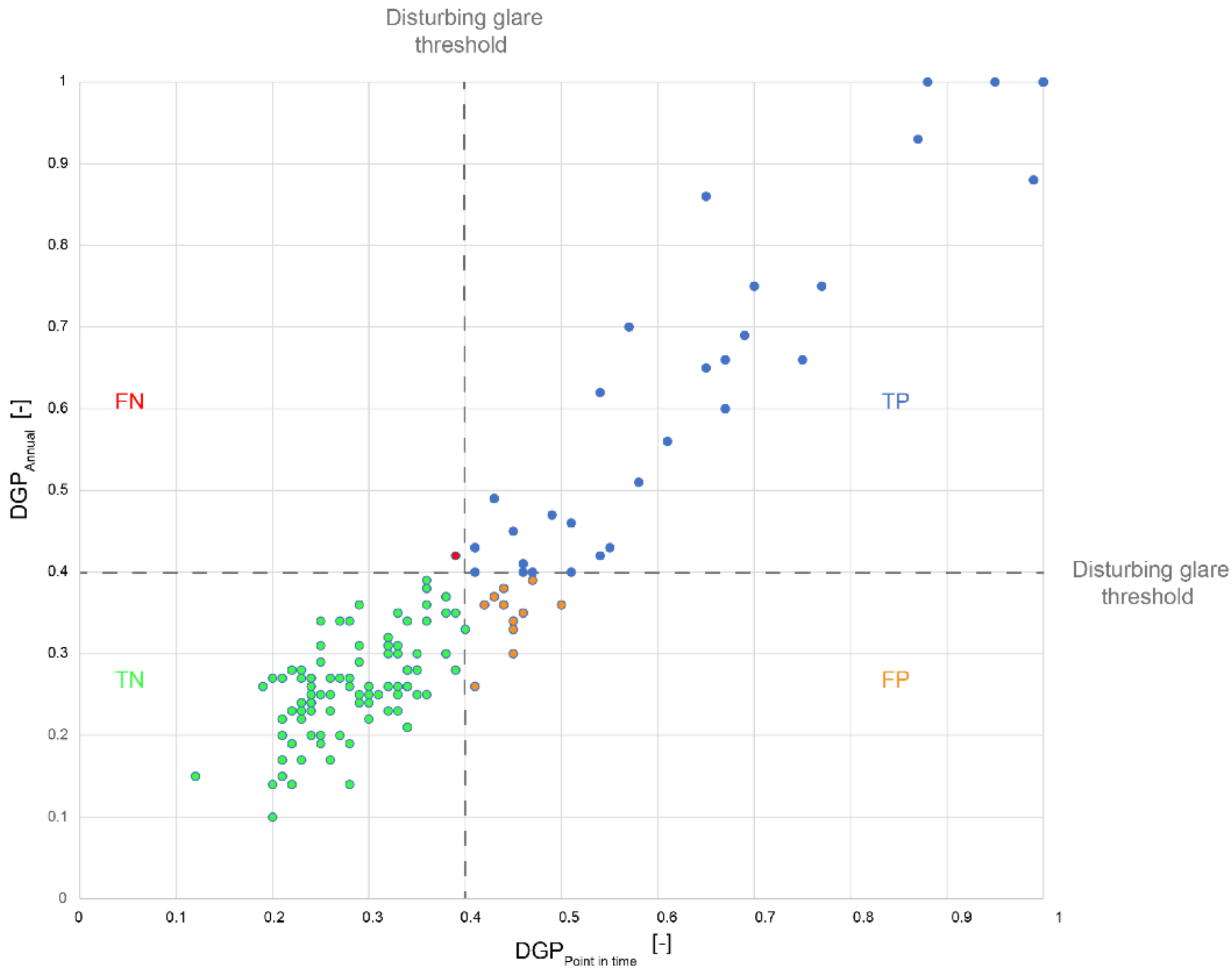

Figure 61. The binary classification of DGP$_{point\text{-}in\text{-}time}$ -DGP$_{annual}$ calculated for scenario one with disturbing glare threshold

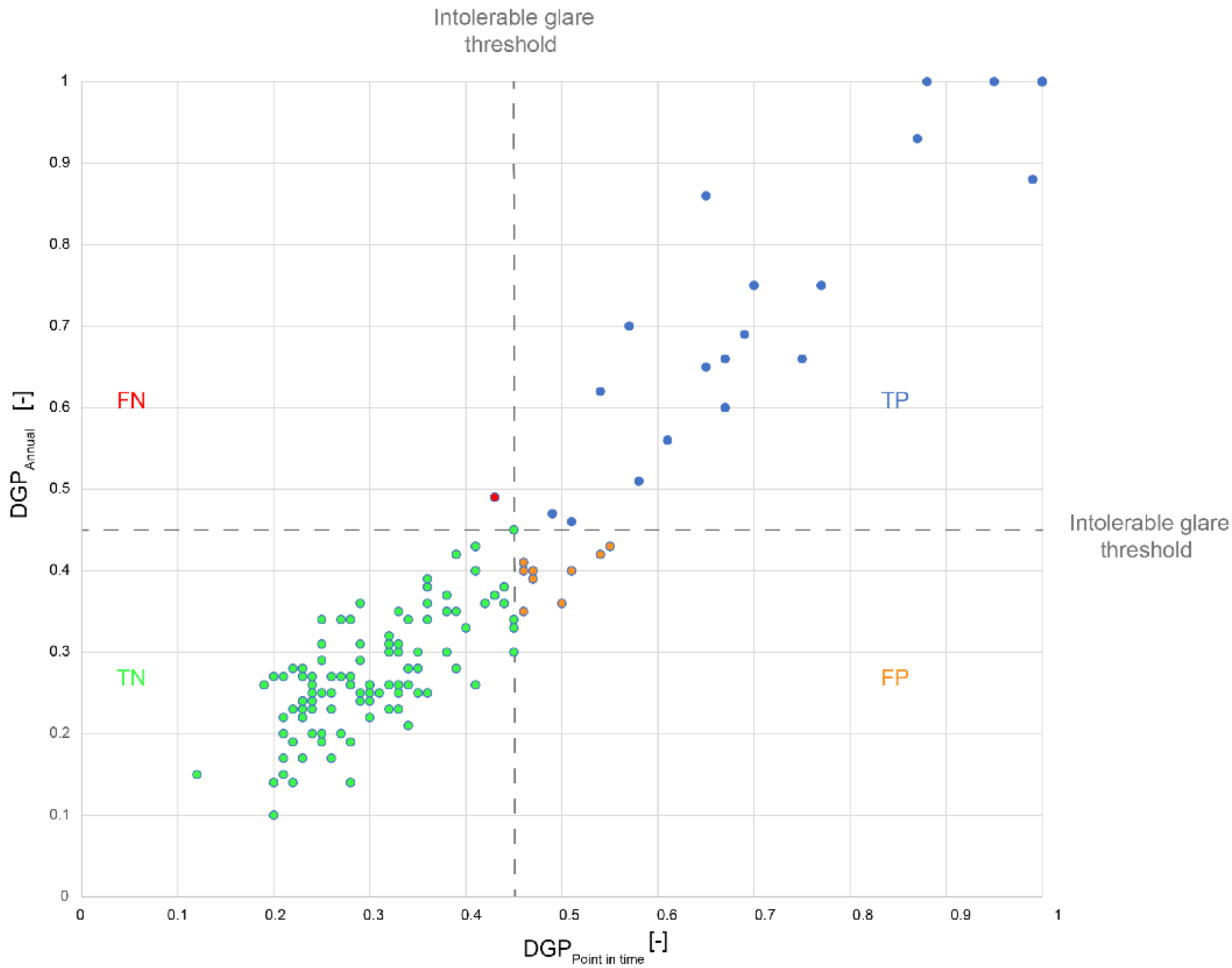

Figure 62. The binary classification of $DGP_{point\text{-}in\text{-}time}$ -DGP_{annual} calculated for scenario one with intolerable glare threshold

Figures 60-62 represent TN with green, TP with blue, FP with orange, and FN with red points. Each point on the chart is defined by a (DGP_{annual}, $DGP_{point\text{-}in\text{-}time}$) pair of values for a specific year time-step. The DGP_{thr} = 0.35, DGP_{thr} = 0.40, and DGP_{thr} = 0.45 is plotted as a dashed horizontal and vertical line in the figure. These two lines divided the graph into four quadrants, each with a different number of points. It is visible from the figures that most of the points were divided into the quadrants of TN and TP. There are only a few points were located in the FN and FP. By increasing the threshold from one glare class to another, the number of points was added to TN and decreased from FP. For statistical analysis of these results, the number of points categorized as TN, TP, FP, and FN is extracted and gathered in Table 32.

Table 32. Summary of the results of the binary classification in scenario one

Discomfort Glare classes	DGP_Annual [-]	DGP_point-in-time class [-]	Common classes	Percentage of each class [%]	TN [%]	TP [%]	FP [%]	FN [%]
Imperceptible glare	124	135	123	64.06				
Perceptible glare	15	16	7	3.65	71.35	22.92	4.69	0.52
Disturbing glare	11	7	2	1.04	77.60	16.15	5.73	0.52
intolerable glare	42	34	32	16.67	82.81	11.98	4.69	0.52
Total	192	192	164	85.42				

In Table 32, the number of each glare class has been extracted separately for DGP_{annual}, $DGP_{point-in-time}$. The corresponding color relates to each discomfort glare class, and the green represents imperceptible glare, yellow represents the perceptible glare, orange and red represent disturbing and intolerable glare conditions, respectively. For example, the number of DGP values with its glare class was counted and reported in this Table. After that, the number of similar classes was estimated correctly with both DGP_{annual}, $DGP_{point-in-time}$ was inserted as the number of similar classes. Then, the percentages of each class were presented. The number of points in each class of TN, TP, FN, and FP was reported in Table. The three thresholds were defined by color, and the percentages show the abundance of points in each GLANCE class.

Based on the results presented in Table 32, the DGP_{annual} estimated the glare condition 64% for imperceptible glare class and 16.67% for intolerable glare. In general, 85.42%

DGP_{annual} predicted correct glare comfort classes. When the threshold was perceptible, the amount of TN was 71.35%, and this amount reached 82.81% when the threshold changed to intolerable glare. In contrast, the percentage of the points in TP was 22.92%, with perceptible glare. As mentioned before, TP and TN show the correct estimation of the glare employing the DGP_{annual}. For example, the sum of TN and TP in the intolerable glare class revealed that more than 96% of the simulated time, DGP_{annual} predicted the glare as the same as $DGP_{point-in-time}$. FN, which is the most dangerous class in terms of glare prediction and considered an error for all the thresholds, was 0.52%. Moreover, FP was 4.69%, 5.73%, and 4.69% for the perceptible, disturbing and intolerable glare threshold.

Figure 63 represented the results with all thresholds and visualized the common glare classes.

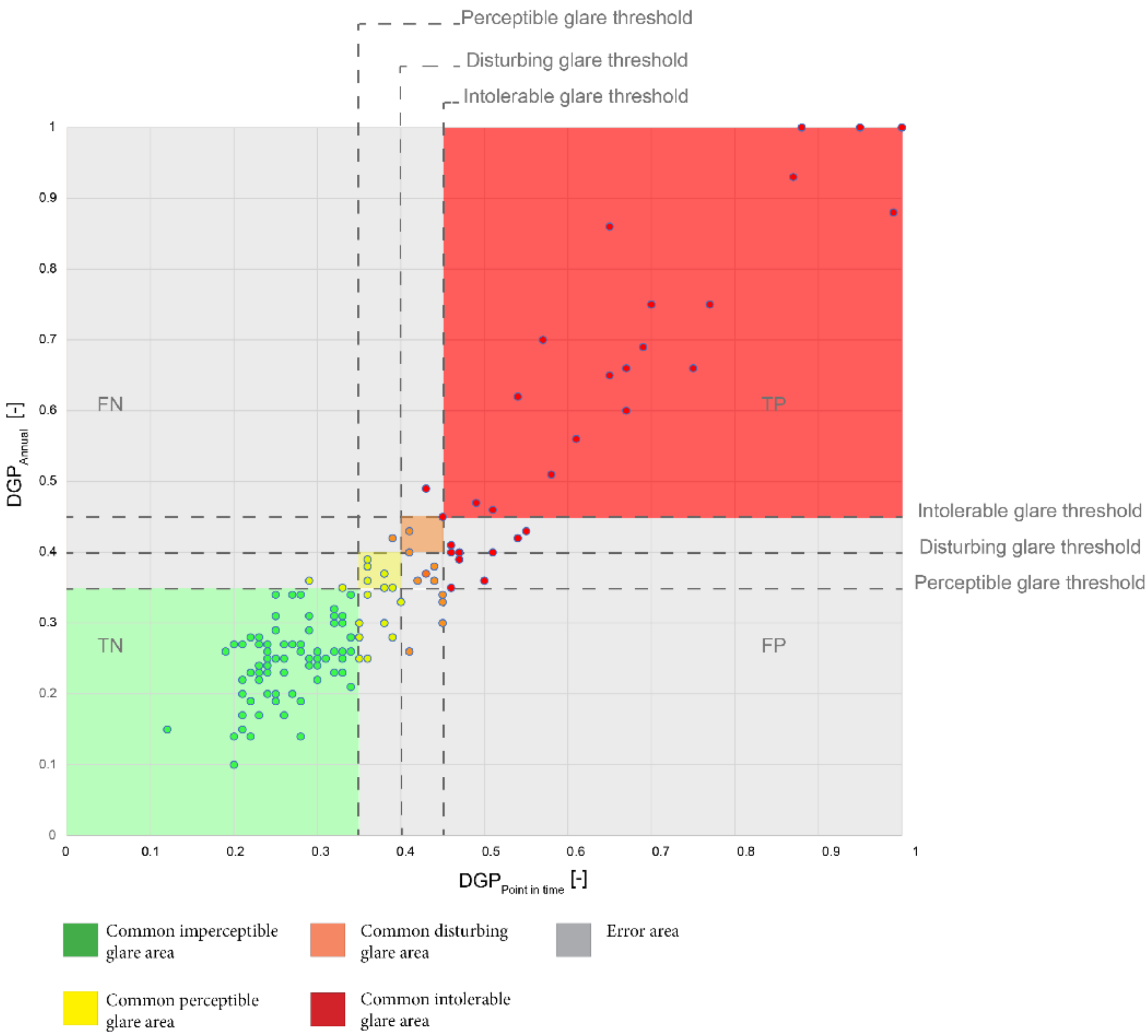

Figure 63. The classification of $DGP_{point\text{-}in\text{-}time}$ -DGP_{annual} calculated for scenario one

The area with green color represents the imperceptible glare condition, and the yellow, orange, and red shows the perceptible, disturbing, and intolerable glare in order. The grey area indicated the error area, which means that at least one glare was overestimated or underestimated by the DGP_{annual}.

4.8.2. Diagnostic analysis for scenario two

Figures 64-66 presents the diagnostic analysis of the results from scenario two. Results of figures 64-66 were shown that most of the points locating in the TN quadrant. Regardless of the DGP_{thr} on each figure, the abundance of the points was in TN and TP.

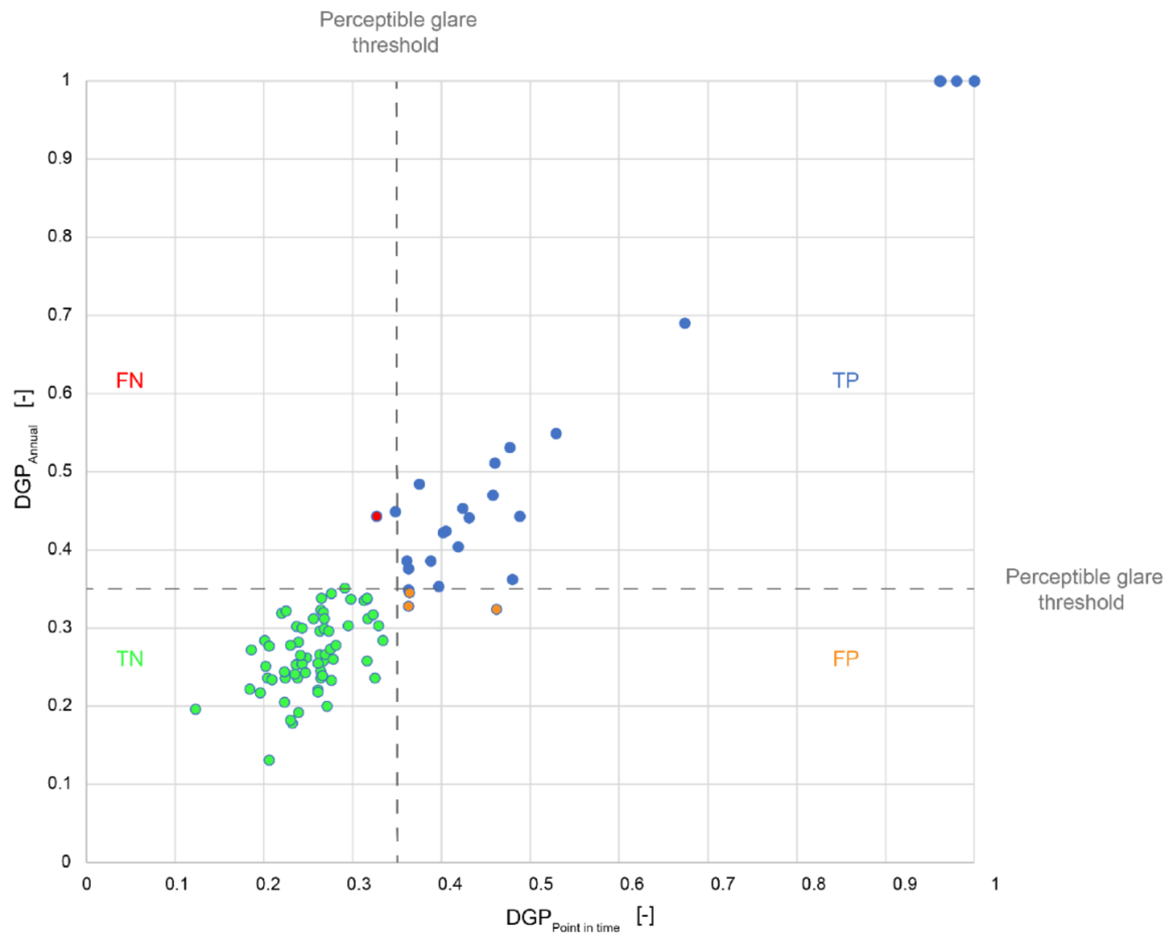

Figure 64. The binary classification of $DGP_{point\text{-}in\text{-}time}$ -DGP_{annual} calculated for scenario two with perceptible glare threshold

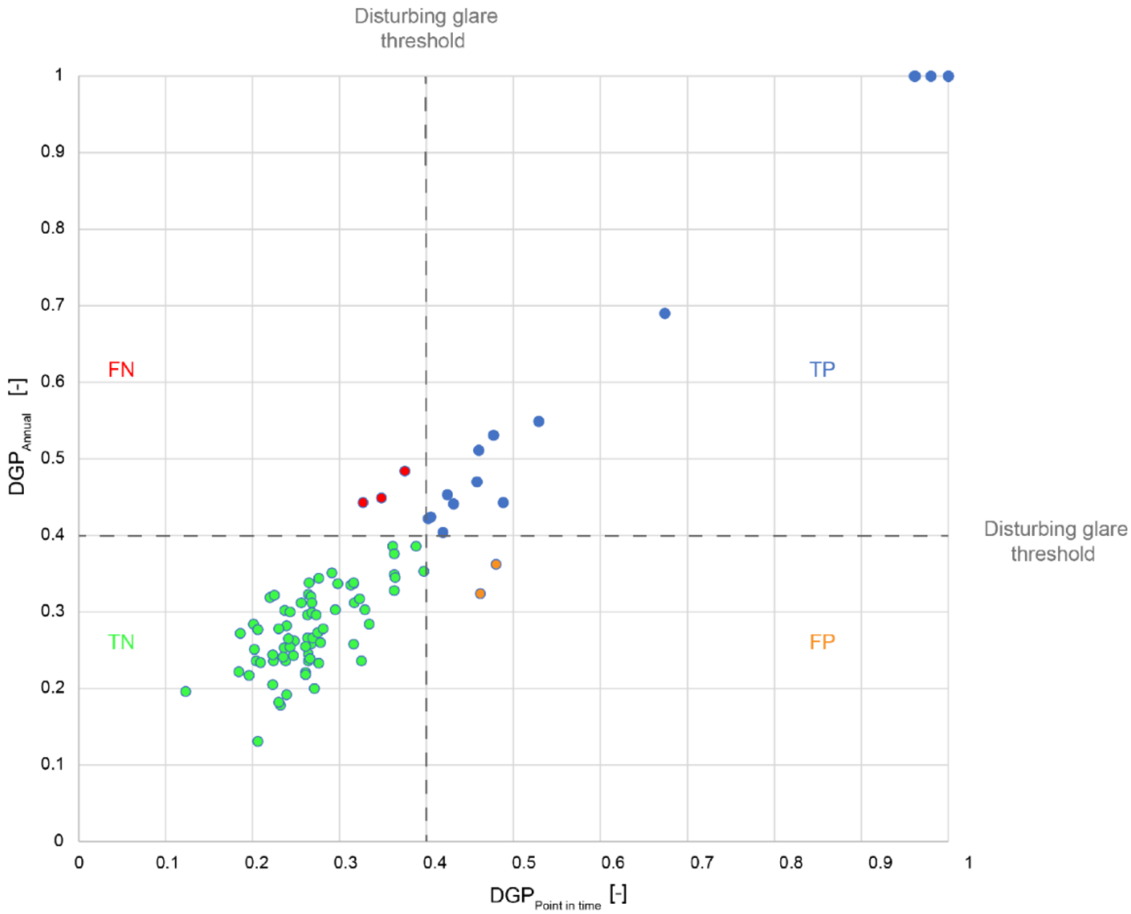

Figure 65. The binary classification of DGP$_{point\text{-}in\text{-}time}$ -DGP$_{annual}$ calculated for scenario two with disturbing glare threshold

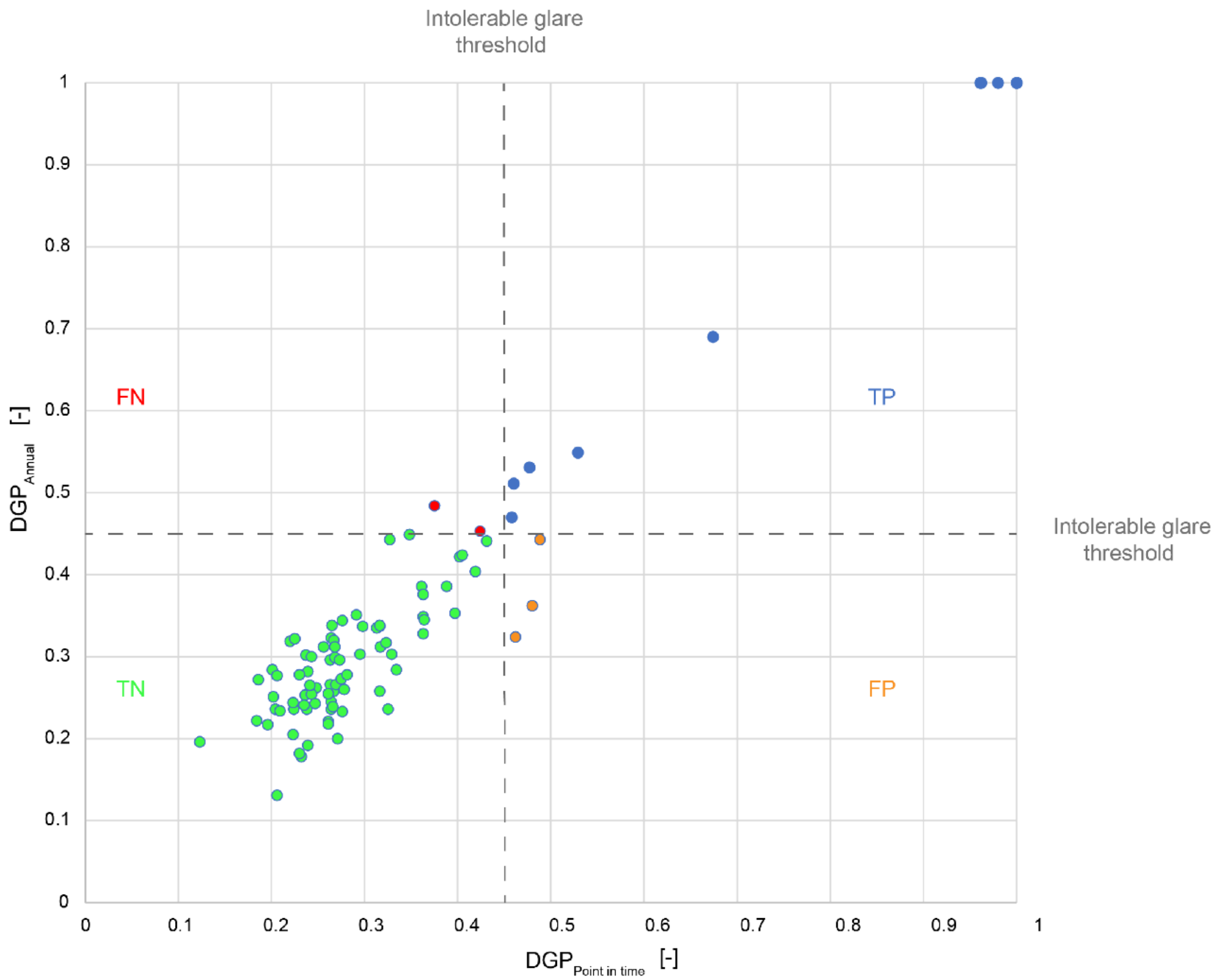

Figure 66. The binary classification of $DGP_{point-in-time}$ -DGP_{annual} calculated for scenario two with intolerable glare threshold

Only a few points were located in the area of FP since this area is the worth area in terms of the dangerous error in estimating the glare. The extracted amount of these points has been shown in Table 33.

Table 33. Summary of the results of the binary classification in scenario two

Discomfort Glare classes	DGP_Annual [-]	DGP_point-in-time class [-]	Common classes	Percentage of each classes [%]	TN [%]	TP [%]	FP [%]	FN [%]
Imperceptible glare	81	81	78	72.22				
Perceptible glare	8	7	5	4.63	75.00	21.30	2.78	0.93
Disturbing glare	5	7	4	3.70	82.41	12.96	1.85	2.78
intolerable glare	14	13	11	10.19	87.04	7.41	3.70	1.85
Total	108	108	98	90.74				

Table 33 represents the detailed information regarding the number of the discomfort glare classes when DGP_{annual} and $DGP_{point-in-time}$ were used. The percentages of common discomfort glare classes showed that 98% of the simulated times, the glare classes were equal in both DGP_{annual} and $DGP_{point-in-time}$. Therefore, if predicting the discomfort glare classes were concerned, the model had the goodness-of-fit.

As shown in Figure 67, except few points located in the gray area (error area), other points were in the common areas of the discomfort glare classes. Moreover, the results showed that when the perceptible glare was considered, the model accurately predicted the glare with more than 96.3%, the sum of TP and TN. The corresponding value for the disturbing and intolerable glare was 95.3% and 94.45%, respectively. However, the error area (FP and FN) was 5.55% for the intolerable glare class. In the disturbing glare class, the sum of the FP and FN was about 4.63%, and the perceptible glare was 3.71%. It should be considered that if only FP were considered as the main dangerous error area, the DGP_{annual} was predicting highly reliable.

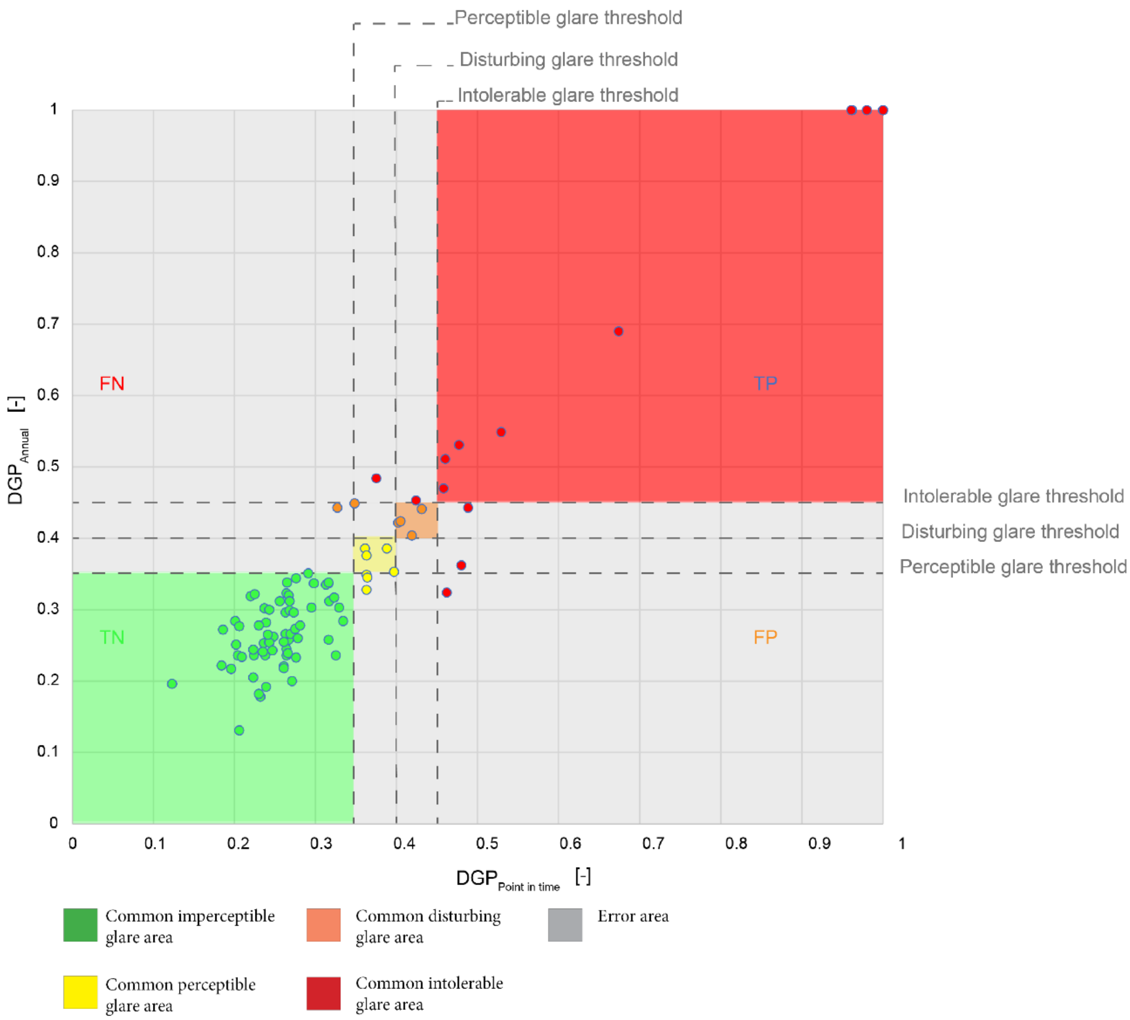

Figure 67. The classification of $DGP_{point\text{-}in\text{-}time}$ -DGP_{annual} calculated for scenario two

4.8.3. Diagnostic analysis for scenario three

The results of the analysis for scenario three are presented in Figures 68-70.

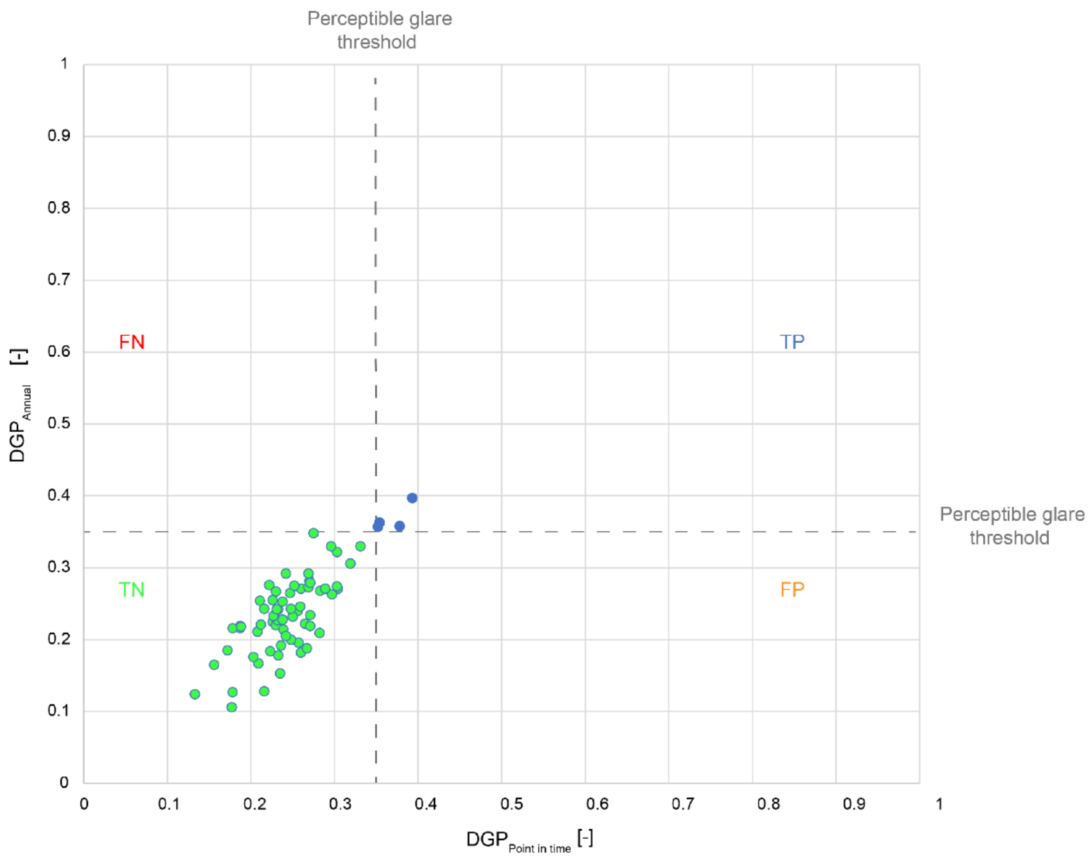

Figure 68. The binary classification of $DGP_{point\text{-}in\text{-}time}$ -DGP_{annual} calculated for scenario three with perceptible glare threshold

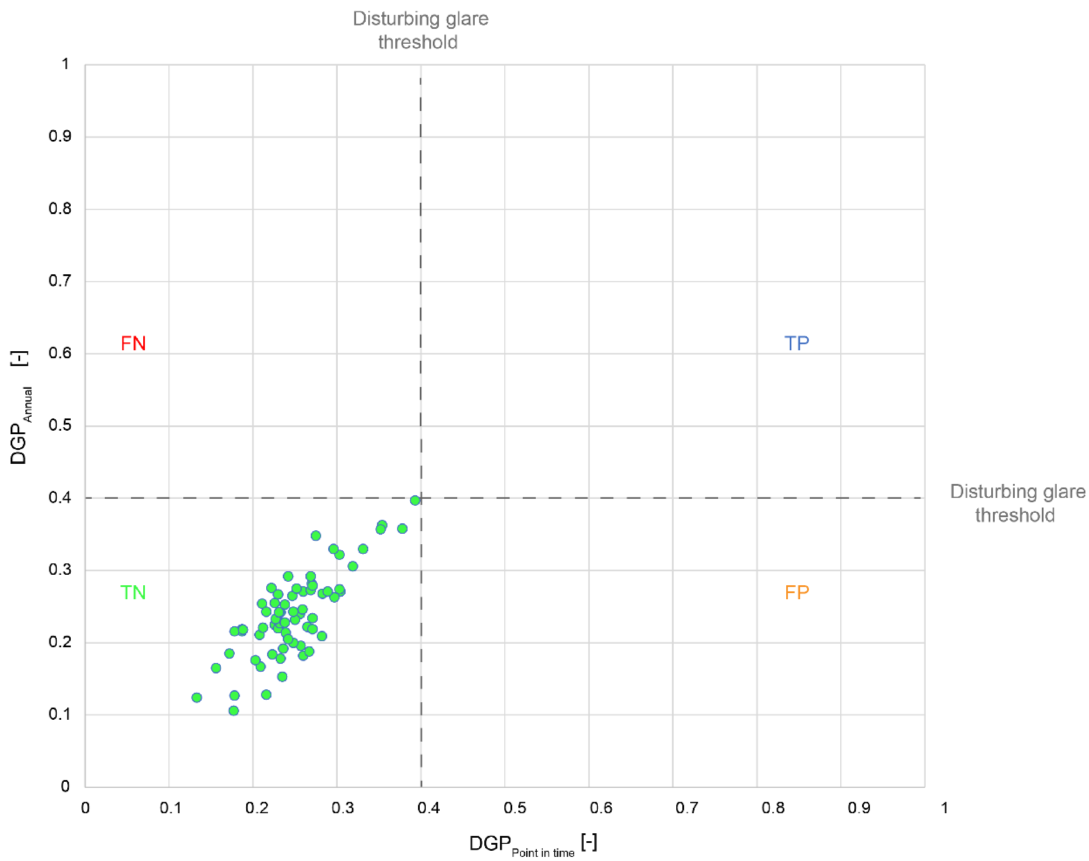

Figure 69. The binary classification of $DGP_{point\text{-}in\text{-}time}$ -DGP_{annual} calculated for scenario three with disturbing glare threshold

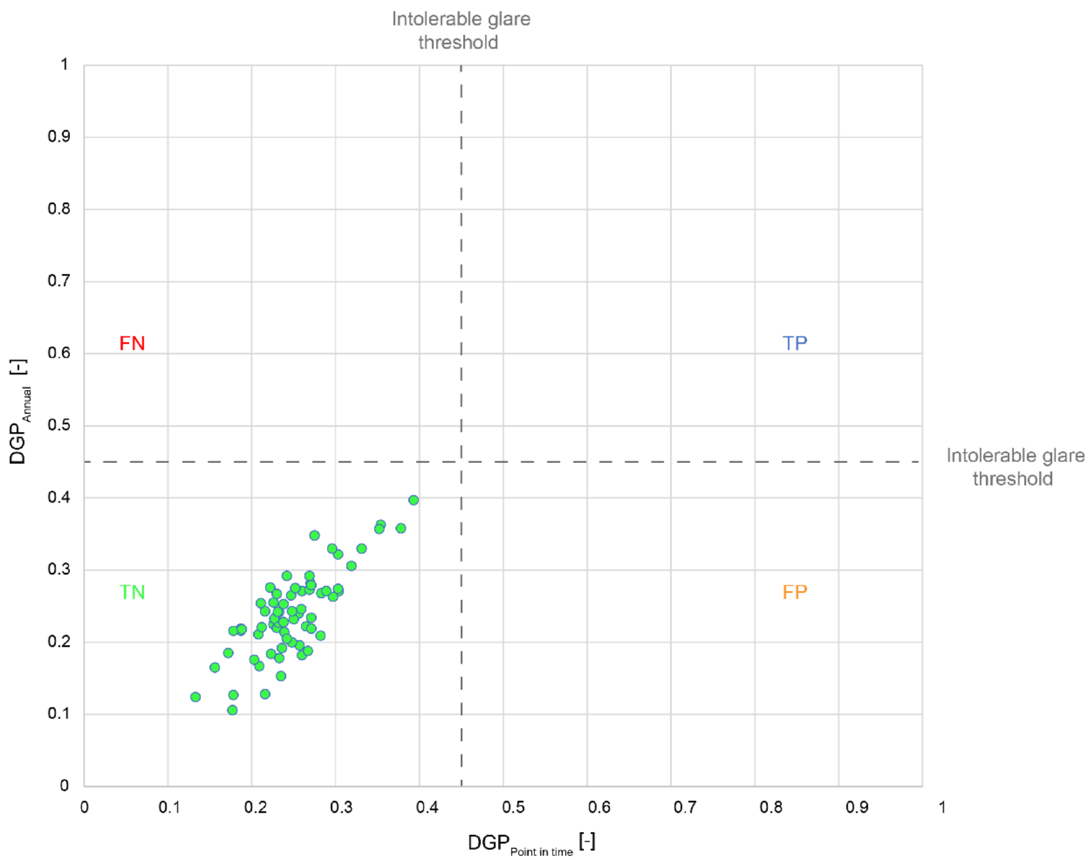

Figure 70. The binary classification of $DGP_{point\text{-}in\text{-}time}$ -DGP_{annual} calculated for scenario three with intolerable glare threshold

According to the results, all points were in the TP and TN for the perceptible glare classes. Only three points were in the area TP with considering the perceptible glare as a threshold. However, when the higher DGP_{thr} were taken into account like disturbing and intolerable, all the simulation results were in the TN. Table 34 statistically analyzed the amounts of DGP_{annual} and $DGP_{point\text{-}in\text{-}time}$ for each discomfort glare class.

Table 34. Summary of the results of the binary classification in scenario three

Discomfort Glare classes	DGP_Annual [-]	DGP_point-in-time class [-]	Common classes	Percentage of each classes [%]	TN [%]	TP [%]	FP [%]	FN [%]
Imperceptible glare	104	104	104	96.30				
Perceptible glare	4	4	4	3.70	96.30	3.70	0.00	0.00
Disturbing glare	0	0	0	0.00	100	0.00	0.00	0.00
intolerable glare	0	0	0	0.00	100	0.00	0.00	0.00
Total	108	108	108	100.00				

The results indicated that DGP_{annual} and $DGP_{point\text{-}in\text{-}time}$ were 96.3% in the imperceptible discomfort glare class and 3.7% in the perceptible glare. There were not observed any disturbing and intolerable glare at scenario three. Furthermore, 96.30% of the points were in the TN area and 3.70% in the TP in the perceptible glare class. In contrast, 100% of the points were in the TN in two other discomfort glare classes. Therefore, there were no DGP values in this scenario's error area (Figure 71). It means that the DGP_{annual} and $DGP_{point\text{-}in\text{-}time}$ were consistent entirely at all the simulated times.

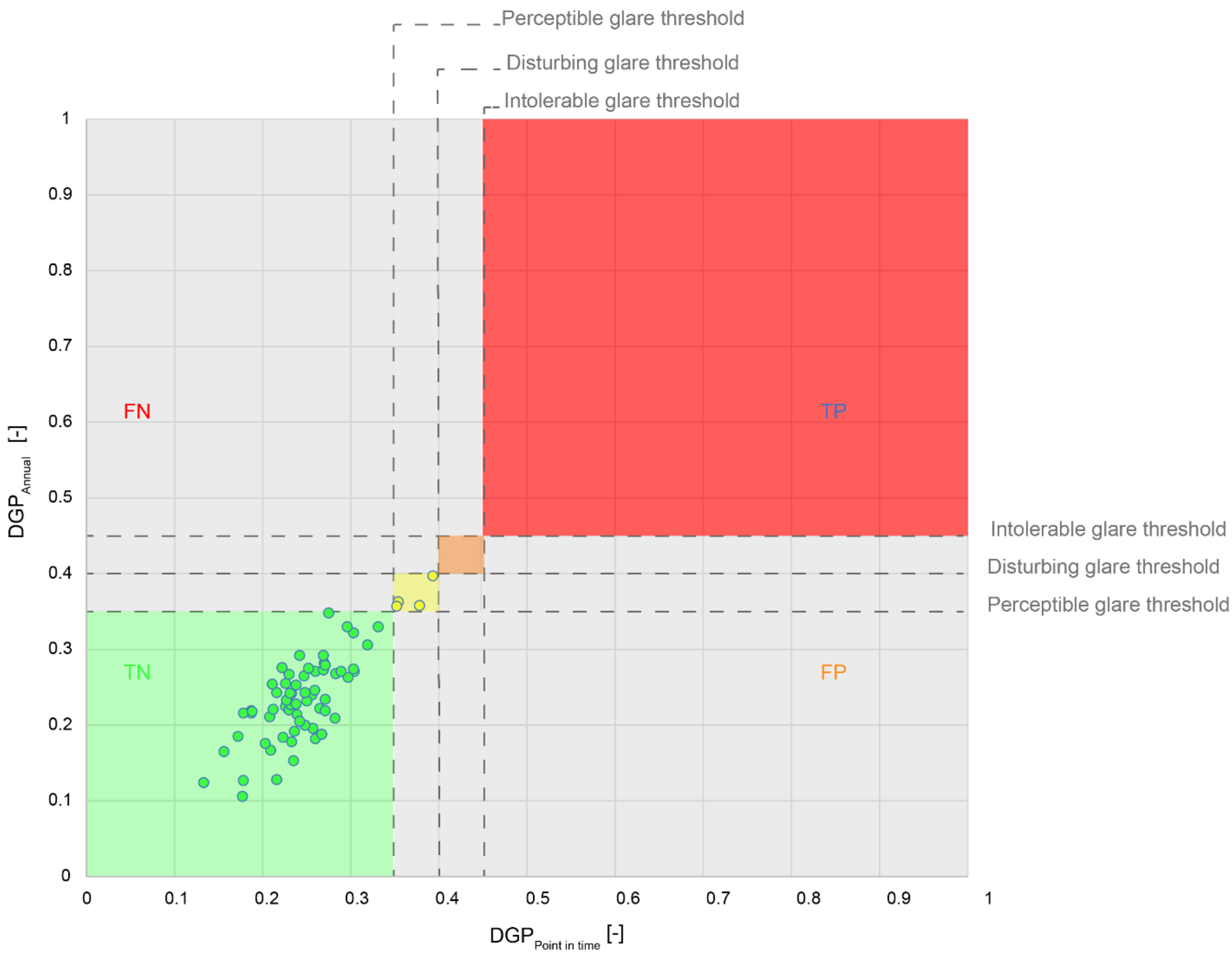

Figure 71. The classification of $DGP_{point\text{-}in\text{-}time}$ -DGP_{annual} calculated for scenario three

5. Discussion

This chapter compiles the thesis discussion, beginning with the essential findings and suggestions that are presented. The study's interpretations, strengths, limits, and challenges are then highlighted. Finally, the implications of practice as well as future research are discussed.

5.1. Summary of the main findings

The visual comfort and daylighting condition at DSF has been studied in this thesis. For calculation of the glare, there are more than 22 glare metrics has been proposed. A recent study showed that among 22 glare prediction metrics, both existing and freshly developed, the DGP is the most robust glare metric for office-like test rooms [105]. Therefore, in this study, DGP has been selected for analysis of the glare. The experimental glare assessment utilizing HDR images was conducted by analyzing 6 different reference points in the DSF test cell. Three of these points had a 45° view angle to the window and three others looking the window directly.

Various factors have been investigated through this thesis. The first one was finding reliable simulation tools in order to do the glare analysis. To this end, the two most commonly used software, Diva for Rhino and Honeybee in Grasshopper, has been selected and the simulation results compared. These tools are the user-friendly interface of Radiance and Daysim for daylighting simulations. The first round of the simulations was done to compare the $DGP_{point\text{-}in\text{-}time}$ values in both simulation tools. It should be noted that this round of simulation has been conducted for the points looking directly to the window. Simulations have been done with CIE sky models (clear sky with sun and overcast sky) and Perez All-Weather sky model. The simulation results with CIE sky models showed that the $DGP_{point\text{-}in\text{-}time}$ value in Diva was higher than the corresponding value in Honeybee almost for all the simulated time. The differences with the CIE overcast sky model were lower than the CIE clear sky. However, the disparity was significant so that in some simulated points, the $DGP_{point\text{-}in\text{-}time}$ values tripled than the $DGP_{point\text{-}in\text{-}time}$ in

Honeybee. Based on a study by Kong et al. [106], the accuracy of the sky model created by the hybrid photo-radiometer (HPR) sky model and the Perez all-weather sky model was experimentally analyzed. They concluded that under HPR and Perez skies, the accuracy of glare prediction was 95.5 % and 93.9 %, respectively. Therefore, the simulations repeated with the Perez sky model in both simulation tools.

Comparison of the results indicated that the $DGP_{point\text{-}in\text{-}time}$ values were precisely the same in both simulation tools at all simulated times and all points. Although the validity and accuracy of the CIE sky models have been investigated and confirmed in various studies [107,108], few studies investigated the results of different simulation tools. Therefore, it seems that the problem of overestimating the $DGP_{point\text{-}in\text{-}time}$ value by Diva when the CIE sky was considered stems from the background algorithms of the tool.

The results of estimation of the glare through DGP_{annual} were compared to the $DGP_{point\text{-}in\text{-}time}$. The GLANCE methodology introduced by Giovannini et al. [30] has been used for this study. The results showed that the DGPannual estimated the glare classes with high accuracy for all scenarios. The estimation rate of DGP_{annual} for discomfort glare classes were 100%, 90.74%, and 85.42% in scenarios three, two, and one, respectively. Therefore, it seems the DGP_{annual} predicted the glare discomfort classes with low light conditions.

In addition to discomfort glare classes, the exact values of DGP_{annual} and $DGP_{point\text{-}in\text{-}time}$ were compared. Results revealed very good correlation in all scenarios. The R^2 of scenarios two and three was the same, with the value of 0.94 and 0.64 for scenario three. It is important to stress that although the correlation in scenario three was lower than others, the glare comfort classes were estimated 100% correctly without any error in this scenario.

Moreover, the diagnostic analysis indicated that the DGP_{annual} has the lowest error related to false prediction (FP+FN) in the perceptible glare class with a value of 3.71% in scenario two and 5.21% in scenario two one. For disturbing glare in scenario two was 4.63% and in scenario one was 6.25%. The same approach was used in the study of [30,109] to evaluate the glare using the vertical illuminance instead of the DGP_{annual}. These studies showed a high correlation between vertical illuminance and DGP values. The results showed that error (FP+FN) for the window with higher visible transmittance was less than 5% in most simulated points. However, the approach was in line with this study, the objectives were different.

In addition, for the study of Giovannini et al. [30], simulations have been done for the space without shading devices, while in this thesis, the effect of shading devices was taken into consideration. It can be stated as another difference between the studies. The results of this study can also be compared with a newly published paper by Sepúlveda et al. [110]. The authors intend to assess cutting-edge approaches for annual glare analysis and explore solutions to minimize computing time without reducing glare calculation accuracy. They concluded that with their proposed sampling methodology (semi-annual and five-day-per-week), simulations of visible sun positions could reduce computation time for annual glare simulations by up to 86% when clear sky conditions were included.

5.2. Strengths and limitations of the study

This research was conducted on simplistic geometry, where all that was used as a test cell. On the other hand, the study's strength is that it is based on worldwide and European regulations, especially for office buildings, where occupant visual comfort is quite crucial. Furthermore, the ideas investigated are widely used, and some of them are novel, such as DGP, Spatial Daylight Autonomy (sDA), and Annual Sunlight Exposure (ASE).

It is also assessed using Grasshopper, a powerful parametric tool. Furthermore, the use of the study is comparable to a few previous research such as while the findings were more comprehensive and reliable. This study provided the guideline for architects and designers to assess the glare condition in the early design stage based on fast simulation DGP_{annual} for the exact place of users. Therefore, this study can also be helpful for façade engineers, dynamic shading device developers, researchers, and daylighting experts.

It should be noted that despite many efforts in the study and accurate simulation, various factors affecting the supply of indicators and appropriate methodology for evaluating and selecting façade technology have some limitations in this study. Among them is the limited number of samples of real sky conditions, the limited consideration of adequate light and glare parameters, such as the material and color of shading devices, the limited selection of types of shadings, etc.

Although the experimental analysis of the glare was conducted on some days with various sky conditions and morning and noontime to have the highest amount of daylight, there was no glare condition in the DSF. The reason can be the month of experimental HDR photography, which was in May. Therefore because of the sun's position, the glare did not happen in the test cell. Therefore, it can be considered as the limitation of this study.

Another limitation of the study was the HDR camera which was not equipped with the fisheye lens, it can also be another reason to have a lower amount of DGP when the scene was measured. As indicated in the paper of Pierson et al. [102], the lower amount of lens field of view results in a higher error. Therefore, the experimental analysis in a higher illuminance scene, such as some days in September and December with the fisheye lens, is highly recommended.

5.3. Interpretation and recommendations

Since it is tedious and time-consuming to calculate the glare at different times of the year, it is inevitable to perform annual simulations to save time and energy consumption from predicting the amount of glare at any time of the year. The annual glare calculation algorithm is different from the point-in-time glare analysis. For example, in the annual algorithm, the value of ambient bounces(-ab) in space is considered zero, which means that the vertical illuminance is the most crucial parameter in the glare calculation at each time step of this algorithm. Different methodologies were proposed and evaluated in order to simplification of glare calculation in the space. Some glare analysis algorithms solely examine brightness to get faster estimates. Wienold [40] created a simpler DGP calculation (DGPs) exclusively based on vertical illuminance. DGPs only applies to views with no direct sun or specular reflections since it ignores specific glare sources. Wienold's DGPs formula matches a vertical eye illuminance of 3500 lux with a 40% threshold for irritating glare. In another study by Giovannini et al., the authors proposed a methodology to predict the glare based on the vertical illuminance [30,109]. In this study, the vertical illuminance has been considered as the index for estimation of the glare. The accuracy of the glare prediction has been compared and validated with the DGP value at the corresponded time.

Nevertheless, in point-in-time glare calculation, (-ab) is considered, and different values can be attributed. As a result, the precision of the point-in-time algorithm in calculating glare is substantially higher than the accuracy of the annual method. For the annual glare analysis, (-ab) was set to 0 or 1 to calculate the HDR image and used for the calculation of the vertical illuminance. However, in the luminance map (-ab) was considered equal to 0 or 1. Therefore, proving the correctness of the expected annual glare using point-in-time glare and checking the error rate helps considerably minimize the computation time and cost of glare calculation. Moreover, confirming this methodology contributes to lower computational accuracy and more reliable results while shortening calculation time. The flexibility to evaluate different thresholds or parameter settings is one advantage of imageless DGP computation [111]. The methodology proposed by Pierson et al. [112] keeps evalglare's capacity to change parameters like brightness threshold, which alter its sensitivity to contrast.

Another reason for the importance of evaluating the annual glare algorithm is that it is needed to prepare the annual schedule for setting and controlling the dynamic shading devices. In the study of Wienold et al. [105], the accuracy of different glare metrics has been evaluated and validated through experimental analysis. The study conducted by Jones [111], proposed the methodology that correctly forecasted DGP under a year's worth of climate-based sky on a grid of sensor sites in a couple of minutes. This computation would take 4600 core hours, or 133,000 times longer, using traditional DGP simulation.

Despite Karlsen et al. [113] findings, which revealed a significant link between contrast-based glare indices and glare, contrast-based glare indices are inefficient in subsequent investigations [114–116]. The relationship between glare and luminosity is affected by dissatisfaction with individual differences, the lack of time parameters (duration of glare), and the possibility of adaptation to conditions (by changing angle, displacement) in evaluating indicators. It is recommended to consider these parameters to have more cohesive results with the real condition with occupants' perception from the glare.

5.4. Implication on practice and future research

In addition to the view direction and angles of the shading studied in this thesis, other factors such as the dimensions of the space, outside vegetation, and barriers, characteristics of the shading, etc., can be influential in receiving daylight and glare conditions. Due to the multiplicity of different combinations of these factors and the study of their impact on each other is a very complex and tedious process. However, the development of simulation and optimization science and parametric design can be related to each other. It is recommended to investigate further, use parametric design software to examine daylight and glare conditions in future studies.

In order to evaluate the glare condition, more simulations step with a higher amount of illuminance can be conducted as a future study. Replication of the method and evaluate the DGP_{annual} and $DGP_{point\text{-}in\text{-}time}$ for other façade technology such as chromogenic glazing family can be investigated further.

Future studies can also include controlling the dynamic shadings based on the annual profile produced based on DGP_{annual} and comparing its results with other control strategies in terms of occupants' visual comfort.

Based on several studies [105,114,116], DGP was the most precise and reliable glare index, the correlation of DGP and other indices can be investigated in future research.

6. Conclusions

In this study, the visual comfort and daylighting condition at DSF were numerically and experimentally evaluated. The introduced DSF was simulated using Honeybee in Grasshopper and Diva for Rhino. Measurements and simulations have been conducted for six points in DSF located at a different distance from the window. Different indicators of daylight and glare were simulated. After that, the effect of the Venetian blind with different degree angles on the selected indicators was investigated. Three scenarios have been defined to investigate the impact of Venetian blind on daylighting and glare. Scenario one was considered when the Venetian blind was raised, while scenarios two and three were performed with the Venetian blind drawn and slat tilt angles of 0° and 30°, respectively. The following conclusions can be extracted from this study:

- The simulation results with CIE sky models showed that the $DGP_{point\text{-}in\text{-}time}$ value in Diva was higher than the corresponding value in Honeybee almost for all the simulated time. The differences with the CIE overcast sky model were lower than the CIE clear sky. However, the disparity was significant so that in some simulated points, the $DGP_{point\text{-}in\text{-}time}$ values tripled than the $DGP_{point\text{-}in\text{-}time}$ in Honeybee.
- Considering the CIE sky, the problem of overestimating the $DGP_{point\text{-}in\text{-}time}$ value by Diva stemmed from the background algorithms of the tool. However, a Comparison of the results indicated that the $DGP_{point\text{-}in\text{-}time}$ values were precisely the same in both simulation tools at all simulated times and all points with the Perez All-Weather sky model.
- By assessing the $DGP_{point\text{-}in\text{-}time}$ and DGP_{annual} for each simulated hour, the closer the evaluated points are to the window, the more the value of glare classifications is inconsistent.
- By utilizing DGP_{annual}, the estimation of glare classes increased from scenarios one to three. Moreover, having the Venetian blind improved the estimation accuracy of the glare classes.

- On sunny days, the mismatch between DGP_{annual} and $DGP_{point\text{-}in\text{-}time}$ more happened; however, on overcast days, DGP_{annual} and $DGP_{point\text{-}in\text{-}time}$ were utterly consistent. Therefore, the greatest quantity of light resulted in the most significant degree of inaccuracy in predicting the glare values.
- DGP_{annual} was overestimated in the morning and underestimated in the afternoon in all situations for the majority of simulated periods and points.
- The studied scenarios confirmed that when the 30° angle has been set, the glare was solved in the simulated points. Therefore, for glare analysis, the higher angle was excluded from the results.
- For all scenarios, the DGP_{annual} estimated the glare classes with high accuracy. The estimation rate of DGP_{annual} for discomfort glare classes were 100%, 90.74%, and 85.42% in scenarios three, two, and one, respectively. Therefore, it seems the DGP_{annual} predicted the glare discomfort classes with low light conditions.
- The diagnostic analysis indicated that the DGP_{annual} had the lowest error related to false prediction (FP+FN) in the perceptible glare class with a value of 3.71% in scenario two and 5.21% in scenarios two and one. For disturbing glare, this prediction in scenario two was 4.63% and in scenario one was 6.25%.
- In addition to discomfort glare classes, the exact values of DGP_{annual} and $DGP_{point\text{-}in\text{-}time}$ were compared. The results revealed a very good correlation in all scenarios. The R^2 of scenarios two and three was the same (0.94). A value of 0.64 was obtained for scenario three. It is important to stress that although the correlation in scenario three was lower than others, the glare comfort classes were estimated 100% correctly without any error in this scenario.

In general, the results demonstrated that the Honeybee as a simulation tool was capable to assess the glare accurately. The statistical analysis has been carried out and high correlation was obtained between the annual and point-in-time glare analyses. The diagnostic analysis results showed that the low amount of error (FP+FN) occurred when the DGP_{annual} was concerned for calculation of the glare. Therefore, the glare analysis can be simplified by employing the annual glare analysis instead of point-in-time.

7. References

[1] Lo Verso VRM, Pellegrino A. Energy saving generated through automatic lighting control systems according to the estimation method of the standard EN 15193-1. J Daylighting 2019. https://doi.org/10.15627/jd.2019.13.

[2] Figueiro MG, Brons JA, Plitnick B, Donlan B, Leslie RP, Rea MS. Measuring circadian light and its impact on adolescents. Light Res Technol 2011. https://doi.org/10.1177/1477153510382853.

[3] Busatto N, Mora TD, Peron F, Romagnoni P. Application of different circadian lighting metrics in a health residence. J Daylighting 2020. https://doi.org/10.15627/jd.2020.2.

[4] Altomonte S. Daylight for Energy Savings and Psycho-Physiological Well-Being in Sustainable Built Environments. J Sustain Dev 2009. https://doi.org/10.5539/jsd.v1n3p3.

[5] Garretón JY, Rodriguez R, Pattini A. Effects of perceived indoor temperature on daylight glare perception. Build Res Inf 2016;44:907–19. https://doi.org/10.1080/09613218.2016.1103116.

[6] Reinhart CF, Mardaljevic J, Rogers Z. Dynamic daylight performance metrics for sustainable building design. LEUKOS - J Illum Eng Soc North Am 2006;3:7–31. https://doi.org/10.1582/LEUKOS.2006.03.01.001.

[7] Quek G, Jakubiec JA. Building climate-based daylighting models based on one-time field measurements. Build. Simul. Conf. Proc., vol. 2, 2019, p. 966–73. https://doi.org/10.26868/25222708.2019.210105.

[8] Reinhart CF, Weissman DA. The daylit area - Correlating architectural student assessments with current and emerging daylight availability metrics. Build Environ 2012;50:155–64. https://doi.org/10.1016/j.buildenv.2011.10.024.

[9] Altomonte S, Kent MG, Tregenza PR, Wilson R. Visual task difficulty and temporal influences in glare response. Build Environ 2016;95:209–26. https://doi.org/10.1016/j.buildenv.2015.09.021.

[10] Wienold J, Christoffersen J. Evaluation methods and development of a new glare prediction model for daylight environments with the use of CCD cameras. Energy Build 2006;38:743–57. https://doi.org/10.1016/j.enbuild.2006.03.017.

[11] Van Den Wymelenberg KG. Visual comfort, discomfort glare, and occupant fenestration control: Developing a research agenda.

LEUKOS - J Illum Eng Soc North Am 2014;10:207–21. https://doi.org/10.1080/15502724.2014.939004.
[12] Nabil A, Mardaljevic J. Useful daylight illuminances: A replacement for daylight factors. Energy Build 2006;38:905–13. https://doi.org/10.1016/j.enbuild.2006.03.013.
[13] Jakubiec JA. The Use of Visual Comfort Metrics in the Design of Daylit Spaces by Signature redacted Signature redacted. Massachusetts Inst Technol 2014:144.
[14] U.S. Green Building Council (USGBC). LEED v4- Reference Guide for Building Design And Construction. US Green Build Counc 2013.
[15] Michael A, Heracleous C. Assessment of natural lighting performance and visual comfort of educational architecture in Southern Europe: The case of typical educational school premises in Cyprus. Energy Build 2017;140:443–57. https://doi.org/10.1016/j.enbuild.2016.12.087.
[16] Plympton P, Conway S, Epstein K. Daylighting in Schools: Improving Student Performance and Health at a Price Schools Can Afford. Am Sol Energy Soc Conf 2000:10.
[17] Serra R. Daylighting. Renew Sustain Energy Rev 1998;2:115–55. https://doi.org/10.1016/s1364-0321(98)00014-8.
[18] Steane MA. The architecture of light: Recent approaches to designing with natural light. vol. 9780203715. 2012. https://doi.org/10.4324/9780203715505.
[19] Mingfang T. Solar control for buildings. Build Environ 2002;37:659–64. https://doi.org/10.1016/S0360-1323(01)00063-4.
[20] Kuhn TE. State of the art of advanced solar control devices for buildings. Sol Energy 2017;154:112–33. https://doi.org/10.1016/j.solener.2016.12.044.
[21] White JR. Didactic daylight design for education. ProQuest Diss Theses 2009:84.
[22] Jakubiec JA, Reinhart CF. Predicting visual comfort conditions in a large daylit space based on long-term occupant evaluations: A field study. Proc. BS 2013 13th Conf. Int. Build. Perform. Simul. Assoc., 2013, p. 3408–15.
[23] Reinhart CF. Lightswitch-2002: A model for manual and automated control of electric lighting and blinds. Sol Energy 2004;77:15–28. https://doi.org/10.1016/j.solener.2004.04.003.
[24] EN. Light and lighting – Basic terms and criteria for specifying lighting requirements. Belgium:EuropeanCommitteeforStandardization 2011. https://doi.org/2004R0726 - v.7 of 05.06.2013.

[25] Technical Committee CEN/TC 169 “Light and Lighting.” Light and lighting - Lighting of work places - Part 1 : Indoor work. Eur Stand 2002;3:1–43.
[26] Wienold J. Daylight Glare in Offices. Fraunhofer Verlag, 2009.
[27] Pierson C, Wienold J, Bodart M. Review of Factors Influencing Discomfort Glare Perception from Daylight. LEUKOS - J Illum Eng Soc North Am 2018;14:111–48. https://doi.org/10.1080/15502724.2018.1428617.
[28] Carlucci S, Causone F, De Rosa F, Pagliano L. A review of indices for assessing visual comfort with a view to their use in optimization processes to support building integrated design. Renew Sustain Energy Rev 2015;47:1016–33. https://doi.org/10.1016/j.rser.2015.03.062.
[29] IESNA. IESNA Lightning Handbook. 2018.
[30] Giovannini L, Favoino F, Lo Verso VRM, Serra V, Pellegrino A. GLANCE (GLare ANnual Classes Evaluation): An approach for a simplified spatial glare evaluation. Build Environ 2020;186. https://doi.org/10.1016/j.buildenv.2020.107375.
[31] Van Den Wymelenberg K, Inanici M. A critical investigation of common lighting design metrics for predicting human visual comfort in offices with daylight. LEUKOS - J Illum Eng Soc North Am 2014;10:145–64. https://doi.org/10.1080/15502724.2014.881720.
[32] Jakubiec JA, Reinhart CF, Van Den Wymelenberg K. Towards an integrated framework for predicting visual comfort conditions from luminance-based metrics in perimeter daylit spaces. 14th Int. Conf. IBPSA - Build. Simul. 2015, BS 2015, Conf. Proc., 2015, p. 1189–96.
[33] Suk J, Schiler M. Investigation of Evalglare software, daylight glare probability and high dynamic range imaging for daylight glare analysis. Light Res Technol 2013;45:450–63. https://doi.org/10.1177/1477153512458671.
[34] Suk JY, Schiler M, Kensek K. Investigation of existing discomfort glare indices using human subject study data. Build Environ 2017;113:121–30. https://doi.org/10.1016/j.buildenv.2016.09.018.
[35] Einhorn HD. Discomfort glare: A formula to bridge differences. Light Res Technol 1979;11:90–4. https://doi.org/10.1177/14771535790110020401.
[36] Jakubiec JA, Reinhart C. The “adaptive zone” - A concept for Assessing glare throughout daylit spaces. Proc. Build. Simul. 2011 12th Conf. Int. Build. Perform. Simul. Assoc., 2011, p. 2178–85.
[37] Scheir GH, Hanselaer P, Bracke P, Deconinck G, Ryckaert WR.

Calculation of the Unified Glare Rating based on luminance maps for uniform and non-uniform light sources. Build Environ 2015;84:60–7. https://doi.org/10.1016/j.buildenv.2014.10.027.
[38] Hopkinson RG. The Multiple Criterion Technique of Subjective Appraisal. Q J Exp Psychol 1950;2:124–31. https://doi.org/10.1080/17470215008416585.
[39] Geerdinck L. Glare Perception in Terms of Acceptance and Comfort. 2012.
[40] Wienold J. Dynamic daylight glare evaluation. IBPSA 2009 - Int. Build. Perform. Simul. Assoc. 2009, 2009, p. 944–51.
[41] Reinhart C. Opinion: Climate-based daylighting metrics in LEEDv4 - A fragile progress. Light Res Technol 2015. https://doi.org/10.1177/1477153515587613.
[42] Walsh JWT. The Early Years of Illuminating Engineering in Great Britain. Light Res Technol 1951;16:49–60. https://doi.org/10.1177/147715355101600301.
[43] Perry MJ. Field study of lighting maintenance factors. Light Res Technol 1999;31:155–64. https://doi.org/10.1177/096032719903100404.
[44] USGBC. Building Design and Construction. Build Des Constr 2013;3096:817.
[45] The Daylight Metrics Committee. Approved Method: IES Spatial Daylight Autonomy (sDA) and Annual Sunlight Exposure (ASE). 2012.
[46] Mardaljevic J, Heschong L, Lee E. Daylight metrics and energy savings. Light Res Technol 2009;41:261–83. https://doi.org/10.1177/1477153509339703.
[47] Böke J, Knaack U, Hemmerling M. State-of-the-art of intelligent building envelopes in the context of intelligent technical systems. Intell Build Int 2019;11:27–45. https://doi.org/10.1080/17508975.2018.1447437.
[48] Casini M. Active dynamic windows for buildings: A review. Renew Energy 2018;119:923–34. https://doi.org/10.1016/j.renene.2017.12.049.
[49] Attia S, Navarro AL, Juaristi M, Monge-Barrio A, Gosztonyi S, Al-Doughmi Z. Post-occupancy evaluation for adaptive façades. J Facade Des Eng 2018;6:001–9. https://doi.org/10.7480/jfde.2018.3.2464.
[50] Favoino F, Loonen RCGM, Doya M, Goia F, Bedon C, Babich F. Building performance simulation and characterisation of adaptive facades – Adaptive Facade Network. TU Delft Open; 2018.
[51] Attia S, Lioure R, Declaude Q. Future trends and main concepts of

adaptive facade systems. Energy Sci Eng 2020;8:3255–72. https://doi.org/10.1002/ese3.725.
[52] Al-Masrani SM, Al-Obaidi KM. Dynamic shading systems: A review of design parameters, platforms and evaluation strategies. Autom Constr 2019;102:195–216. https://doi.org/10.1016/j.autcon.2019.01.014.
[53] Loonen RCGM, Favoino F, Hensen JLM, Overend M. Review of current status, requirements and opportunities for building performance simulation of adaptive facades†. J Build Perform Simul 2017;10:205–23. https://doi.org/10.1080/19401493.2016.1152303.
[54] Shameri MA, Alghoul MA, Sopian K, Zain MFM, Elayeb O. Perspectives of double skin façade systems in buildings and energy saving. Renew Sustain Energy Rev 2011;15:1468–75. https://doi.org/10.1016/j.rser.2010.10.016.
[55] Hamza N. Double versus single skin facades in hot arid areas. Energy Build 2008;40:240–8. https://doi.org/10.1016/j.enbuild.2007.02.025.
[56] Poirazis. H. Double Skin Façades for Office Buildings. Lund Inst Technol Sweden 2004:192.
[57] Alibaba HZ, Ozdeniz MB. Thermal comfort of multiple-skin facades in warmclimate offices. Sci Res Essays 2011;6:4065–78. https://doi.org/10.5897/sre11.319.
[58] Çıldır AS, Köktürk G, Tokuç A. Design approaches for retrofiting offices to reach nearly zero energy: A case study in the Mediterranean climate. Energy Sustain Dev 2020;58:167–81. https://doi.org/10.1016/j.esd.2020.08.004.
[59] Poirazis H. Double-skin façades - A literature review. IEA SHC Task 34 2007.
[60] GhaffarianHoseini A, GhaffarianHoseini A, Berardi U, Tookey J, Li DHW, Kariminia S. Exploring the advantages and challenges of double-skin facądes (DSFs). Renew Sustain Energy Rev 2016;60:1052–65. https://doi.org/10.1016/j.rser.2016.01.130.
[61] Lee KS, Han KJ, Lee JW. The impact of shading type and azimuth orientation on the daylighting in a classroom-focusing on effectiveness of façade shading, comparing the results of da and udi. Energies 2017;10. https://doi.org/10.3390/en10050635.
[62] Bellia L, Marino C, Minichiello F, Pedace A. An overview on solar shading systems for buildings. Energy Procedia, vol. 62, 2014, p. 309–17. https://doi.org/10.1016/j.egypro.2014.12.392.
[63] Srisamranrungruang T, Hiyama K. Balancing of natural ventilation, daylight, thermal effect for a building with double-skin perforated facade

(DSPF). Energy Build 2020;210. https://doi.org/10.1016/j.enbuild.2020.109765.
[64] Yi YK, Yin J, Tang Y. Developing an advanced daylight model for building energy tool to simulate dynamic shading device. Sol Energy 2018;163:140–9. https://doi.org/10.1016/j.solener.2018.01.082.
[65] Al-Masrani SM, Al-Obaidi KM, Zalin NA, Aida Isma MI. Design optimisation of solar shading systems for tropical office buildings: Challenges and future trends. Sol Energy 2018;170:849–72. https://doi.org/10.1016/j.solener.2018.04.047.
[66] Ochoa CE, Aries MBC, Hensen JLM. State of the art in lighting simulation for building science: A literature review. J Build Perform Simul 2012;5:209–33. https://doi.org/10.1080/19401493.2011.558211.
[67] Ward G and SR. Rendering with Radiance: The Art and Science of Lighting Visualization. Morgan Kaufman 1998.
[68] Reinhart CF, Walkenhorst O. Validation of dynamic RADIANCE-based daylight simulations for a test office with external blinds. Energy Build 2001;33:683–97. https://doi.org/10.1016/S0378-7788(01)00058-5.
[69] Mardaljevic J. Validation of a lighting simulation program under real sky conditions. Light Res Technol 1995;27:181–8. https://doi.org/10.1177/14771535950270040701.
[70] Walkenhorst O, Luther J, Reinhart C, Timmer J. Dynamic annual daylight simulations based on one-hour and one-minute means of irradiance data. Sol Energy 2002;72:385–95. https://doi.org/10.1016/S0038-092X(02)00019-1.
[71] Tregenza PR, Waters IM. Daylight coefficients. Light Res Technol 1983;15:65–71. https://doi.org/10.1177/096032718301500201.
[72] Perez R, Seals R, Michalsky J. All-weather model for sky luminance distribution-Preliminary configuration and validation. Sol Energy 1993;50:235–45. https://doi.org/10.1016/0038-092X(93)90017-I.
[73] Urbano Gutiérrez R, Du J, Ferreira N, Ferrero A, Sharples S. Daylight control and performance in office buildings using a novel ceramic louvre system. Build Environ 2019;151:54–74. https://doi.org/10.1016/j.buildenv.2019.01.030.
[74] Jakubiec JA, Reinhart CF. DIVA 2.0: Integrating daylight and thermal simulations using rhinoceros 3D, DAYSIM and EnergyPlus. Proc. Build. Simul. 2011 12th Conf. Int. Build. Perform. Simul. Assoc., 2011, p. 2202–9.
[75] Solemma 2021. https://www.solemma.com/.
[76] Kharvari F. An empirical validation of daylighting tools: Assessing

radiance parameters and simulation settings in Ladybug and Honeybee against field measurements. Sol Energy 2020;207:1021–36. https://doi.org/10.1016/j.solener.2020.07.054.
[77] Roudsari MS, Pak M. Ladybug: A parametric environmental plugin for grasshopper to help designers create an environmentally-conscious design. Proc. BS 2013 13th Conf. Int. Build. Perform. Simul. Assoc., 2013, p. 3128–35.
[78] Davidson S. Grasshopper Algorithmic Modeling for Rhino. Add-Ons Grasshopp 2015. https://www.grasshopper3d.com/.
[79] Kumaragurubaran V, Inanici M. Hdrscope: High dynamic range image processing toolkit for lighting simulations and analysis. Proc. BS 2013 13th Conf. Int. Build. Perform. Simul. Assoc., 2013, p. 3400–7.
[80] Bleicher T. Wxfalsecolor By Tbleicher 2021. http://tbleicher.github.io/wxfalsecolor/.
[81] Andersen M, Stokes E, Gayeski N, Browne C. Using digital imaging to assess spectral solar-optical properties of complex fenestration materials: A new approach in video-goniophotometry. Sol Energy 2010;84:549–62. https://doi.org/10.1016/j.solener.2009.02.005.
[82] Greenberg DP. A Framework for Realistic Image Synthesis. Commun ACM 1999;42:44–53. https://doi.org/10.1145/310930.310970.
[83] Muneer T. Evaluation of the CIE overcast sky model against Japanese data. Energy Build 1998;27:175–7. https://doi.org/10.1016/s0378-7788(97)00028-5.
[84] Inanici M, Hashemloo A. An investigation of the daylighting simulation techniques and sky modeling practices for occupant centric evaluations. Build Environ 2017;113:220–31. https://doi.org/10.1016/j.buildenv.2016.09.022.
[85] Ubbelohde MS, Humann C. Comparative Evaluation of Four Daylighting Software Programs. ACEE Summer Study Energy Effic Build 1998;1988:16.
[86] Vinet L, Zhedanov A. A “missing” family of classical orthogonal polynomials. J Phys A Math Theor 2011;44. https://doi.org/10.1088/1751-8113/44/8/085201.
[87] Tsangrassoulis A, Bourdakis V. Comparison of radiosity and ray-tracing techniques with a practical design procedure for the prediction of daylight levels in atria. Renew Energy 2003;28:2157–62. https://doi.org/10.1016/S0960-1481(03)00078-8.
[88] Ward G, Mistrick R, Lee ES, McNeil A, Jonsson J. Simulating the daylight performance of complex fenestration systems using

bidirectional scattering distribution functions within radiance. LEUKOS - J Illum Eng Soc North Am 2011;7:241–61. https://doi.org/10.1080/15502724.2011.10732150.
[89] McNeil A, Lee ES. A validation of the Radiance three-phase simulation method for modelling annual daylight performance of optically complex fenestration systems. J Build Perform Simul 2012;6:24–37. https://doi.org/10.1080/19401493.2012.671852.
[90] Bourgeois D, Reinhart CF, Ward G. Standard daylight coefficient model for dynamic daylighting simulations. Build Res Inf 2008;36:68–82. https://doi.org/10.1080/09613210701446325.
[91] LNBL. WINDOW | Windows and Daylighting 2013. https://windows.lbl.gov/software/window.
[92] Hirning MB, Isoardi GL, Cowling I. Discomfort glare in open plan green buildings. Energy Build 2014;70:427–40. https://doi.org/10.1016/j.enbuild.2013.11.053.
[93] Bian Y, Ma Y. Subjective survey & simulation analysis of time-based visual comfort in daylit spaces. Build Environ 2018;131:63–73. https://doi.org/10.1016/j.buildenv.2018.01.007.
[94] The Daylight Metrics Committee. Approved Method: IES Spatial Daylight Autonomy (sDA) and Annual Sunlight Exposure (ASE). 2012.
[95] Gennaro G. Strategie di controllo avanzate di vetri elettrocromici per il risparmio energetico negli edifici: caratterizzazione sperimentale e analisi numeriche. Politecnico di Torino, 2019.
[96] Pepe D. Controllo dinamico della radiazione solare con smart glazing per il comfort termico ambientale: caratterizzazione sperimentale e analisi numeriche. Politecnico di Torino, 2007.
[97] Jones NL, Reinhart CF. Experimental validation of ray tracing as a means of image-based visual discomfort prediction. Build Environ 2017;113:131–50. https://doi.org/10.1016/j.buildenv.2016.08.023.
[98] Jakubiec JA, Wymelenberg K Van Den, Inanici M, Mahic A. Accurate Measurement of Daylit Interior Scenes. CIE 2016 Light Qual Energy Effic 2016:1–10.
[99] DiLaura DL, Houser KW, Mistrick RG, Steffy GR. The Lighting Handbook. 2018.
[100] Velux Commercial. EN 17037 Daylight in buildings - Designing Buildings. Eur Stand 2020.
[101] Inanici M. Research Methods in Daylighting and Electric Lighting. Res. Methods Build. Sci. Technol., 2021, p. 71–93. https://doi.org/10.1007/978-3-030-73692-7_4.

[102] Pierson C, Cauwerts C, Bodart M, Wienold J. Tutorial: Luminance Maps for Daylighting Studies from High Dynamic Range Photography. LEUKOS - J Illum Eng Soc North Am 2021;17:140–69. https://doi.org/10.1080/15502724.2019.1684319.
[103] Wienold J. evalglare.pdf — Radsite 2016:2. https://www.radiance-online.org/learning/documentation/manual-pages/pdfs/evalglare.pdf/view.
[104] MIT OpenCourseWare. Choice Rev Online 2007;44:44-6573-44–6573. https://doi.org/10.5860/choice.44-6573.
[105] Wienold J, Iwata T, Sarey Khanie M, Erell E, Kaftan E, Rodriguez RG, et al. Cross-validation and robustness of daylight glare metrics. Light Res Technol 2019;51:983–1013. https://doi.org/10.1177/1477153519826003.
[106] Kong Z, Utzinger DM, Humann C. Evaluation of a hybrid photo-radiometer sky model compared with the Perez sky model. Energy Build 2018;178:318–30. https://doi.org/10.1016/j.enbuild.2018.08.022.
[107] Darula S, Kittler R. CIE General sky standard defining luminance distributions. ESim 2002 Can Conf Build Energy Simul 2002:8.
[108] Mardaljevic J. Sky Models for Lighting Simulation. Daylight Simul Validation, Sky Model Daylight Coefficients 1999:163–209.
[109] Giovannini L, Favoino F, Lo Verso VRM, Pellegrino A, Serra V. A simplified approach for the annual and spatial evaluation of the comfort classes of daylight glare using vertical illuminances. Buildings 2018;8. https://doi.org/10.3390/buildings8120171.
[110] Sepúlveda A, Bueno B, Wang T, Wilson HR. Benchmark of methods for annual glare risk assessment. Build Environ 2021;201. https://doi.org/10.1016/j.buildenv.2021.108006.
[111] Jones NL. Fast climate-based glare analysis and spatial mapping. Build. Simul. Conf. Proc., vol. 2, 2019, p. 982–9. https://doi.org/10.26868/25222708.2019.210267.
[112] Pierson C, Wienold J, Bodart M. Daylight discomfort glare evaluation with evalglare: Influence of parameters and methods on the accuracy of discomfort glare prediction. Buildings 2018;8. https://doi.org/10.3390/buildings8080094.
[113] Karlsen L, Heiselberg P, Bryn I, Johra H. Solar shading control strategy for office buildings in cold climate. Energy Build 2016;118:316–28. https://doi.org/10.1016/j.enbuild.2016.03.014.
[114] Van Den Wymelenberg K, Inanici M. Evaluating a New Suite of Luminance-Based Design Metrics for Predicting Human Visual Comfort

in Offices with Daylight. LEUKOS - J Illum Eng Soc North Am 2016;12:113–38. https://doi.org/10.1080/15502724.2015.1062392.
[115] Van Den Wymelenberg K, Inanici M, Johnson P. The effect of luminance distribution patterns on occupant preference in a daylit office environment. LEUKOS - J Illum Eng Soc North Am 2010;7:103–22. https://doi.org/10.1582/LEUKOS.2010.07.02003.
[116] Nezamdoost A, Van Den Wymelenberg KG. Revisiting the Daylit Area: Examining Daylighting Performance Using Subjective Human Evaluations and Simulated Compliance with the LEED Version 4 Daylight Credit. LEUKOS - J Illum Eng Soc North Am 2017;13:107–23. https://doi.org/10.1080/15502724.2016.1250011.